SEARCH FOR RARE NEUTRAL TWO-BODY CHANNELS IN THE $\bar{p}p$ ANNIHILATION AT REST

performed by

measurements of high energy γ-rays using a modular NaI(Tℓ)-spectrometer

VETENSKAP OCH KONST

SEARCH FOR RARE NEUTRAL TWO-BODY CHANNELS IN THE $\bar{p}p$ ANNIHILATION AT REST

performed by

measurements of high energy γ-rays using a modular NaI($T\ell$)-spectrometer

Lars Adiels

STOCKHOLM 1986

Adiels, L.: Search for rare neutral two-body channels in the p̄p annihilation at rest (Roya Institute of Technology, Department of Physics, and Research Institute of Physics, Stockholn 1986).

Abstract

Proton-antiproton annihilation at rest in liquid hydrogen has been studied with a modu- lar NaI(Tℓ)γ-spectrometer. For the purely neutral two-body channels the followin branching ratios, some of them not known before, have been obtained:
$\mathrm{BR}(\bar{p}p \rightarrow \pi^0\omega) = (2.38 \pm 0.65)\%$, $\mathrm{BR}(\bar{p}p \rightarrow \pi^0\eta) = (0.82 \pm 0.10)\%$,
$\mathrm{BR}(\bar{p}p \rightarrow \pi^0\gamma) = (0.0015 \pm 0.007)\%$ and $\mathrm{BR}(\bar{p}p \rightarrow \pi^0\pi^0) = (0.06 \pm 0.04)\%$.
The upper limit for the branching ratio $\mathrm{BR}(\bar{p}p \rightarrow \pi^0\eta')$ was found to be 1.1%. For the ratio $\mathrm{BR}(\bar{p}p \rightarrow \pi^0\omega + \pi^0\rho^0 + \pi^0\eta + \pi^0\eta')/\mathrm{BR}(\bar{p}p \rightarrow \eta\omega + \eta\rho^0 + \eta\eta + \eta\eta')$ an uppe limit of 0.50 could in addition be obtained. It was also concluded that a substantial par of the annihilation comes from P-wave processes.

In a search for Baryonium or other exotic states, peaks appeared in the singles gamm spectrum corresponding to four possible states with masses 1210 ± 5, 1638 ± 3, 1694 ± 2 and 1771 ± 1 MeV, respectively, with yields having upper limits of 0.1, 0.3, 0.16 an 0.18 %, respectively. Two of these peaks are consistent with data obtained from p̄H annihilation. A considerable effort was made to establish the existence of Baryoniu created in p̄p annihilation but it must be concluded that the yield of such states, if the are narrow, seems to be much lower than anticipated. Possible interpretations of thes results are briefly discussed.

A pilot experiment for further studies of the π^0 and the η spectra at LEAR was als performed.

Descriptors: Barionium, γ-ray spectorscopy, p̄p annihilation at rest, p̄He annihilation at rest Glueballs.

ISBN 91-7170-986-X
Sundt Offset Stockholm

> ”Jag skall berätta vad jag hört om glas
> och då skall ni förstå. I varje glas
> som står tillräckligt länge oberört
> förflyttas glasets blåsa efterhand
> oändligt sakta mot en annan punkt
> i glasets kropp och efter tusen år
> har blåsan gjort en resa i sitt glas.”
>
> HARRY MARTINSON, *Aniara*

Till Marianne

TABLE OF CONTENT

PREFACE

Acknowledgements

1 THEORETICAL AND EXPERIMENTAL BACKGROUND

Comments on the $\bar{p}p$ annihilation process

Annihilation and quarks 1

Other annihilation models 1

Baryonium and other exotic states 1

Early experimental evidence of Baryonium 1

Theoretical background 1

The nuclear potential model 1

The MIT-bag model for quarks and gluons 1

Glueballs 2

Lattice QCD and glueballs 2

Conclusion 2

2 EXPERIMENTAL SETUP 2

Requirements on the experimental equipment 2

The experimental equipment 2

The antiproton beam 2

The beam telescope 2

The γ -ray calorimeters 2

The SECTOR-detector 2

The light pulser of the SECTOR 2

12" NaI(Tℓ) 3

Multiplicity counters 3

3 CALIBRATION, DATA-TAKING, MONITORING 3

Calibration 3

Stabilization 3

Data-taking system 3

4 ANALYSIS 3

Singles γ-ray inclusive spectrum analysis 40

Off-line reconstruction of the inclusive singles γ-spectrum 40

Tonne analysis 42

Monte-Carlo simulation of annihilation channels 43

Parametrization of the many-body final state background 44

Analysis of two-body final states at higher energy 45

Errors 45

Analysis of the two-body final states at lower energy 46

Analysis of $\bar{p}$He to γ + anything 46

Coincidence analysis 47

5 CONCLUSIONS AND DISCUSSION 49

A SOME KINEMATICS FORMULAE 53

A.1 Notation and some basic formulas 53

A.1.1 Conserved quantities 53

A.1.2 Lorentz transformations 53

A.1.2.1 Lorentz transformation of energy and momentum 53

A.1.2.2 Lorentz transformations of angles 54

A.1.2.2.1 General 54

A.1.2.2.2 The Lorentz-transformation for a massless particle (photon) 54

A.1.3 The two-body decay kinematics 54

A.1.3.1 Introduction 54

A.1.3.2 Formulas 54

B SOME DECAY PROPERTIES OF THE π^0 AND THE η 57

B.1 Decay properties for π^0 and η to $\gamma\gamma$ 58

B.2 THE BOX SHAPE OF THE (monoenergetic) π^0 DECAY SPECTRA 59

C COINCIDENCE BACKGROUND 63

D THE QUARK CONTENT OF THE ORDINARY MESONS 65

E PAPER I-V 67

F PROPOSAL FOR EXPERIMENT PS182

REFERENCES

PREFACE

"I sit beside the fire and think
of people long ago,
and of people who will see a word
that I shall never know."

J. R. R. TOLKIEN *The Lord of the rin*

This thesis is part of the requirement for a Swedish PhD. It is written entirely in Englis (with the exception of some quotations) and will be defended in Swedish at the Roy Institute of Technology, Department of Physics. The thesis is based on work which th author have performed in the Basle – Karlsruhe – Stockholm collaboration at CER during 1978 – 1984. The scientific work have been published in five papers, enclose in Appendix E. Finally in Appendix F the proposal to the experiment PS182, whic followed on the results obtained documented here, is enclosed. The experiment PS18 at LEAR has taken data since 1984 and the analysis is in progress.

Since I joined the group in november 1978 I have worked mainly with the analysi once the experiment was set-up. When the data taking was finished in 1981 I got th opportunity to take care of the on-line software for the experiment PS182 and since 198 I gradually moved over to the new experiment. I left CERN in mid 1984 to complet my thesis at my home institute in Stockholm, after a very interesting and stimulatin delay as responsible for the data-taking of PS182. Before the summary I would like t give my thank to some of all the persons involved in the development of this work.

Acknowledgements

The scientific work on which this thesis is based is a team work and could not have com through without all my colleagues and co-writers in the group. It was also dependen on CERN and its experimental as well as computer facilities. The hospitality of CER and the very international scientific ambience at CERN has been a great source o inspiration during my stay.

Among all the persons in the group and others closely related at the participatin institutes to whom I feel indebted I wish to take the opportunity to give a special than to prof. I. Bergström for giving me the opportunity to join the group, to A. Kerek an I. Bergström for taking special care of me during their sabbatical at CERN coincidin with my first year there. I would also like to thank L. Tauscher who in reality acted a my supervisor both in physics and in skiing for several years. K. Fransson, who travelle a lot between CERN and Sweden induced inspiring discussions as well as P. Pavlopoulo whose original experiment also to a great extent motivated the effort. Among the othe senior physicits I would also like to thank A. Nilsson and R. Guigas who never hesitate to take time from their work to help me progress with my tasks. For several parts of the analyses I have worked in close contact with B. Richter whose time in the group will not be forgotten. From a group of three students S. Carius, H. Danared and H. Johansson unfortunately only S. Carius has continued in the group but his help and discussions have been so much more fruitful. Other students D. Hatzifotiadou, J. Repond, D. Tröster C. Findeisen and R. Buser, some of them joining the group so late that they do not appear in those papers, have been very helpful also in private matters. I would also like to give a special thanks to two of the technicians Å. Engström and K. Agehed with whom I have worked in close contact during the set-up of the experiments. Two visitors in the group M. Cooper and M. Hasinoff have been very helpful to me by virtue of their personal qualities and their new ideas. Among the CERN staff I would in particular like to thank the computer-librarian H. Renshall, M. Sendall and his group (DD/OC) and P. Darriulat who once introduced me to particle physics.

The work would not have been possible without the unlimited support from my wife Marianne and my family who have always supported my work with their hearts and souls.

This manuscript was excellently typed by E. Oppenheimer who has also helped in revising the language together with Marianne, any remaining mistakes are however introduced by me afterwards. The manuscript is produced by our TeX* setting-system and I would finally, still not being able to mention several persons to whom I owe great thanks to, like to thank N. Elander who helped me acquire the necessary equipment for the TeXnology at the institute.

* TeX is a trademark of the American Mathematical Society

CHAPTER 1
THEORETICAL AND EXPERIMENTAL BACKGROUND

"Wheresoever the carcase is, there will

the eagles be gathered together"

St. Matthew xxiv.28

Ever since the Dirac-equation [1] was explored and the positron and antiproton were discovered, the subject of matter-antimatter has fascinated many physicists and even laymen. The study of the matter-antimatter annihilation process has played an important role in elementary particle physics for many years. As a consequence of the increasing understanding of the proton and antiproton structure, the antiproton itself has become an important probe for investigating matter, as for example was manifested in the recent $\bar{p}p$-collider project at CERN which led to the discovery of the W- and Z-particles.

Although the proton-antiproton system has been extensively studied, the annihilation process is not understood in detail. In particular, experimental information is poor regarding rare neutral two-body annihilation channels, which are hard to study with bubble chamber techniques. In addition, current well established theories are only able to predict the main features of the annihilation process. In the late 70's several groups found evidence for exotic objects named Baryonium, when investigating the proton-antiproton annihilation process. The masses of these objects were reported to be in the 2 GeV region. The interpretation of these results, some of them suffering from poor statistics, was not very clear. As a result, a large number of papers on both experimental and theoretical aspects of the proton-antiproton annihilation were published. Independently, new calculations based on the major theory for strong interaction, Quantum chromodynamics (QCD), have led to predictions of exotic states in the same energy range. Such exotic particles could for instance be objects composed of two quarks and two antiquarks, Baryonium, or of gluons only, Glueballs.

Comments on the $\bar{p}p$ annihilation process

The most striking feature of the proton-antiproton interaction is the annihilation process. This means that when a particle and an antiparticle are brought together they disintegrate into lighter particles by strong interaction. These particles ultimately decay to stable leptons and photons. The $\bar{p}p$ annihilation process was studied extensively in the 1960's. Information about the most frequent annihilation channels based on $\bar{p}p$ annihilation at rest in a liquid target of H_2 is collected in Table 1, where it should be observed that the bubble chamber technique then available was rarely able to distinguish channels with more than two neutrals in the final state.

Table 1

Branching ratios from $\bar{p}p$ annihilation at rest in a liquid target

Annihilation channel	Resonant channel	Branching ratio BR (%)	Reference
$\pi^+\pi^-\pi^0$		3.7	2
$\pi^+\pi^-\pi^0$	$\rho^{\pm}\pi^{\mp}$	2.7	2
$\pi^+\pi^-2\pi^0$		9.3	3
$\pi^+\pi^-3\pi^0$		23.3	3
$\pi^+\pi^-4\pi^0$		2.8	2
$2\pi^+2\pi^-\pi^0$	$\omega\pi^+\pi^-$	3.8	2
$2\pi^+2\pi^-\pi^0$	$\rho^0\pi^0\pi^+\pi^-$	7.3	2
$2\pi^+2\pi^-\pi^0$	$\rho^{\pm}\pi^{\mp}\pi^+\pi^-$	6.4	2
$2\pi^+2\pi^-2\pi^0$		16.6	3
$2\pi^+2\pi^-3\pi^0$		4.2	3
$3\pi^+3\pi^-\pi^0$		1.3	2
$\pi^+\pi^-\eta$		1.2	2
$2\pi^+2\pi^-\eta$		0.6	2
$\pi^0\rho^0$		1.4	2
$\eta\rho^0$		0.22	2
$m\pi^0$		3.2	2
$\pi^+\pi^-$		0.4	4
$4\pi^+4\pi^-$		6.9	4
$3\pi^+3\pi^-$		2.1	4
$K\bar{K}m\pi(m \geq 0)$		6.82	2
$\pi^0\pi^0$		0.014/0.048	5/6

Compared with the electron-positron system, for which the annihilation is well unde stood, the annihilation of the proton-antiproton system is much more complicated f many reasons. Experimentally the antiprotons have been very hard to produce, requi ing very large and expensive accelerator facilities. In contrast to e^+e^--annihilatio where the interaction is entirely electromagnetic, the electromagnetic interaction in th $\bar{p}p$ case is followed by the strong interaction which in this case is entirely responsib for the annihilation process. No reliable theory is so far available since this annih lation process is nonperturbative and involves composite particles. A strong effort t gain a better understanding of $\bar{p}p$ annihilation both experimentally and theoretical is in particular motivated by the fact that the annihilation process is a genuine quar phenomenon also in the low energy regime. As pointed out the results in Table 1 we obtained using a liquid H_2-target. The results from a gaseous target are quite differe (see below). The experiment presented in this thesis deals with $\bar{p}p$ annihilation at re in a liquid H_2-target where the annihilation products are two neutral objects. The ex perimental set-up was able to detect decay channels with one γ + any neutral particl and one π^0 + any neutral particle or one η + any neutral particle, in the latter cases by studying the subsequent decay of π^0 and η, respectively, into two γ 's (see Table 2). Thus the experiment covers most of the frequent energetically possible neutral two-body channels, since phase space favours the light π^0- and η-mesons.

Annihilation and quarks

As can be seen from Table 1 the most frequent annihilation channels are those in which three or more hadrons are produced. This can be qualitatively understood by the application of the quark concept. The idea of quarks was introduced [7] in the early 60's when it first served as a simple tool to formulate SU_3 symmetry in strong interactions. Nowadays the quark concept is so well established that it serves as the starting point of any theory of hadrons and their interactions.

Figure 1
Schematic figure of a) Mesons b) Baryons

a) A meson is built from a quark and an antiquark and kept together by gluons

b) A baryon is built from three quarks and kept together by gluons

From the five well established basic quarks* (u, d, s, c, and b) all known hadronic (i.e. strongly interacting) particles can be built. As is well known they are divided into two groups, baryons and mesons. The baryon consists of three quarks and the meson of a quark and an antiquark, both of them kept together by gluons (see Figure 1). All mesons decay (see Table 2) by strong or weak interaction, but the lightest baryon, the proton, is remarkably stable. To our present knowledge the proton does not decay. The lifetime is larger than 10^{32} years and thus very much longer than the age of the universe. The quark content of the proton (antiproton) and the mesons built from only u and d quarks is given in Appendix D.

* Several experiments have been carried out in order to search for a sixth quark predicted by theory long ago. It may have been observed by the UA1 collaboration [8] in the above mentioned $\bar{p}p$ collider project, but so far no final conclusion has been reported.

Table 2

The most common decays of the lightest mesons. The decays of special interest for this analysis are indicated (ref. [10]).

Particle	Mass [MeV]	Decay channel	Final products	Decay fraction for channels relevant in this thesis (%)
π^0	135.0	$\gamma\gamma$	$\gamma\gamma$	98.8±0.03
π^+	139.6	$\mu^+\nu$	$\mu^+\nu$	
π^-	139.6	$\mu^-\bar{\nu}$	$\mu^-\bar{\nu}$	
η	548.8	$\gamma\gamma$	$\gamma\gamma$	39.0±0.8
		$3\pi^0$	$\gamma\gamma\gamma\gamma\gamma\gamma$	
		$\pi^+\pi^-\pi^0$	$\mu^+\mu^-\gamma\gamma\nu\bar{\nu}$	
ρ^0	769	$\pi^+\pi^-$	$\mu^+\mu^-\nu\bar{\nu}$	
ρ^+		$\pi^+\pi^0$	$\mu^+\gamma\gamma\nu$	
ρ^-		$\pi^-\pi^0$	$\mu^-\gamma\gamma\bar{\nu}$	
ω	782.6	$\pi^+\pi^-\pi^0$	$\mu^+\mu^-\gamma\gamma\nu\bar{\nu}$	
		$\pi^0\gamma$	$\gamma\gamma\gamma$	8.7±0.5

As already emphasized (Table 1) most $\bar{p}p$ annihilation channels involve the emission c pions. The charged pion has a mean life of $2.6 \cdot 10^{-8}$ s while the mean life of the π^0 i only $0.8 \cdot 10^{-16}$ s. This means that the charged pions survive distances much longer tha the detector dimensions while the π^0 decays (mostly into 2 photons) in the target, fact which has consequences for the detector design and data analysis.

Most naturally [9] one can consider a model where the three quarks and antiquark in the proton and antiproton are rearranged into three mesons (see Figure 2a). Th immediate conclusion of this model is that only three-body annihilations can occur. Thu the final state should contain three or more mesons due to further decay of the primar mesons. Furthermore, no strange mesons should appear and especially the productio of ϕ ($s\bar{s}$) must be suppressed. This simple model fits 80-90 % of the total experiment data (cf. Table 1). However, $\approx$ 7 % of the annihilation channels do contain strang particles and there are at least 10 % two-body annihilations. For the understanding c the annihilation process in finer details a more refined model is needed, in particula to treat channels with more than one neutral particle in the final state. For obviou reasons such channels were hard to study with bubble chamber techniques.

Some possible extensions to allow 2-body annihilation channels within the framework c the simple rearrangement model mentioned above are indicated in Figures 2b and 2c, bu most theoretical works tend to avoid this question so far. The experimental informatio

Figure 2
Schematic annihilation mechanisms.

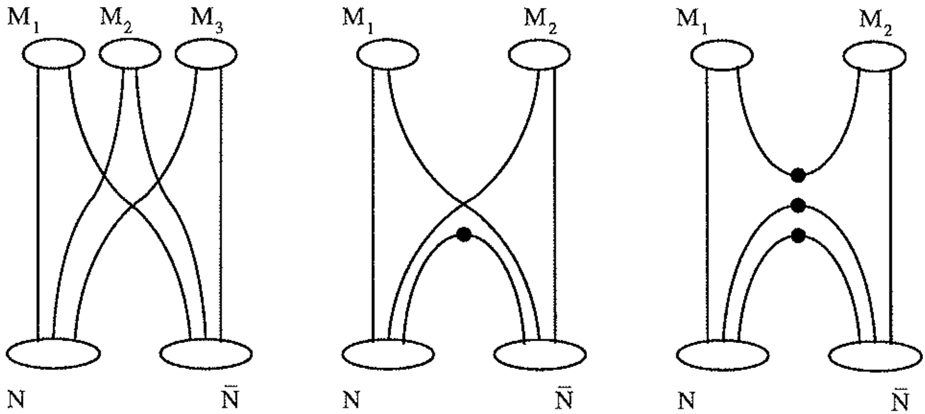

a) rearrangement into three mesons

b) rearrangement into two mesons with one annihilation vertex

c) rearrangement into two mesons with annihilation and creation vertices

on the yields of two-body annihilation channels is not only rare, but sometimes also contradictory when it exists. For instance for the annihilation channel $\bar{p}p \rightarrow \pi^0\pi^0$ the yield is reported by two different groups to be (0.014 ± 0.003) % and (0.048 ± 0.010) %, respectively (cf. Table 1).

Other annihilation models

Among several theoretical approaches to the understanding of the $\bar{p}p$-system (for a review until 1983 see Green [11] and references therein) the potential concept has been extensively used. The potential used has developed from a simple phenomenological nucleon-nucleon interaction potential to more refined potentials in which the quark nature of the associated particles is taken into account. A potential approach predicts only the appearance of two-body annihilation channels, but as shown in Table 1 many-body channels dominate the experimental data. This deficit of the model can, however, be cured to some extent by the construction of many-body channels from weakly coupled resonant two-body channels.

Baryonium and other exotic states

One striking feature of the nuclear potential models, observed first in 1956 [12,13] and developed by Shapiro [14], is that a nucleon-antinucleon force is necessarily strongly attractive. The corresponding deep potential well should thus contain several bound states as well as states in the continuum (Figure 3). Such states were named Baryonium in analogy with the name positronium (e^+e^-). The level energies and widths of Baryonium are, however, difficult to calculate because of the uncertain radial position of th hard core and the interference with the annihilation process itself.

In the energy region 0 - 2 GeV the standard QCD theory is not calculable in a perturb tion approach. However, there are some models, using simplifications, approximatio or further assumptions to make the theory calculable, which agree reasonably well wi the measured meson mass spectrum. Furthermore, qualitative arguments show that a possible mesons in this region are found. With "all possible" we mean $q\bar{q}$ systems whe q is u, d or s. Other flavours are heavier and thus resulting in objects with masses larg than 2 GeV. However, the question must be raised why there would not be meson-lil states of the type $qq\bar{q}\bar{q}$, or states with only gluons, often named Glueballs. This nam is a little bit misleading since spherical Glueballs are not stable in QCD according t Robson [15] and a Glueball has to have a torus shape or more complicated geometr to be stable. Therefore, names like "Gluerings" have been suggested. There are se eral models predicting such objects. In many experiments such exotic states have bee searched for.

Early experimental evidence of Baryonium

In 1974 an experiment by A. Caroll et al. [16] claimed the observation of a narro resonance in the $\bar{p}p$ and $\bar{p}d$ total cross section at 1932 ± 2 MeV having a width $\Gamma = 9 \pm 4$ MeV. Similar results were also obtained by Chalupka et al. [17]. As n mesons were known or expected in this energy region these objects were interprete as being something else than ordinary mesons. The interpretation chosen at this tim was a $\bar{p}p$-state slightly above threshold, i. e. a Baryonium state in the continuum. Thes measurements stimulated an intensive search also for bound Baryonium states, sever experiments claimed evidence for structures in this energy region. The results of som of these experiments are collected in Table 3 together with some results from olde experiments on $\bar{p}p$ annihilation and some results from observations of e^+e^- collision All experiments claimed states below 1850 MeV and were suggested to be candidat for eihter Baryonium or Glueballs. In Table 4 suggestions are collected for Baryoniu states in the continuum. The present thesis is very much related to the search for boun Baryonium states, i.e. narrow objects with a mass less than $2m_p$, and was particular motivated by the findings of Pavlopoulos [18] et al.

Theoretical background

A general review of Baryonium is presented in the theoretical work by Rossi an Veneziano [25] . The general impression from this and other surveys is that Baryo nium should exist, though different authors may use the name in slightly different way Two basic theoretical approaches have been applied extensively to explain Barioniu states; the nuclear potential model and the concept of four-quark states. Here, som nuclear potential results and one four-quark model, the MIT-bag model, will be briefl commented.

The nuclear potential model

The first work by Shapiro mentioned above [14] and later reports [31] cover the essen tial ideas for the possible existence of bound states and resonances in the $\bar{N}N$-system

Figure 3

Transformation from particle-particle to particle-antiparticle potentials for the strong interaction (below) and, for comparison the Coulomb interaction (above). The curves are schematic and the scales cannot be compared.

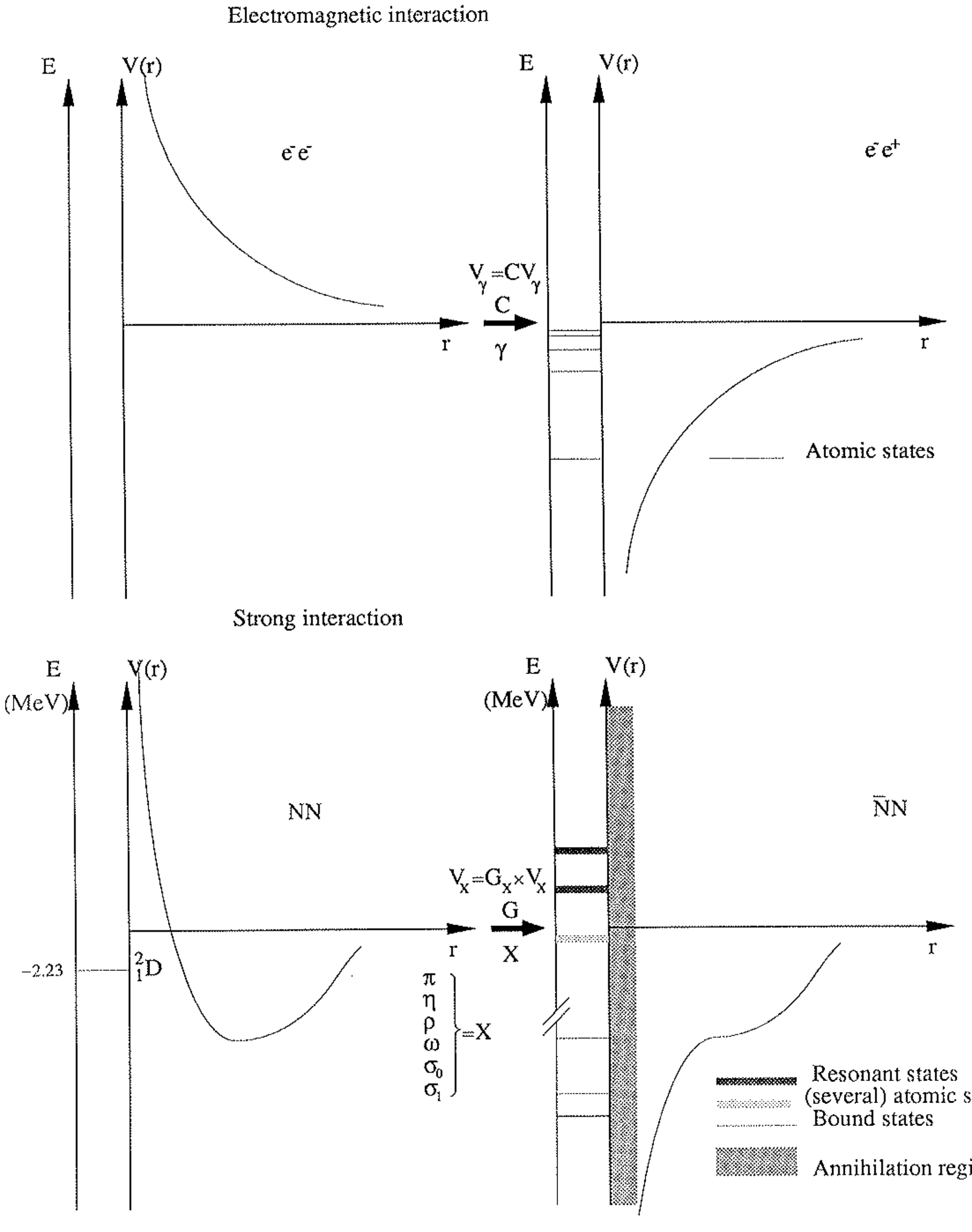

Table 3

Some experiments claiming objects with a mass below the $2m_p$ threshold of $\bar{p}p$ annihilation at rest. All those "states" has been discussed as possibly being Baryonium or Glueballs (but not necessarily by the original authors).

Mass (MeV)	Width (MeV)	"Name"	Reaction	ref	Year
1394±23	<46		$\bar{p}p \rightarrow \gamma + X^0$	18	1978
1423±10	45±20	E(1420)	$(3\text{-}4)\bar{p}p \rightarrow$	19	1967
1425±7	80±10	$\iota(1440)$	$\bar{p}p$(at rest)$\rightarrow$	20	1967
1640±50	220±100	$\theta(1690)$	$J/\Psi \rightarrow \gamma\ 2\eta$	21	1982
1646±11	<24		$\bar{p}p \rightarrow \gamma + X^0$	18	1978
1652±17			$e^+e^- \rightarrow X^0$	22	1979
1683±8	<21		$\bar{p}p \rightarrow \gamma + X^0$	18	1978
1708±30	156±60	$\theta(1690)$	$e^+e^- \rightarrow \gamma + K^+K^-$	23	1982
1772±6			$e^+e^- \rightarrow X^0$	22	1979
1794.5±1.4			$\bar{p}p \rightarrow p + X^-$	24	1971

Most later calculations are done after a similar scheme based on boson exchange mo els. The general features of the one boson exchange potential model can be deduced a systematic way [32], providing a specific coupling strength for each exchange part cle. This model or more elaborate ones, taking also two boson exchange into accoun parametrized as the exchange of the hypothetical mesons σ_0 and σ_1, is fitted to lo energy NN scattering data. In analogy with the transformation of the e^-e^- system in an e^+e^- system by charge conjugation the NN system can be transformed to an $\bar{N}$ system like $\bar{p}p$ by a G-parity transformation (cf. Figure 3). It then turns out that t NN force, which is repulsive with the exeception of the small attractive well which allo the only bound state ${}^2_1$D, changes to a strongly attractive force for a large part of i range, mainly due to the fact that the ω-exchange is strongly attractive in the $\bar{N}N$ cas

The major problem with such an approach is that the hard core NN potential due ω-exchange is difficult to determine experimentally. Its G-parity transform which dor inates the $\bar{N}N$ behaviour is thus sensitive to the least known part of the NN potenti In addition, the levels of possible bound or resonant states are pushed and broadened an uncontrolled way by annihilation. Furthermore, the whole approach assuming poi like objects must be questioned, since it leads to predictions for effects on such sma distances that the quark substructure of the nucleons should be taken into account.

Some of the main features of the nuclear model are compared with the MIT-bag mod (to be discussed below) and some other models in Table 5. In Figure 4 one of t potential calculations of level energies is compared to one of the MIT-bag calculatio

Table 4

Some experiments claiming non-strange resonances above the $2m_p$ threshold of $\bar{p}p$ annihilation at rest

Mass (MeV)	Width (MeV)	"Name"	Reaction	ref	Year
1932±2	9±4	S	$\bar{p}p$,$\bar{p}d$ cross section	17	1976
1935±3	16±11		$\bar{p}p$ cross section	16	1974
1935±1.0	2.8±3.0		$\bar{p}p$ cross section	26	1979
1937±2	21±10		$\bar{p}p$ cross section	27	1980
2190±5	85	T_1	$\bar{p}p$,$\bar{p}d$ cross section	28	1967
$2192.7^{+1.2}_{-1.5}$	$97.6^{+8.1}_{-5.9}$		$\bar{p}p$ cross section	29	1973
2155±15	35±75		$\bar{p}p$ cross section	30	1977
2345±10	140	U_1	$\bar{p}p$,$\bar{p}d$ cross section	28	1967
$2359.4^{+1.4}_{-1.2}$	$169.4^{+17.0}_{-7.6}$		$\bar{p}p$ cross section	29	1973
2380±10	140	U_0	$\bar{p}p$ cross section	28	1967
2345±15	135^{+150}_{-65}		$\bar{p}p$ cross section	30	1977

The MIT-bag model for quarks and gluons

In the MIT-bag model the quarks and gluons are put in a spherical cavity of radius r. The eigenstates are then found using a proper completely antisymmetric wave function. The masses of the states are obtained by minimizing with respect to r the quantity

$$E(r) = E_q + E_v + E_o + E_g$$

where E_q is the quark kinetic energy, E_v is an energy contribution from the confining pressure, E_o is an estimate of the effects of zero-point fluctuations of fields in a confining sphere and E_g is the quark - gluon interaction. The only limitation from colour is that the system is a colour singlet. In the MIT-bag model there is room for multiquark states of the $(q)^n(\bar{q})^m$ (n+m > 3) type besides the usual $q\bar{q}$-mesons and qqq-baryons. The most interesting case in this thesis is n = m = 2, and the further discussion will be restricted to this case and n = m = 0, i. e. a state containing only gluons. Following Jaffe [39] the discussion about Baryonium-like states will be divided into two parts depending on the angular momentum and the internal geometrical composition of states.

(i) *S-wave* $qq\bar{q}\bar{q}$ *states analogous to the usual S-wave mesons and baryons.* An S-wave state of $qq\bar{q}\bar{q}$ is analogous to the usual $q\bar{q}$-mesons and qqq-baryons, which are "well"

Table 5

A comparison of different models (from reference [25]). All models are not discussed i this thesis. Further references to these models and theories are: for the Colour chemistr models [35] and for the Topological bootstrap theory [36]. The references in the tabl (54,55) are given as references [37,38] respectively in this thesis.

Comparison among various approaches to baryonium physics

Baryonium properties	QCD inspired dual topological picture	Nuclear physics approach	MIT-bag model	Colour chemistry model	Topological bootstrap
Spectrum	Baryonium states other than $M_4^4(qq\bar{q}\bar{q})$: $M_2^4(q\bar{q})$ and M_0^4(no q's) Mixing between exchange degenerate trajectories	No EXD $I = 1$ states cluster near threshold and have low L[(a)] $I = 0$ states more deeply bound	Linear EXD trajectories for $l^{(b)} > 1$ No mixing effects generally considered	Two kinds of states: T- and M-baryonia. Linear EXD trajectories $l^{(b)} > 1$. Mixing with normal trajectories allows for M-baryonium production	Only the $qq\bar{q}\bar{q}$ kind of baryonium states
Trajectory parameters	Computed via duality from the multiperipheral structure of the crossed channel	—	Slopes and intercepts computed in terms of parameters of the model	Same slopes as in MIT-bag model. T- and M-baryonium intercepts from the assignment of the T-2.15 GeV and the 2.95 GeV states respectively	Linear EXD traject be computed self c in the "planar boot approximation (see for instance re
Assignements	No specific assignement attempted Problems with high mass narrow states	Difficult, but many experiments need confirmation	Room for S, T, U resonances and for those of ref. [54]	S, T, U resonances and those of ref. [54] are T-baryonia Narrow high mass states are M-baryonia	No specific assignm attempted. Possible problems v spin high mass narr
Isospin G-parity	Degeneracy	No degeneracy	Degeneracy	Degeneracy Small splitting of G-parity doublets for M-baryonium	Degeneracy
Coupling to mesonic channels (ann.)	Suppressed by JOZI Lack of detailed calculations	Suppressed by the wave function being small in the annihilation region	Suppressed by centrifugal barrier. Lack of detailed calculations	Suppressed by centrifugal barrier. Problems with low M-baryonia in specific non-relativistic quark model calculations	Topologically forbi at lowest order
Coupling to $N\bar{N}$ channels (scatt.)	Allowed	Allowed	Allowed	Allowed for T-baryonium Forbidden for M-baryonium	Allowed
Candidates for narrow width states	High spin states near threshold. M_2^4 and M_0^4	Bound states near threshold Resonances with $I = 0$	High spin states near threshold or states with exotic internal colour configuration	M-baryonium and other states with exotic internal colour configurations. S is a T-baryonium narrow because near threshold	Low angular momentum, lowest mass states. Best candidates: states under threshold

[(a)] L is the angular momentum of the $N\bar{N}$ system.
[(b)] l is the angular momentum of the (qq)-$(\bar{q}\bar{q})$ system.

this table (5 comp diff models) is not yet ready

Figure 4
Low-lying non-strange Baryonium masses according to different models

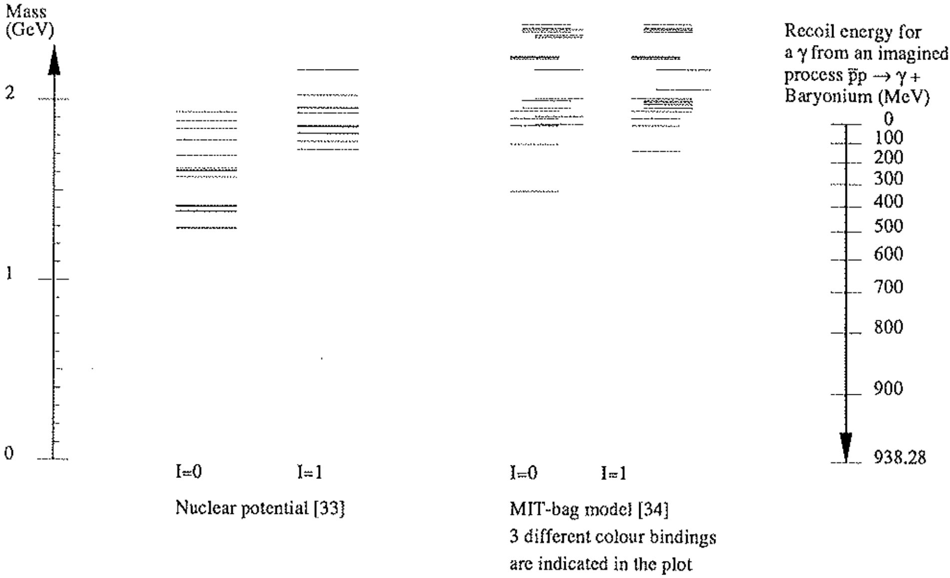

understood within the model. The major contribution to the mass of the states comes in this case from the kinetic energy of the quarks and antiquarks. Thus the model predicts, in first approximation, a ratio 2:3:4 $\simeq$ 700:1100:1500 MeV for the masses of $q\bar{q}$ (mesons), qqq (baryons) and $qq\bar{q}\bar{q}$ ("Baryonium") respectivly. This would possibly be an explanation for the absence of exotic states in the low mass region. Jaffe [39] has associated four-quark states of this type with the mesons $\epsilon(700)$, $S^*(980)$, $\sigma(980)$ and $\kappa(?)$*. Other authors have proposed to associate such states with bumps seen in e^+e^- annihilation in the mass region 3.6 – 4.4 GeV [40]. However, states of this type also have a large width into mesonic channels and are therefore not Baryonium-like states with the definition usually chosen which require Baryonium to have relatively long half-life.

(ii) *High ℓ (angular momentum)* qq *(diquark) -* $\bar{q}\bar{q}$ *(diquark) states corresponding to elongated bag structures.* The coupling to mesonic states is supposed to be suppressed by centrifugal barrier effects. A motion which possesses a non-zero angular momentum is plausible to result in an elongated object. If there are two quarks in one end of this structure and two antiquarks in the other, one can assume that they are kept apart by a centrifugal force and thus the coupling to mesons are reduced since it is not possible to form a colour singlet from qq or $\bar{q}\bar{q}$. It seems reasonable to

* This work was done when these "mesons" where still "alive". They are not listed in the 1984 version of reference 10.

assume that it is the colour flux lines that keep the system together while the angula momentum provides a centrifugal barrier that prevents the quarks and antiquarl to combine to ordinary mesons. Using the assumption that string-like hadrons ar tubes of colour flux lines which terminate on colour charges at the ends K. Johnso [41] found that the first narrow state, with spin 2, has a mass about 1.6 GeV. Th bag model also predicts that states of high spin (high mass) should be more narrov States of this type could be candidates for Baryonium states.

Glueballs

One distinctive feature of the MIT-bag model is that also a state consisting of only gluor must have a mass [42], a prediction which is not a priori true for other models. A naïv MIT-bag model gives a mass of 960 MeV for the lowest glueball state. However, mor realistic calculations increase this mass to above 1300 MeV. Some MIT-calculations o masses for glueballs are collected in Figure 5.

Figure 5

Low lying Glueball masses according to MIT-bag models and Lattice theories

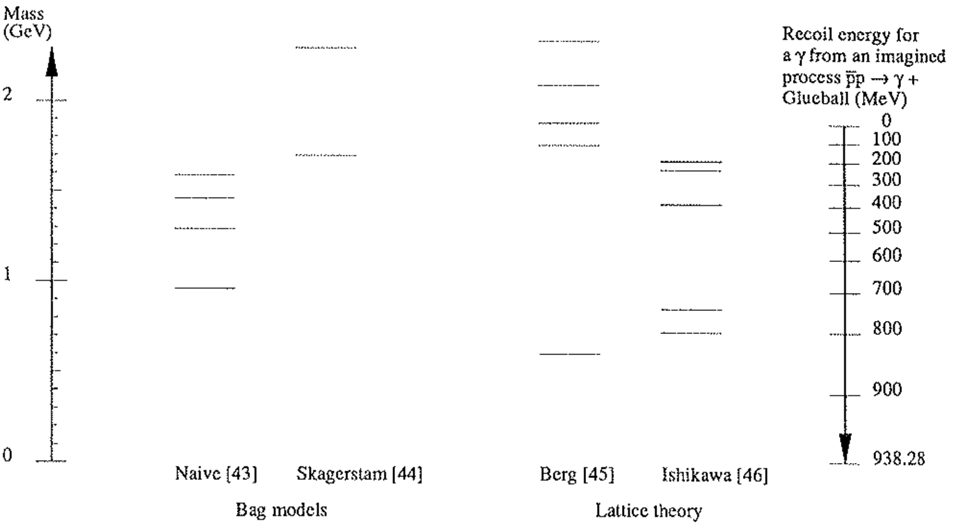

Lattice QCD and glueballs

For a long time the use of the bag models was the only method to make reasonab numerical estimates of masses of particles, as it is not known how to make calculatior of many observables with basic QCD (see below). However, recently there are ne calculations on glueball masses done with a new approach to the QCD problems, namel the use of the lattice gauge concept. These calculations emerged from attempts to solve basic problems with QCD but has also resulted in estimates of glueball masses which gave similar results as the bag model. Unfortunately, the masses of the bosons and mesons are still difficult to calculate.

Quantum chromodynamics (QCD), as all quantized field theories, has to be regularized and renormalized in order to give results which can be compared with experimental data. Generally, this is accomplished with a perturbative expansion, but in QCD there are problems which are not amenable to a perturbative treatment. This problem is not unique to QCD, but the availability of nonperturbative methods of analysis is particularly important, since the calculation of mass spectra hinges on them.

In order to solve these problems, Wilson proposed [47] in 1974 a formulation of QCD to provide a nonperturbative regularization, which has led to the very important result of proving confinement, as well as to estimations of glueball masses. The theory is defined on a hypercubical lattice in Euclidian space-time with a spacing a. Matter fields are only defined at the lattice points, but the gauge dynamical variables are finite group elements U_x^μ associated with links, from x to x + $\hat{\mu}a$, on the lattice. There is an action S consisting of $S_g + S_m$ where S_g is the gauge field action and and S_m is the action from the matter fields. S_g is built up from terms depending on colour exchange in each lattice point. In the continuum limit a $\rightarrow$ 0 this formalism is able to regularize the theory with the proper normalization. Numerical "experiments" show that a lattice spacing of $\approx$ 0.11 fm or less is enough to obtain stable results which is reasonable since the typical scale for hadronic phenomena is 1 fm.

Several authors [45,46] have calculated the mass for glueballs within the framework of lattice theories. However, the technical (computer resource) problems are substantial. The results from different attempts are slowly converging (sometimes with a scale-factor) and some results are given in Figure 5. A comparison with the theoretical estimates of the masses from bag models is also done.

Conclusion

There exists several models predicting new exotic states in the 0–2 GeV region, but they all suffer from lack of experimental data, since they contain parameters which have to be fixed by experiments. From the experimental point of view there are a number of claims that new states have been found. However, some of these claims suffer from poor statistics and others are questioned by new experiments. The work described in this thesis was to a great extent inspired by the fact, that it should be possible to reach four-quark states (qq-$\bar{q}\bar{q}$) as well as Glueballs in the annihilation of $\bar{p}p$ at rest and it might be possible that such states (X^0) are populated in the two-body process $\bar{p}p \rightarrow \gamma X^0$, where the energies of the γ-rays should fall in the energy region 0-1 GeV, which can be studied with NaI(Tℓ)-detectors at a reasonable cost.

CHAPTER 2

EXPERIMENTAL SETUP

"It is a capital mistake to theorize
before one has data."

Sir ARTHUR CONAN DOYLE, *Scandal in Bohemia*

Requirements on the experimental equipment

As emphasized in the preceding section the main aim of the work presented in th thesis was to search for Baryonium states and for rare two-body channels where one both particles decay by gamma-emission. Thus, the main experimental device need was a gamma detector with good efficiency and resolution. Studies of the p̄p-syste at rest means that the highest available momentum is equal to the proton mass. Th the detector had to cover a range up to 1 GeV. The device chosen was a big modul NaI(Tℓ) detector described in detail below and in Paper I.

Furthermore, it is desirable to determine the multiplicity of the pions since the decay Baryonium could be dominated by one channel and thus a window on the multiplici spectrum could help to reduce the background. Since the dominant neutral particle the π^0 which decays mainly to two γ-rays (cf. Table 2) it is also desirable to have tv γ-detectors operating in coincidence mode. The ideal detector is one having 4π sol angle, including a magnetic spectrometer for the charged π and having almost no ma acting as a secondary source of radiation, could not be constructed nor for technic neither for economic reasons. Furthermore, since the experiment had the character o pilot experiment for further studies, the detector had to be simple and a poor solid ang had to be accepted. This simple equipment offers still some experimental possibiliti but also some obvious experimental difficulties.

Below some experimentally important remarks are made before the final set-up is d scribed.

- Neutral decay products

One objective of the experiment was to study poorly known neutral p̄p annihilati channels. All the neutral particles, to be considered, decay on a time scale whi makes it difficult to measure their energy before they have decayed. The final dec products are usually two or several γ-rays which results in a continuous spectrum w an approximately exponential fall towards higher γ-energies. However, both π^0 anc (and to some extent ω) have interesting decay properties which makes it possible study monochromatic particles by measuring only one of its decay γ-rays (see belov

- Two-body annihilation channels

Experimentally two-body annihilation channels play a special role, since the system is well determined if one of the two decay particles is detected. This fact permits experiments with much less costly equipment than when simultaneously several particles have to be detected for the reconstruction of a certain event.

- Decay kinematics

In appendix A the kinematics relevant for this thesis is presented in greater detail. One central observation is that one can detect monoenergetic particles decaying into two γ-rays by measuring only one of the decay γ-rays and thus measure neutral two-body channels with one single γ-detector. This is due to the fact that the two decay γ-rays form a uniform distribution, with a maximum (and minimum) value depending only on the velocity of the decaying particle.

- Target

For several reasons we have used a **liquid H_2** target:

(i) One obtains different results from annihilation in a gas target and a liquid target. This is due to the fact that annihilation occurs from different initial states. In a gas target the annihilation occurs predominantly from a P-wave, whereas in a liquid target Stark-mixing is shaking the system down to an S-wave state before annihilation takes place. As the $\pi^0\pi^0$ channel is restricted to come from P-wave its branching ratio is dramatically different in a gas and a liquid target.

(ii) The poor quality of the $\bar{p}$-sources (before LEAR) and the big momentum spread implies that one must have a big enough stopping power in the target region. This is difficult with a gas target.

(iii) The $\bar{p}p$ is not in a well defined initial isospin state. However, a neutron target is not feasible and for a heavy nuclide the Fermi motion is distorting the relevant part of the spectrum.

For the Baryonium search (see above) a He target was also used.

The experimental equipment

As emphasized above the purpose of the experiment was to study the proton-antiproton annihilation at rest resulting in γ + any other particle(s), or (π^0 or η) + any other particle. As is well known (cf. Table 3) the π^0 and sometimes the η decay into two γ-rays. The fact that studies of these particles in two-body channels can be done by measuring accurately only one photon means that one good NaI(Tℓ) γ-calorimeter was needed. A second NaI(Tℓ)-calorimeter was used to study coincidences. However, the coincidence count rate was very low and this detector combination served only as a pilot experiment for later studies at LEAR.

In addition a good $\bar{p}$-beam with a beam telescope was needed in order to provide a trigger and separate the antiprotons from other particles in the beam in particular negative pions. The experiment included also multiplicity counters for both γ-rays

and charged particles. Below the experimental set-up is described item by item. Th
schematic layout can be seen in Figure 7.

The antiproton beam

As a source for p̄'s the electrostatically separated so-called K_{23} beam at the CER
proton synchrotron (PS) was used. The beam elements together with its optical equiv
alent is shown in Figure 6. The optimum efficiency was found at a beam momentu
of 600 MeV/c in an earlier experiment [48] using the same beam line. At this bea
momentum the beam was fine-tuned several times a day to optimize the stop rate.
maximum stop rate of ≈ 250 p̄'s per machine burst was obtained. The same beam lin
was used in both the 1979 and the 1980 runs.

Figure 6
The beam K_{23} and its optical equivalent.

The symbols stands for, PT = Production target, Q = Quadrupole magnets, B = Bendin
magnets, SM = correcting magnets to the Separator S, ΔP = momentum slits, BS = Bea
stopper, ΔM = mass slits and FT = Target.

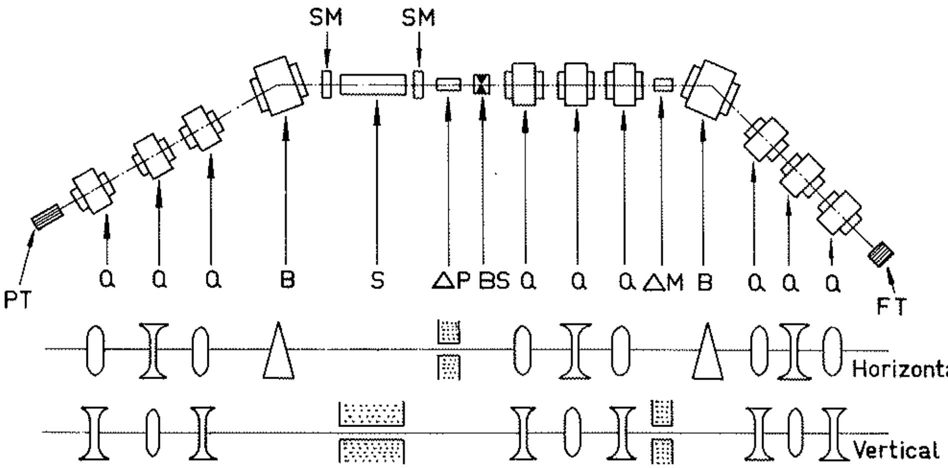

The antiprotons are produced by letting the proton beam of the PS hit an internal tungsten target. The particles around a given momentum (in our case 600 MeV/c) are collected with a $\Delta p/p$ of 1 % into a total acceptance of 8.7 msterad. This beam of particles is focussed and bent into an electrostatic separator. After passing the momentum defining slit (ΔP) the beam is again focussed and passing a mass slit (Δm). Finally, the beam is bent into the experimental area and focussed. However after all this beam manipulation the beam still contains all the long-lived negative particles with the same momentum produced in the production target.

The beam telescope

In order to distinguish between $\bar{p}$ from K^-, π^- and e^- with the same momentum, a beam telescope was constructed, which consisted of four scintillation counters (T_0, T_1, T_2, T_3) and one Čerenkov detector (Č). The lay-out is shown in Figures 6 and 7. Between the counter T_2 and the multi-wire proportional chambers (MWPC) (see Figure 7) there were placed carbon plates (6–7 cm) to degrade the beam in order to obtain the maximum of the stopping distribution at the center of the target.

The counter combination $T_0 - T_1 \bullet T_2$ was used in the time-of-flight mode, and the Čerenkov counter discriminated at $\beta = 0.67$. From this we could define two triggers, one for $\bar{p}$ and one for π^- as follows

$$T(\bar{p}) = (T_0 - (T_1 \bullet T_2))_{time=\bar{p}} \bullet \bar{\check{C}} \bullet T_3^h$$

$$T(\pi^-) = (T_0 - (T_1 \bullet T_2))_{time=\pi^-} \bullet \check{C} \bullet T_3^t$$

(Here $\bar{\check{C}}$ indicates that the Č is in anti-coincidence mode, $\bullet$ coincidence and $-$ (minus) a delayed coincidence. The index h or t refers to the discriminator level which is set high for $\bar{p}$ and at just above noise threshold for π^-). The time separation between $\bar{p}$ and π^- was nominally 21.6 ns. The first trigger was also used as a $\bar{p}$ stop trigger. The separation power is shown in Table 6. The counter T_3 placed just in front of the target defined a beam size which was smaller than the target. In order to keep the annihilation process within a reasonably small region, **liquid** hydrogen (helium) was used which enabled the target to be sufficiently thick to stop $\bar{p}$ within the target after $\approx$ 15 cm. A target container with a cooling system was provided by the CERN target group [49] for each data-taking period. The target used in 1979 could also be used for helium and thus data for the process $\bar{p}He \rightarrow \gamma$ + any other particles (Paper IV) were consequently produced only in the 1979 run. The possibility to tune the beam to both π^- and e^- was also used for calibration purposes.

The $\gamma-$ray calorimeters

For the main part of the experiment, two different NaI(Tℓ)-calorimeters were used. The so-called SECTOR, which was by far superior for $E_\gamma \geq 100$ MeV, was a modular (54 units) detector in a single housing covering 1/13 of 4π. In addition a 12" $\times$ 10" cylindrical mono-crystalline NaI(Tℓ) was used for the construction of π^0 and η energy spectra (Paper V). The π^0 and η spectra so obtained were merelly used for tests for a later experiment at LEAR (see Appendix D) and thus the performance of the 12" NaI(Tℓ)-detector was less important.

Table 6

The beam telescope perfomance.

With a trigger which required only T_0 T_1 and T_2 in coincidance a ratio of ≈ 1 for $\pi^-/$
was obtained. Then by using the beam telescope we can gain the factors given belov
It should be noted that although the trigger is virtually free from unwanted particle
($\pi^-/\bar{p} \approx 10^{-4}$) after this telescope, secondary particles are also produced in the targe

Improvement in the intensity ratio $\pi^-/\bar{p}$	gain factor
T_3^h in coincidence	> 5
also $\check{C}$ in anti-coincidence	> 12
also time requirement on T_0 - ($T_1 \bullet T_2$)	> 175

The SECTOR-detector

The SECTOR-detector was the main component of the experimental set-up and Paper
is devoted to describing its development and performance. It was the prototype of wha
became known as the Crystal Ball at SLAC [50]. The layout is shown in the followin
Figure 8 as well as in addition to several relevant figures in Paper I.

The SECTOR-detector* was built from 54 NaI(Tℓ) modules. All modules were sim
lar in shape but had for geometrical reasons differences in dimension of up to 12 %
Each module was a truncated equilateral triangular pyramid (b $\approx$ 13.5 cm at the wid
base, h $\approx$ 39 cm) of polycrystalline NaI(Tℓ)and was wrapped in white paper and
aluminized mylar for optical separation. Through a hole with a diameter of 50 mm
the outer triangular surface an air light-guide was fitted towards the glass window
the aluminium housing. A photomultiplier tube† was connected to each module by
second air light-guide into which light could also be injected from the light pulser (se
below)**. The multipliers were magnetically shielded by 1 mm of μ-metal and a housin
of $\approx$ 5 mm iron. The specifications†† were tested individually for each module befo
packing into the common housing. All modules met the resolution requirement. Nir
modules did not fully meet the uniformity requirements and were therefore placed
the outer ring of the assembly (No. 25-54 in Figure 9) where less energy was accepted
each event and thus the performance was less critical. Figure 10 shows the performanc
of a typical module.

As mentioned all the 54 individually wrapped modules were closely packed in a seale

* Manufactured by Harshaw Chemical Co., Solon, Ohio, USA.

† The PM's were SRC L50BOI or KTC XP2202B, which are semi-fast, ϕ 50 mm, 1
stage tubes

** These two air light-guides were the main reason for the relatively poor light outpu
of the modules, 7 % of a 2" × 2" cylindrical NaI(Tℓ) placed directly on the tube whic
however, was acceptable for the energy range used.

†† See Paper I for details about the specifications.

Figure 7
Lay-out of the experimental set-up.

A vertical and a horizontal cut through th experiment. The main detector systems are described in detail in following figures.
The symbols are as follows, T=H_2 Target
S=scintillation counters T_0–T_3, M=moderator
(6-7 cm carbon),MW=Multi Wire Proportional Chambers,
Č=Čerenkow detector
and FP= Front plastic (veto scintillation counters)

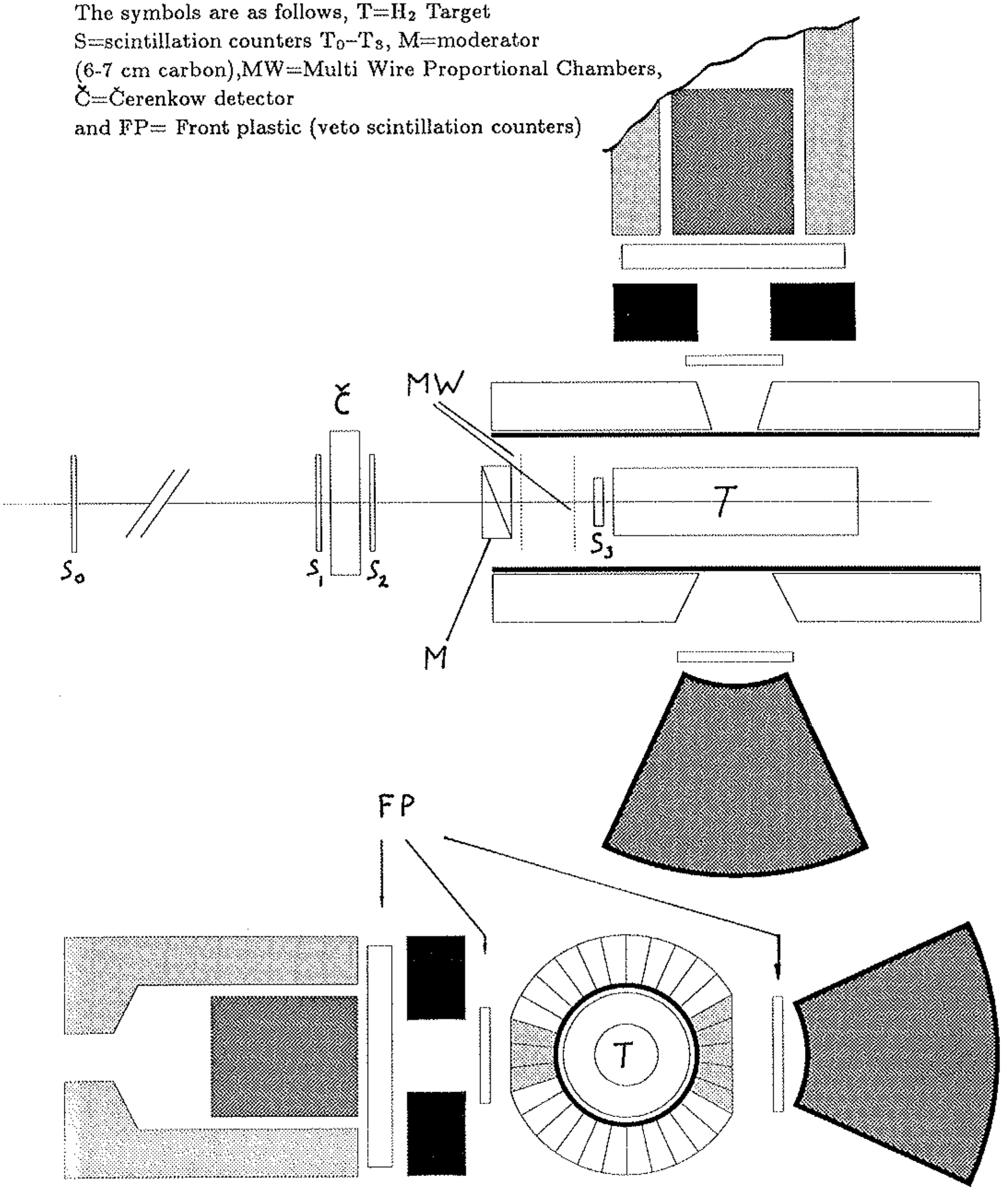

Figure 8
THE SECTOR

Schematic picture of the SECTOR-detector set-up. Only the modules are shown. Technical details and specification can be found in Paper I.

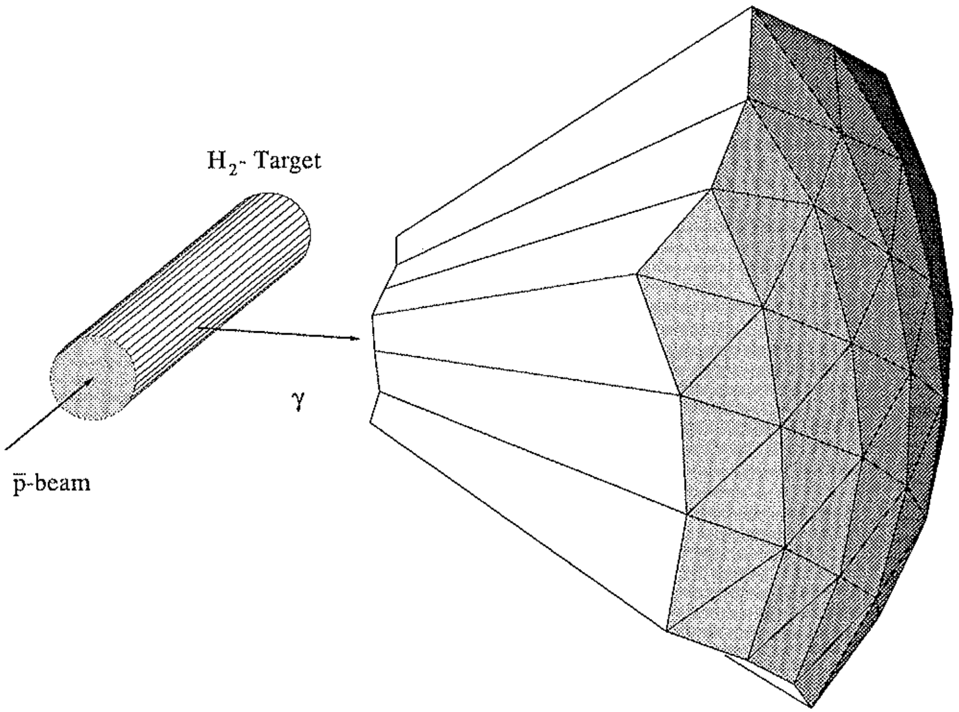

single aluminium housing. The stacking was done so that the arrangement cut out a honeycomb from a hollow sphere with an inner radius of 25 cm and an outer radius of ≈ 64 cm. The honeycomb-shaped projection can also be seen as three rings with 6, 1 and 30 modules in each (see Figure 18 in chapter 4).

To discriminate charged particles from neutrals entering the γ-ray detector there was thick scintillation plastic veto-counter between the target and the detector (see Figu 7). Furthermore, in all places where the mechanics and support allowed it, the part clo to the target was covered by four plastic counters to veto charged particles entering fro other sources than the main interaction region.

All PM's for the SECTOR itself and surrounding plastic counters were fed with hig voltage (HV) from individual channels. Once the calibration was done this HV was ke constant for each data taking-period, and any drift in the calibration was taken care

Figure 9
Projection of the SECTOR. You stand in target and look on the SECTOR.

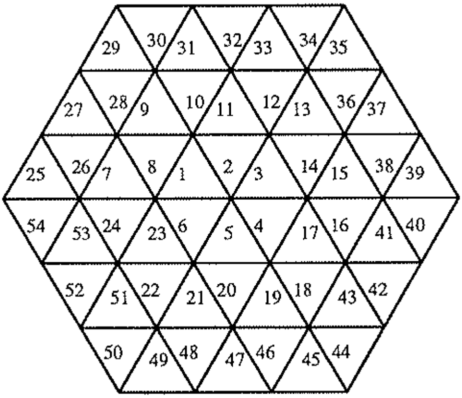

in the off-line analysis (see below).

In the 1979 run a negative HV was used. This had the drawback that irrecoverable gain losses occurred (up to several % in one day). Thus the HV voltage was changed to positive for the 1980 data taking, which however had the drawback of causing non-linear response for high energy inputs. The different PM bases are shown in Figure 11.

Each PM was read out individually in two different lines in order to have both a large dynamic range and still keep a good precision in the low energy range where most modules have some energy deposit due to escapes from the module actually hit. Each line fed an 11 bit ADC (LeCroy 2249 W). The ranges were set to $\approx$ 0–1 GeV for the high channel and 0–100 MeV for the low channel.

The light pulser of the SECTOR

In order to monitor and control the stability of the SECTOR-detector, a light pulser was developed. The construction used is schematically described in Figure 12. The pulser consisted of a light source, a light attenuator, a light diffuser, a distribution system, and a reference module with a radioactive source. The set-up was constructed in a modular way so that the main unit, the light diffuser box with a filter wheel containing six filters, and its remotely controllable electronics also served as a holder for the light source tower and electronics. The reference module (a 2" $\times$ 2" NaI(Tℓ) crystal and a ^{22}Na source) were placed in a lead shield in the same thermally shielded box as the SECTOR itself. The light pulse was produced by a xenon flash tube of the type FX 280*. This pulse was shaped so that it resembled the pulse from the NaI(Tℓ) modules. The intensity

* Manufactured by EGG Electro Optics Division, Salem, Mass., USA.

Figure 10
Performance of one typical (bad) module

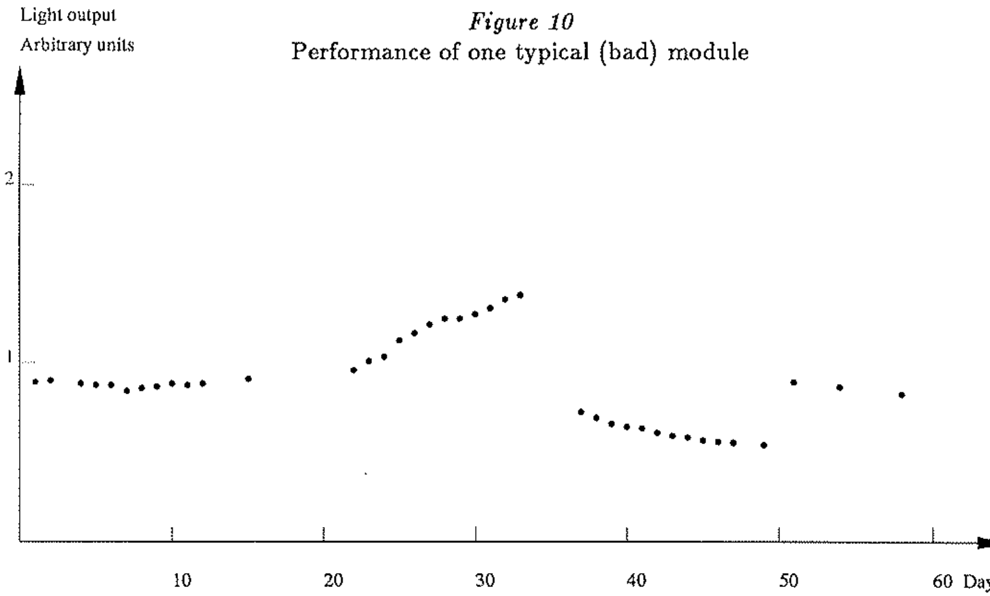

Relative light output about 8 o'clock in the morning for module 30 illustrating the difficulties with gain stability using a negative PM high-voltage.

could be adjusted continuously so that the light output after filter attenuation covere a range corresponding to 20-1000 MeV. But, once set, it was kept constant during th run.

After attenuation the light was diffused in the diffusion box. Then it was distribute by 56 fiber light guides* each one of them with a diameter of 1 mm and a length 2 m. 54 of these fibers were connected went to their respective modules via a small ho in the second air light guide, one fiber was led to the reference crystal, and finally or fiber led to a special PM serving as a light pulser trigger. The possibility to check th LP against the 1.27 MeV line of ^{22}Na showed that running the LP continuously with Hz deteriorated the light output from the flash bulb by ≈ 1 % per week. A resolutio of 2-4 % was obtained for selected flash bulbs. The LP was also used to check th linearity of the electronics and read-out system of the modules up to an energy rang corresponding to 1 GeV.

12" NaI(Tℓ)

The second calorimeter was the same detector as the one used by the collaboration an earlier experiment [18] on $\bar{p}p \rightarrow \gamma +$ anything. In our work, however, it was on used for the coincidence analysis where the performance was less critical.

* Manufactured by Fiberoptik-Heim AG, CH 8707 Uetikon am See, Zurich, Switze land.

Figure 11

Analog electronic schemes used for the SECTOR-detector bases in a) 1979 and b) 1980.

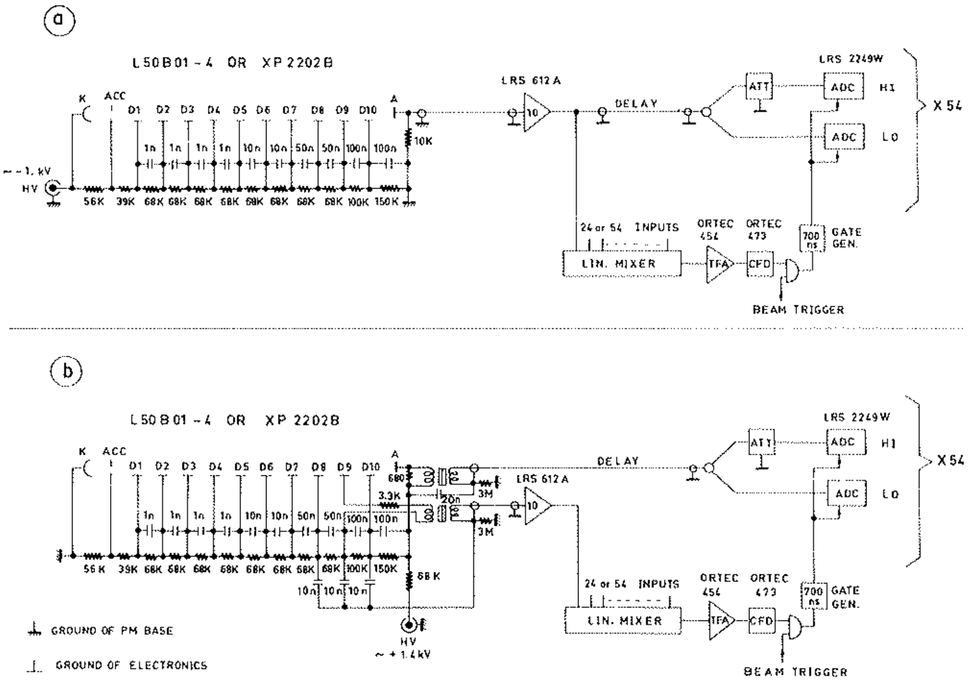

The cylindrical detector is described in reference [51] and in Figure 13. The NaI(Tℓ)-crystal (12" $\times\, \phi$ 10" cylindrical) was surrounded by thick scintillation counters to enable electronic collimation. The γ-rays were further collimated by a lead collimator (ϕ_{inner} 12 cm $\times$ 12 cm deep). In front of the crystal there was one thick and one thinner scintillation veto counter to discriminate between charged particles and γ-rays entering the detector. The collimation had to be weak in order to maintain a large solid angle for the coincidence experiment.

Multiplicity counters

With the aim of reducing the background and identifying the decay of a possible exotic state, a set of multiplicity counters covering a solid angle of about 80% was constructed. This set of detectors are in the text below named the TONNE (inner, outer) from the German word for barrel. However in the quantitative analysis the requirement of identifying the final state of a decay channel reduced the statistics too much because of the pooroverall efficiency, and thus the information from the TONNE detectors was not of much use in the final analysis. The detectors are shown in Figures 14 and 15.

Figure 12
The lightpulser of the SECTOR (from paper I)

The light pulser(schematic). Not shown are the motor and the encoder for the diaphragm, an
an additional retractable filter betwen the diaphram and the filter wheel.

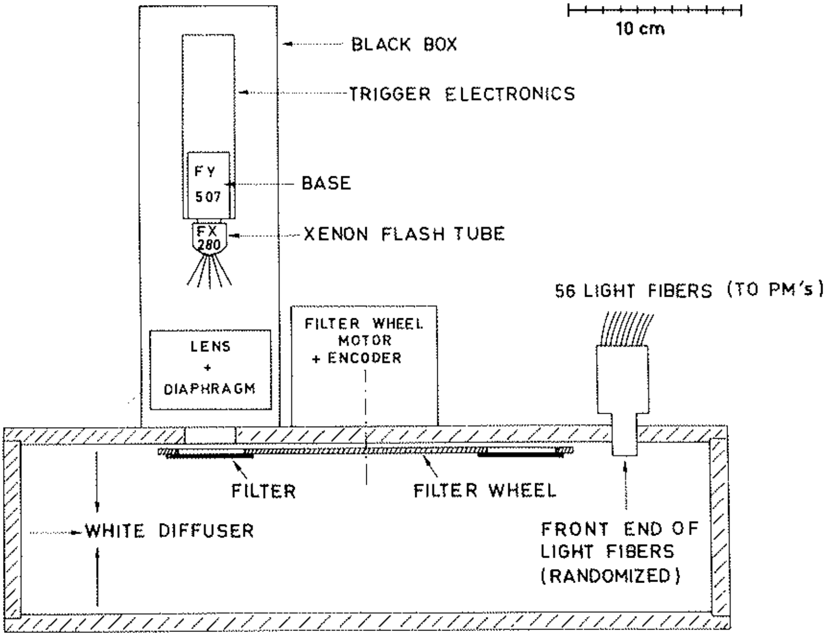

The inner TONNE-detector was constructed to measure the charged particle multiplici and consisted of 30 scintillator strips, each one 1 m long and 1 cm thick, arranged in cylindrical shape with a diameter of 30 cm. They were kept in position from the outsi by an aluminium cylinder. From the inside they were supported by the slightly wedg shape of the slabs and by a black paper cylinder, which also served as protection f an aluminized mylar wrapping applied for the optical separation of each module. Ea detector strip was coupled individually to a photomultiplier (PM). The signals we amplified and the threshold was set for optimizing the efficiency of minimum ionizi particles. The signals from all 30 strips were read out by two 16 bit pattern units CAMAC.

The outer TONNE-detector was constructed to measure the photon multiplicity, an was located outside the inner TONNE on a 0.7 cm thick iron cylinder. It was made 60 identical modules, each one 0.5 m long and having an angular width of 12 degree

Figure 13
The 12" NaI(Tℓ)-detector

A cut through the cylindrical 12" by 10" NaI(Tℓ)detector. The crystal volume X is surrounded by thick plastic scintillator (MP). In front of the detector there is two front plastic (FP) charge veto detectors and a lead collimator (Pb).

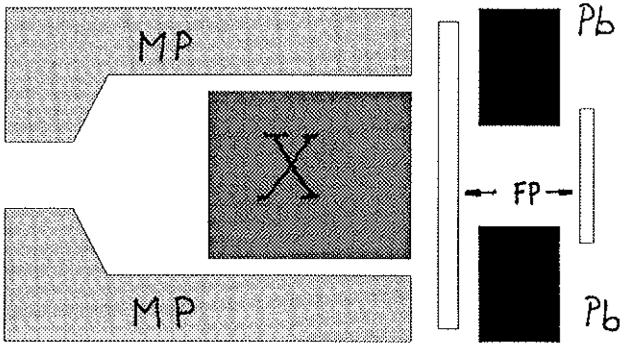

Figure 14
A cut through the TONNE multiplicity counter

The inner TONNE consists of 30 plastic (IP) scintillator strips inside and an aluminum and iron cylinder (B). The outer TONNE consists of lead (Pb) plastic (Sc) scintillator sandwich with tungsten (W) walls.

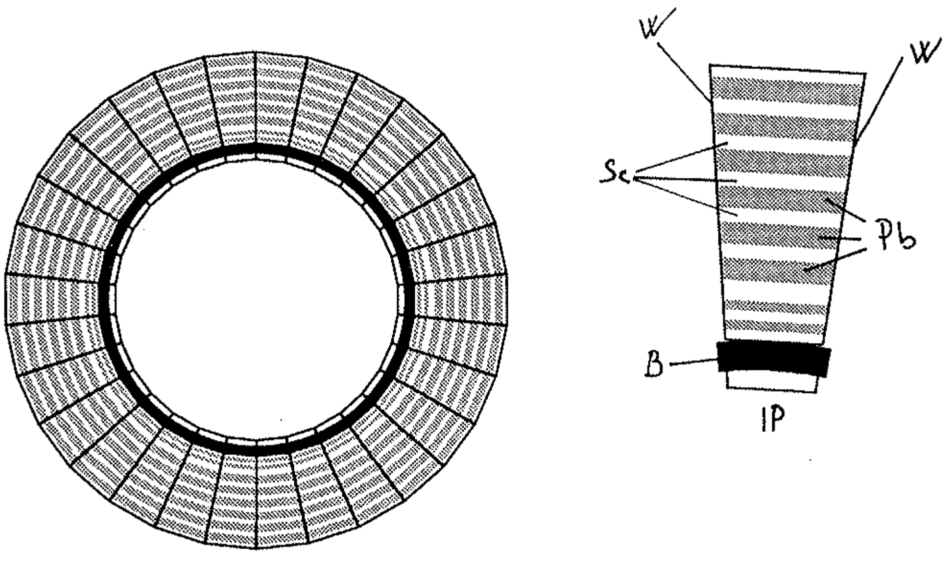

Figure 15
Schematic picture of the TONNE multiplicity counter

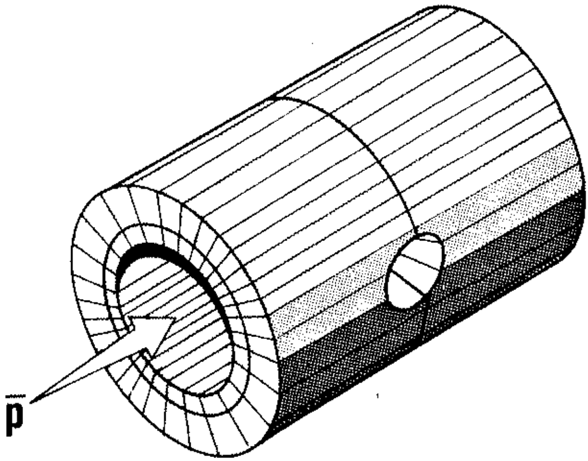

The modules were sandwiches of lead and scintillator plastic (see Figure 15 for details
Each module was connected to a PM via a light guide and read out individually via a b
pattern unit in CAMAC. The thresholds were adjusted so that an isotropic count rat
was obtained when a small carbon target was irradiated in the center of the TONNI
Two holes were cut out in the 2×3 central modules on each side of the cylinder in orde
to avoid any interaction with matter before the γ-rays reached the NaI(Tℓ)-detecto
(Figure 14 and 7).

CHAPTER 3

CALIBRATION, DATA-TAKING, MONITORING

"Tant de bruit pour une omelette au lard."

JACQUES VALLÉ DES BARREAUX

"Much Ado About Nothing."

WILLIAM SHAKESPEARE

Before data could be taken the equipment had to be tested and calibrated. The requirement for the inter-calibration of the modules was that the energy calibration for any module should not vary by more than ≈ 10 % from its nominal value. Once this calibration was established it had to be monitored. However it was not corrected on-line. Instead any variation during data-taking was corrected off-line in conjunction with the final calibration (see next chapter). Furthermore, all equipment had to be monitored during the run so that any temporary malfunction of the equipment could be corrected for.

Calibration

Before the run there were three possibilities for calibration, a source calibration up to a few MeV, the use of an electron beam or the 129.4 MeV γ-rays produced from the reaction $\pi^- p \rightarrow n + \gamma$. None of these methods could however be used during data-taking without interrupting it, but a source calibration record was made every morning. Finally, off-line after the run the upper edge of the γ-spectrum ($E_{max} = m_p$) and the energy of γ-rays originating from the reaction

$$\bar{p}p \rightarrow \pi^0 + \omega \text{ or } \rho^0$$
$$\searrow \gamma\gamma$$

could be used for calibration. For the 12" NaI($T\ell$) crystal the calibration was somewhat easier since it consisted of one big module and hence no inter-calibration had to be done. Furthermore, minimum ionizing particles due to high energy cosmic rays could be used to check the stability of the 12" NaI($T\ell$)system in contrast to the more complicated SECTOR case. This cosmic ray calibration could be performed simultaneously with interuptions done for the source-calibration of the SECTOR. The 2.38 MeV Compton edge of ^{228}Th was used for inter-calibration and absolute calibration of the SECTOR modules at low energies. The high voltage of the PM's was adjusted so that all modules had the same gain after feeding the signal through the same amplifier. The sam procedure without any adjustment of the high voltage was also applied once early eve morning to check the stability. This procedure was performed also inbetween bea periods to keep record of the stability of the equipment. For the 12" NaI(Tℓ)detect we used ^{228}Th (E_γ=2.62 MeV) for calibration at low energies.

Before the final set-up the beam was tuned for electrons in order to check the energ calibration and the linearity by putting the detector in the target position. This chec was limited by the precision in momentum to which the beam could be tuned ($\approx$ 2 % In the 1979 run the non-linearities were negligible (from calibration points in the $\bar{p}$ data and from the light pulser (LP) data) and no correction was neccesery. In th 1980 set-up a few modules became non-linear above 400 MeV. This deviation was sti reflected in the resolution at high energies after correction. The response of the 12 NaI(Tℓ)detector was well-known from earlier experiments [18], and the detector wa therefore not calibrated in the electron beam in this experiment.

The calibration described above was not sufficient for the experiment, where the energ of the γ-ray was distributed in several modules. Thus the calibration was important i the energy range where the shower properties are dominant. At an energy $\approx$ 100 Me three calibration points can be obtained by tuning the beam for π^- (see Figure 18 i chapter 4). These were:

$\pi^- p \to n\gamma$	$E_\gamma = 129.4$	[MeV]
$\pi^- p \to n\pi^0$	$E_{\gamma_{min}} = 54.9$	[MeV]
	$E_{\gamma_{max}} = 83.0$	[MeV]

The beam was thus tuned to stopping π^- before and after each $\bar{p}p$ data-taking perio and the $\pi^- p$ data were stored on magnetic tape and used in the final calibration, whic was done off-line after each run period. The data were also used for calibration for th on-line data-taking monitoring program.

<u>Stabilization</u>

Once the calibration was established it had to be stable over a long period of tin however with no possibility to control it in a direct way. In order to maintain th calibration, data were taken with the light-pulser source described above approximate once every 4 hours for a few minutes and stored on magnetic tape. A survey of the data and a comparison with the source data showed that the accuracy was much bett for the LP data, and thus the source data were only used for a consistency control.

This scan of the data from the light pulser showed very different features for the differe run periods of 1979 and 1980. As a consequence, the high voltage supply of the phot multipliers was changed between the runs. The modification thus made proved to l satisfactory and the 1980 LP data did not vary by more than $\pm$1.2% for any modu except for short periods which were anyhow disregarded in the data analysis for oth reasons. Therefore it was decided after tests that no off-line correction were needed f the 1980 data and therfore the following procedure was only applied to the 1979 dat

The off-line calibration was done after the full run period so that all the information about the performance of the modules was known in advance. Therefore, after comparing the LP-data and the source data the decision was taken not to further correct the 1980 data. After establishing a reference value, the LP data were fitted for each time interval with a second degree polynomial. This procedure gave an individual time-dependent expression for each module. The coefficients thus obtained were then introduced into the off-line analysis program "SECTOR".

Once it was known that the light-pulser data and the source data gave consistent results we could use the LP results alone since they were more accurate and more frequent.

Finally, the light-pulser itself had to be stabilized in order to avoid additional errors from instabilities in the light bulb or gain shifts in the PM's and amplifiers. Thus a time-dependent coefficient for the reference value A_{ref}, defined as $A_{ref} = P_{Source}(0) / P_{Source}(t)$ where $P_{Source}(t)$ is the peak position at time t was applied to the data.

Data – taking system

The data-taking, the control of the experiment and the monitoring were all done with a PDP 11/34* computer. For interfacing between the computer and the electronics a standard CAMAC interface was used.

The fast trigger T was built from standard NIM units (see Figure 16). The master trigger was defined as

$$M = T(\bar{p}_{stop}) \bullet s_\gamma$$

where s_γ denotes that the inner 24 modules contained more than 10 MeV equivalent energy and no veto plastic scintilator was fired. This trigger opened a gate (700 ns) for the all ADC's of the "Sector". After conversion the data were read into a buffer in the computer, together with the other relevant information. In order to take data for tests and calibration (e.g. LP-data), the computer could change the trigger by means of output registers in a well defined way. Only in the case of π^- data the trigger had to be changed manually.

The data-taking program used was meanwhile developed by the CERN DD/OC group to be CERN's standard data-taking program for PDP's. As this program was not final at the set-up of the experiment a considerable time was invested in testing the program to secure data integrity.

* PDP 11/34 is a trademark of Digital equipment corporation

Figure 16
The fast trigger

The main trigger and the different test triggers are all built together. The open ends ar constant levels used by the computer to control the experiment. The symbols are T = Timin filter amplifier, C = Constant fraction amplifier and FP = Front plastic (the charge vet counters).

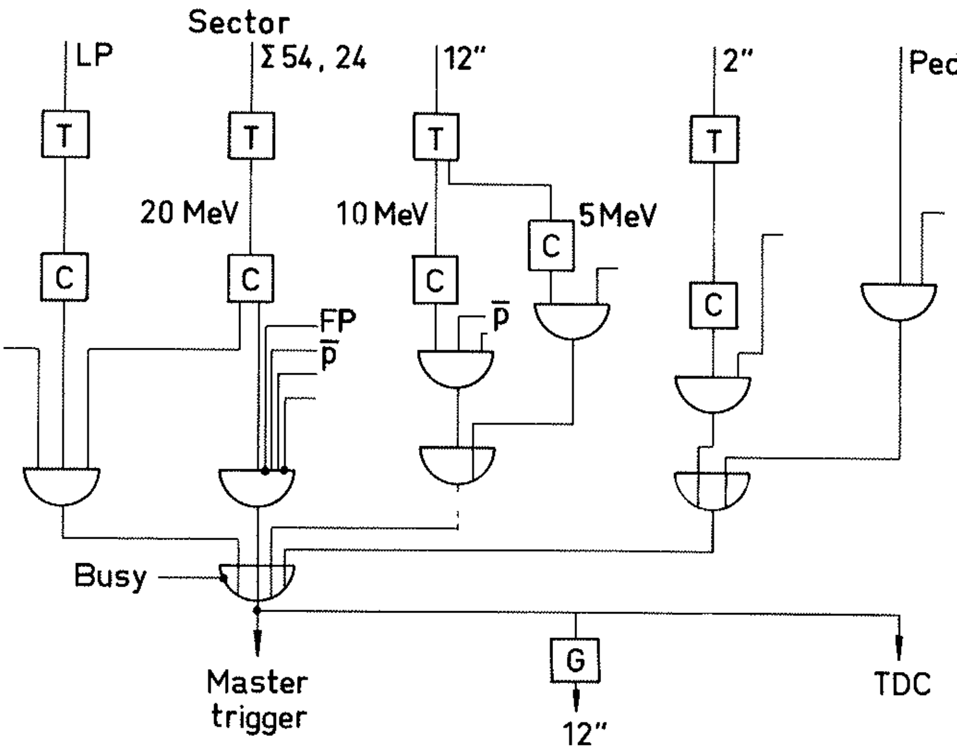

CHAPTER 4
ANALYSIS

'"What are *you* doing?"
"Hunting," said Pooh.
"Hunting what?"
"Tracking something," said Winnie-the-Pooh very mysteriously.
"Tracking what?" said Piglet, coming closer.
"That's just what I ask myself. I ask myself, What?" '

A. A. MILNE, *Winnie-the-Pooh*

The object of the analysis was the inclusive γ-spectra from $\bar{p}p$ and $\bar{p}He$ annihilation at rest. If the annihilation at rest results in two particles they both have well defined energies depending on their masses only. On the other, when hand an annihilation at rest results in three or more particles, it gives rise to a continuous energy distribution. Thus, when one particle is produced together with a single γ-ray the recoil of the particle is visible in the γ-spectrum as a monoenergetic peak. Also, if one particle is produced together with a π^0 this can be seen in the γ-spectrum, since the γ-rays from a monoenergetic π^0 decay in motion will be distributed as a "box" in the laboratory frame. Details about the relevant kinematics for two-body annihilation are given in Appendix A.

The analysis consists of three parts.

1) Analysis of the singles γ-ray inclusive spectra from $\bar{p}p$ annihilation at rest, where we were interested in:

   monoenergetic γ-rays with 90 MeV $< E_\gamma <$ 938 MeV

   monoenergetic π^0 revealing themselves as box edges with $E_{\gamma_{max}} <$ 933 MeV where beacause of statistical reasons only the high energy box edge ($E_{\gamma_{max}}$) can be observed.

2) Analysis of the singles γ inclusive spectra from $\bar{p}He$ annihilation at rest. This analysis is different from the search for monoenergetic γ-rays in $\bar{p}p$ data. Here we studied in particular the region 50 $< E_\gamma <$ 500 MeV because of the presence of neutrons and Fermi motion of the nucleons.

3) Analysis of the coincidence spectra between the two detectors, the SECTOR and the 12" NaI(Tℓ). Where we studied the π^0 and η spectra at low momenta. This in-

vestigation should be considered mainly as a pilot experiment for future experiment at LEAR.

Items 1,2,3 are commented more in detail in the following subchapters.

Singles γ-ray inclusive spectrum analysis

In the singles γ-spectrum we searched the data for any structures corresponding to $\bar{p}p \rightarrow \gamma + X$ where 90 MeV $< E_\gamma <$ 550 MeV. For the region $E_\gamma >$ 550 MeV the analysis was restricted to the data from 1979 because of the worse resolution at high energy in the 1980 data. For the same reason the search for structures corresponding to $\bar{p}p \rightarrow \pi^0 + X$ (which is visible at higher energies only) was limited to the 1979 data sample.

The analyses of the processes $\bar{p}p \rightarrow \gamma + X$ and $\bar{p}p \rightarrow \pi^0 + X$ described below require an estimate of the shape of the inclusive γ-spectrum. As the detector is modular and the shower properties are such that the energy is distributed in several modules the γ-spectrum had to be constructed off-line after the data-taking was finished. This estimate and the construction of the resulting from background processes were common for both analyses and consisted of the following steps.

1) Off-line reconstruction of the energy spectrum including final calibration and stabilization.

2) Monte-Carlo (MC) simulation of the background originating both from known two and multi-body final states.

3) Parametrization of this background.

The analysis of the singles γ-spectrum is described below in two parts ($\bar{p}p \rightarrow \gamma + X$ where X is unknown and $\bar{p}p \rightarrow \pi^0 + X'$ where X' is a known meson).

Off-line reconstruction of the inclusive singles γ-spectrum

The modular structure of the SECTOR and the nature of shower production distribute the energy from one γ into several modules. Thus, the energy deposited in different modules had to be added up. To do that in a consistent and correct way we had to intercalibrate the modules absolutely and keep track of any drift during data-taking. Furthermore, we had to veto any charged particles and assure that one and only one γ is measured. This was done with the veto plastic scintillators and some topological cuts in the algorithm used for adding the individual energy information from each module.

The first step in the off-line analysis was to establish the absolute intercalibration. This was done with data from the reactions

$$(\pi^- p)_{rest} \rightarrow n\gamma \qquad \text{and} \qquad (\pi^- p)_{rest} \rightarrow n\pi^0 \rightarrow n\gamma\gamma$$

taken before each run period as described above.

We found a calibration factor a_ν for each module (ν) in the following iterative way. Starting with the rough source calibration by setting $a_\nu^{(1)} = 1$ we calculated the peak position c_ν for each module whenever that module contained more than 60 % of the total energy. Now a new calibration factor $a_\nu^{(2)}$ could be calculated as

$$a_\nu^{(2)} = 1 + \left(\frac{\bar{c} - c_\nu}{c_\nu}\right)$$

where $\bar{c}$ denotes the average peak position. The process converged satisfactorily after three iterations. This procedure worked well for the inner 24 modules but for the other 30 a small correction had to be applied to correct for energy escapes. This correction was estimated with a Monte Carlo simulation using the program EGS [53]. The result of this intercalibration can be seen in Figure 17a, where we in this way obtained an FWHM of 5.5 % as compared to 12 % from the rough source intercalibration. The energy scale was determined from the peak position 129.4 MeV for $\pi^- p \to n\gamma$ and the two box edges (54.9 and 83.0 MeV) from $\pi^- p \to n\pi^0 \to n\gamma\gamma$ corrected for the detector resolution. In the final fitting procedure we could also check the calibration at 774 MeV and 938 MeV (see below).

Figure 17

Result of intercalibration (from paper I)

The spectra from the reaction $\pi^- p$ *to* $n\pi^0$and $\pi^- p \to n\gamma$ [(a) as obtained from the calibration run, (b) 2 month later]. Open dots (O) in (a) show the 129.4 Mev peak as obtained from the source calibration alone. Open dots (O) in (b) show the 129.4 MeV peak as obtained without light-pulser correction.

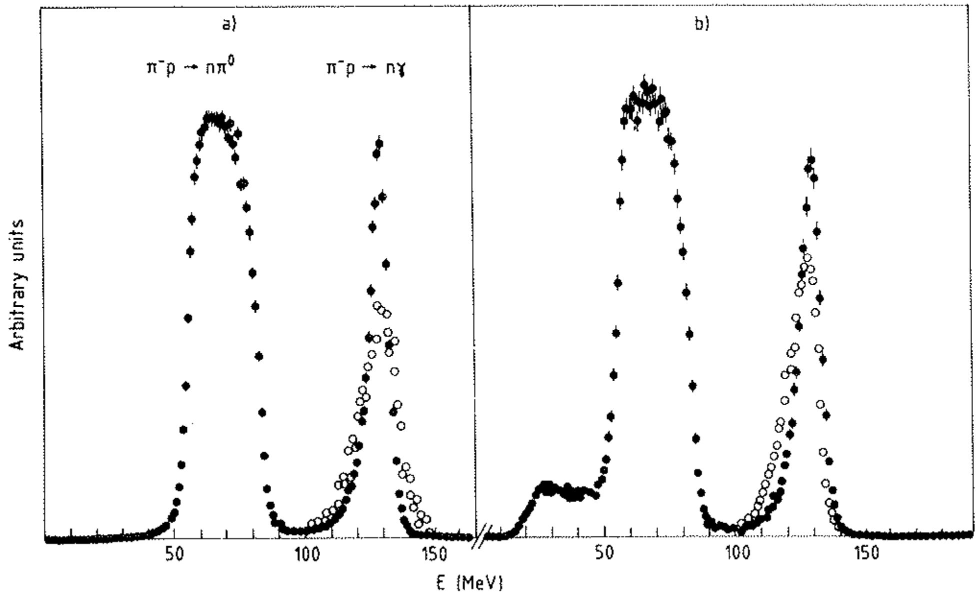

To maintain this calibration during the whole data-taking period we used the data taken with the light-pulser described above. Tests showed that the modules were stable over the data-taking period in 1980, but corrections had to be made for the 1979 data. As we stored the real time for each event on tape we prefered to have a continuous time-dependent correction in order not to introduce any discrete effects in the energy spectra. Thus, we constructed a time-dependent reference value

$$A_{ref}(t) = \frac{P_{LP}^{ref}(0) \cdot P_{Source}(t)}{P_{LP}^{ref}(t) \cdot P_{Source}(0)}$$

where P_{LP}^{ref} is the peak position of the light pulser signal for the reference and P_{Source} is the source peak position for the reference. From this reference value the final time dependent calibration factors a_ν were obtained for each module as

$$a_\nu = \frac{P_{LP}^{\nu}(0)}{A_{ref} P_{LP}^{\nu}(t)}.$$

The result of this stabilization can be seen in Figure 17b where an improvement of almost 50 % for a two month period is displayed. For stabilization "switched on" we got a FWHM of ≈ 7% for a period of two months, as compared to ≈ 11% without stabilization. The resulotion 7% should be compared with the value of ≈ 5.5% obtained as best value at the start of the period.

Before the final adding of the energy output from the modules there were some cuts applied in order to avoid the counting of double hits and to obtain a good resolution for showers. Thus, one of the inner 24 modules, the trigger module, had to contain at least 40% of the total energy registered in each event. Further, the trigger module plus its twelve closest neighbours had to contain 90 [1 - exp (-E (MeV) /58)] % of all energy deposited except for the lowest total energies. Only the trigger module plus the two neighbouring rings were added to avoid noise from modules into which no part of the showers could enter (Figure 18). No event with the plastic veto counter firing was taken into account.

Using this process of adding several modules which were individually stabilized off-line we got a reconstruction of the inclusive γ-spectra which above 70 MeV was energy independent, giving a resolution of $3.3\ \%/\sqrt[4]{E(GeV)}$. This result could be kept almost stable for several weeks.

Tonne analysis

The Tonne-detector was the result of an attempt to construct a simple and fairly cheap facility to measure the charged and neutral multiplicity related to the $\bar{p}p$ annihilation in a relatively large solid angle. It showed several drawbacks, e. g. (i) charged particles might give a signal also in the neutral photon detector, (ii) photon showers might spread into two or three adjacent detectors, (iii) there was no coincidence requirement for the charged particle detector which lead to noise and efficiency problems, (iv) geometrical overlap made it possible for charged particles from certain annihilation positions in the target to fire two charged particle detectors, (v) the detector did not cover the full solid angle.

Figure 18
How the modules are added up.

We see two rings of "12" and "24" modules around the module hit, i.e. the one with most energy deposited in it. These rings are added up separately and compared with each other and the total energy. The distribution has to be reasonable in order to accept the event. In the right case some of the inner 24 modules come outside the physical detector.

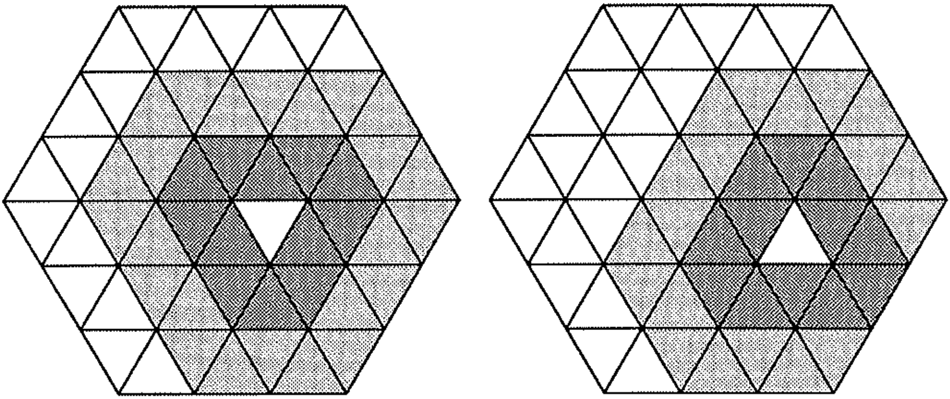

All these drawbacks made it difficult to uniquely determine the charged and/or neutral particle multiplicity of a given event. Furthermore, some effects were so difficult to control that a reliable Monte Carlo simulation could not be made. The conclusion is that unfortenately we were not able to use this detector for any quantitative analysis. As an example the full linear spectrum is compared with the best approximation of two charged particles as a recoil to the detected γ-ray in Figure 19, which shows how the ρ/ω "box" becomes visible for the unguided eye. However, the fit quality and normalization are better for the original spectrum due to the Tonne detector limitations discussed above.

Monte-Carlo simulation of annihilation channels

A Monte-Carlo simulation of the γ-ray spectra expected from the annihilation channels as known from bubble-chamber experiments (Table 1) was performed in two steps both dealing only with phase-space and containing no apparatus effects.

The many-body channels marked MC in Paper II, Table 2 were simulated by the CERN standard routines for many-body decays. They were then added in the correct proportions. As the purely neutral channels were poorly known it was in this step assumed that these channels — as well as other ones containing strange particles — did not change the spectral shape in any significant way This assumption is correct in a first approximation beacause of the weak intensity of these channels.

The γ-spectra from a two-body channel of the type π^0 or η + one other particle ($\pi^0, \eta, \rho^0, \eta', \omega, \gamma$,...) can be described analytically as a monoenergetic π^0 or η decaying into two γ-rays, giving a box-like distribution in the laboratory system (see Appendix A). The spectral intensity of such a channel ν is given by the expression:

$$B_\nu(E_\gamma) = B_{\bar{p}p\to ab} = \frac{\Gamma_{a\to\gamma's}}{\Gamma_a^{tot}} B^a(E_\gamma) + \frac{\Gamma_{b\to\gamma's}}{\Gamma_b^{tot}} B^b(E_\gamma)$$

and where $B^{a,b}(E_\gamma)$ is defined by the function:

$$B^{a,b}(E_\gamma) = \frac{N_\gamma^{a,b}}{E_{max}^{a,b} - E_{min}^{a,b}} \qquad \text{for} \quad E_{min}^{a,b} \leq E_\gamma < E_{max}^{a,b}$$

where $N_\gamma^{a,b}$ is the number of monoenergetic γ-rays into which the particles a or b decay at rest.

Parametrization of the many-body final state background

The simulated spectrum from the known many-body final states was fitted with the following purely phenomenological shape function:

$$f(E_\gamma) = N\left[(E_0 - E_\gamma)^{\alpha_1} \cdot e^{\beta_1} + (E_0 - E_\gamma)^{\alpha_2} \cdot e^{\beta_2} + \beta_3 \cdot e^{\alpha_3 E_\gamma}\right]$$

where $E_0 = 938.28$ (MeV) and N is a normalization constant (the average number of γ-rays per annihilation). The other six parameters were fit parameters and were kept fixed after this fit. The fit gave a χ^2/df of 1.33 with the following values of the fit parameters: $\alpha_1 = 4.1548$, $\alpha_2 = 1.6732$, $\alpha_3 = -0.0327$ (MeV^{-1}), $\beta_1 = -33.4948$, $\beta_2 = -19.9818$, $\beta_3 = -0.006921$. The average number of γ-rays from $\bar{p}p$ annihilation, N, is a sum of several N_i (one from each channel). With $N_i = R_i N_{\gamma_i}$, where R_i is the branching ratio to channel i and N_{γ_i} the average number of γ-rays from this channel, and using our final results giving 0.11 γ-rays per annihilation from two-body annihilation we get $N = N_\gamma - 0.11 = 3.82$ (± 0.24), where N_γ is the average total number of γ-rays as found from Paper II, Table 2 (or calculated from Table 1 in this thesis).

The total γ-spectrum from the $\bar{p}p$ annihilation at rest was then assumed to be a superposition of the many-body final state MC-spectra and the two-body final state (analytical) box-shaped spectra. Thus, the final spectra to be compared with the measured spectra had the form

$$F(E_\gamma) = A_0[f(E_\gamma) + \Sigma_\nu R_\nu B_\nu(E_\gamma)]$$

where A_0 represents the total number of annihilations contributing to the measured spectrum when the intergral a

---

Figure 19
Result from multiplicity counting

The spectra shows the raw spectra and our best approximation of two charged particles and no neutral particles in the TONNE. One can see the upper "box" edges from the annihilation channels: $\bar{p}p \rightarrow \pi^0 + \rho/\omega$, since ρ (and ω) decays into low multiplicity channels.

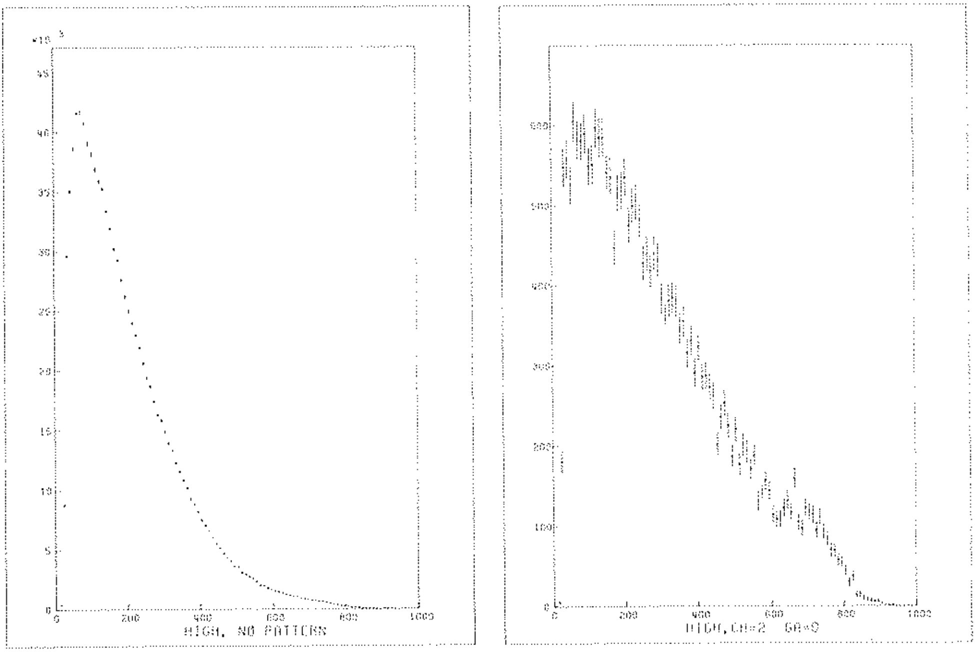

$$\int_0^\infty \frac{F(E_\gamma)}{A_0} dE$$

was normalized to be the average number of γ-rays per annihilation N_γ. The value of A_0 was determined by fitting $F(E_\gamma)$, after folding with the experimental energy resolution, to the measured spectrum in the range from 400 to 600 MeV. The number 0.11 for two-body annihilation was the second free parameter determined at this moment. The accuracy of this determination of A_0 was $\pm 5\%$ and independent of errors in solid angle, stop rate and other experimental parameters.

Analysis of two – body final states at higher energy

After fitting $A^{box}(E_\gamma) = A_0 \sum_\nu R_\nu B_\nu(E_\gamma)$, folded with the resolution of the apparatus, to the measured spectrum minus the many-body background $f(E_\gamma)$, the only remaining free parameters were the searched branching ratios R_ν. Unfortunately, all R_ν are not independent. Particularly the η meson channels are strongly correlated with π^0 for the same recoil meson. The $\pi^0\rho^0$ channel interfered with the resolution and was thus not treated independently. Variation of the parameter α_2 showed a correlation with $\pi^0\omega$ and $\pi^0\eta$ yields but no other channel, but the parameter was still kept fixed as derived from the Monte-Carlo calculations.

The channel $\pi^0\rho^0$ was well known from bubble chamber experiments. Thus, during the final analysis we kept it fixed, but for tests we also varied it in steps for different detector resolutions. The value $R(\bar{p}p \rightarrow \pi^0\rho^0) = 1.6$ % adopted to the final fits is higher but compatible with the values listed in Table 1 and favoured by the present data. We also kept the favoured value for the resolution $5\%/\sqrt[4]{E(GeV)}$ fixed for the final fits.

It was impossible to resolve the channels (η + meson) and (π^0 + meson). Instead we used a fixed ratio η/π^0 of 0.16, taken from bubble chamber data (Table 1). In order to estimate systematic errors the η/π^0 ratio was also varied in steps between the limits $0 \leq \eta/\pi^0 \leq 0.33$.

Also the $\pi^0\pi^0$ channel was kept fixed with a branching ratio of 0.4 %, a value favoured by our error analysis (see below) and one earlier measurement [6] but in contradiction to another one [5].

The fitting was then done similarly for the channels $\pi^0\eta'$, $\pi^0\omega$, $\pi^0\eta$, and $\pi^0\gamma$.

Errors

In order to get a good fit we had to introduce one more parameter which we treated as a hypothetical process $\bar{p}p \rightarrow \pi^0 X$ or γX where m_X correspond to ≈ 680 MeV. For the fitting procedure this two processes worked equivalently well but if they were real physical processes, $\bar{p}p \rightarrow \pi^0 X$ would have been strongly favoured. The statistical errors were obtained from a MINOS [54] error analysis. To estimate systematic errors we used the maximum and minimum values for each branching ratio obtained under different conditions for the following "fix" parameters; the $\pi^0\pi^0$ branching ratio, the $\pi^0\rho^0$ branching ratio, the η/π^0 ratio, the detector resolution and the constant α_2.

The results summarized in Table 7 were obtained in an all-parameters-free fit but with the above-mentioned restrictions on the channels $\bar{p}p \rightarrow \pi^0\pi^0$, $\pi^0\rho^0$ and the η/π^0 ratio. To obtain a reasonable χ^2/df we had to introduce a **correction** which however also could be an unknown particle with a rest mass ≈ 680 MeV.

Analysis of the two – body final states at lower energy

For the region below 400 MeV a small background remained after subtracting the MC distribution which was probably due to the absence of purely neutral and strange channels in this background distribution. After subtracting a smooth function (a third degree polynomial) the remaining structures were fitted with all parameters free except for the width which was limited downwards by the detector resolution. The structures then found were only considered as candidates of the process $\bar{p}p \rightarrow \gamma + X$ rather than $\bar{p}p \rightarrow \pi^0 + X$, although some unsuccessful attempts were made to fit a box edge instead of a line shape.

The results should be compared with the data obtained in a previous experiment [18] made by a Basle-Karlsruhe-Stockholm collaboration (see Paper III, Table 1 and Figure 1). We found similar structures but the yields were systematically lower in the new experiments. Further, we found new structures with a similar significance. These new results do not contradict the old data since the statistics in the former case were much lower and the efficiency not energy-independent. Although no single experiment confirmed structures with a high significance the significance of the combined experiments is quite high since the experiments should be considered as independent.

As a conclusion we confirmed two narrow structures at energies 1694 and 1638 MeV also found in an earlier experiment but then with a higher yield. We also measured the branching ratios for the annihilation channels $\bar{p}p \rightarrow \pi^0\omega$, $\pi^0\eta$, $\pi^0\pi^0$, $\pi^0\gamma$ and an upper limit for $\bar{p}p \rightarrow \pi^0\eta'$ in an analysis of "box edges".

Analysis of $\bar{p}$He $\rightarrow \gamma$ + anything

Having indications for several narrow states from $\bar{p}p$ annihilation at rest, the most natural continuation was to study the $\bar{p}$ annihilation on nuclei. Hence, we studied the reaction $(\bar{p}^4\text{He})_{rest} \rightarrow \gamma + X +$ nucleons by measuring the γ spectrum in the same fashion as we studied the $\bar{p}p$ annihilation.

In 1979 we stopped about one fifth of the available antiprotons in ^{4}He. We treated these data in exactly the same way as the $\bar{p}p$ data described above and after calibration and stabilization we obtained the raw spectra in Paper II, Figure 1 (and figure 19). A comparison with $\bar{p}p$ data shows a similar shape but the energy range is extended to 1150 MeV. Furthermore, the spectra has a monotonic increase towards the lowest energies. Finally, one can see that the "ρ^0, ω box" is less pronounced.

The very similar shapes of the raw γ spectra from $\bar{p}p$ and $\bar{p}$He suggest that the annihilation mechanisms are closely related. In order to relate the spectra quantitatively we adopted the working hypothesis that the antiproton annihilates on one single nucleon.

The main differences between $\bar{p}$ annihilation on p and ^{4}He is that the antiproton can annihilate on both protons and neutrons and that the neutron are not at rest, but perform a Fermi motion. The implications of the possible annihilation on neutrons will be discussed later.

To estimate the number of γ-rays per $\bar{p}$He annihilation we assume that the multipionic final state branching ratios are the same for $\bar{p}p$ and $\bar{p}n$ annihilations. Then charge conservation implies that the number of γ-rays per annihilation is the same for $\bar{p}p$ and $\bar{p}$He for all the channels in the Monte-Carlo calculation. The continuous background thus obtained plus the contribution from two-body final states scaled from results obtained as described above (see also Paper IV, Table 1) then leads to a γ-spectrum in the $\bar{p}$N rest frame. However, the $\bar{p}$N system was not at rest when annihilating, since the nucleon performes Fermi motion and since in addition the $\bar{p}$ gains momentum when falling from an atomic orbit.

When we took the Fermi motion into account (details in Paper IV) we were able to fit the experimental spectrum with the shape based on the $\bar{p}p$ data with only two new free parameters, the number of annihilations and the total branching of two-body channels. Also in this case there had to be an arbitrary contribution at low energies.

After subtracting the background one clearly sees two peaks in the region 100 - 300 MeV. The fit shows that those peaks are compatible with or slightly broader than what could be expected by the detector resolution plus the Fermi motion and the above-mentioned momentum gain.

The somewhat lower γ-energy for the peaks in the $\bar{p}$He spectrum is compatible with the binding energy difference between the initial state and possible final states of ^{3}H or ^{3}He in one case and ^{3}H or ^{3}He or 3N in the other (here 3N denotes three free nucleons). The yield, ≈ 1 %, was about three times the yield from $\bar{p}p$, but no structures corresponding to 100 and 550 MeV could be seen. This is, however, compatible with different possible assignments of the isospin for the corresponding states. Thus, only $I \geq 1$ states would be visible in $\bar{p}$He with our present statistics. The increased widths of the peaks can also be an indication of a possible charge splitting.

Coincidence analysis

The two γ-rays emerging from a decaying π^0 or η are correlated, and having two γ-energy calorimeters enabled us to measure $\bar{p}p \rightarrow \pi^0 +$ anything and $\bar{p}p \rightarrow \eta +$ anything. However, for several reasons the effective solid angle for such a measurement becomes very small and we detected only about 10^3 true π^0 and still fewer η. Thus, the experiment should be seen mainly as a pilot test for a further experiment at LEAR (see Appendix D).

There are three decay parameters (see Appendix A and B) describing the π^0 (η) decay: E_{γ_1}, E_{γ_2} and $\phi_{\gamma_1\gamma_2}$. From those parameters there exist several possible estimators to estimate the π^0 or η energy. However, most of the γ-rays did not even originate from the same π^0 or η. Figure 2 in Paper V indicates that in the invariant mass peak region for π^0 there was a signal to noise ratio of 1 to 3 and for the η the situation was even worse. Assuming that all γ-pairs were uncorrelated we could estimate the background for the invariant mass as

$$\text{back}_m = \sqrt{F_1(E_{\gamma_1})F_2(E_{\gamma_2})}$$

where $F_1(E_{\gamma_1})$ and $F_2(E_{\gamma_2})$ were individual shape functions for the two detectors. The normalization of this background was taken from regions well outside the physical in variant masses, since estimates based on solid angles are good only to ≈ 20 %. In thi way we could identify 1000 ± 55 π^0 and 272 ± 48 η.

After cutting the invariant mass spectra the π^0 and η energies were estimated by th sum $E_{\pi^0,\eta} = E_{\gamma_1} + E_{\gamma_2}$.

The resulting (Figure 4a in Paper V) spectra still contained about 2/3 backgrounc However, with the estimator above it was simple to estimate the background. Th final π^0 total energy spectra were, as expected, dominated by a Panofsky peak a 138.3 MeV. For higher energies the very unfavourable detector efficiency decreased th number of counts and we could only give an upper limit of 8 % for a reaction $\bar{p}p \rightarrow \pi$ + X ($m_X \approx 1650$ MeV) where the π^0 total energy corresponds to 220 MeV.

As regards the η we could detect them only in the most favourable region and as nothin was known earlier about the shape of the η spectrum this result was not conclusive.

CHAPTER 5
CONCLUSIONS AND DISCUSSION

> " 'Forty-two!' yelled Loongquawl. 'Is that all you've got to show for seven and a half million years' work?'
> 'I checked it very thoroughly,' said the computer, 'and that quite definitly is the answer. I think the problem, to be quite honest with you, is that you've never actually known what the question is.' "
>
> DOUGLAS ADAMS, *The Hitchhikers guide to the galaxy*

In spite of the large effort spent on studying certain aspects of the p̄p annihilation it is not well understood. In particular the knowledge is poor about p̄p going to only neutral particles and p̄p resulting in many neutral particles + charged particles. In the stage of evaluation there are several experiments at LEAR which will hopefully give very accurate new information on such processes. Before this facility was constructed we were stimulated by other related works and performed a study of p̄p annihilation at rest for three particular cases: (i) p̄p $\rightarrow \pi^0$(or η) + one other particle, by studying the γ-rays from the decaying π^0 or η, (ii) p̄p $\rightarrow \pi^0$ or η + one other particle, by studying the decay γ-rays from π^0 or η in coincidence, (iii) p̄p $\rightarrow$ γ + anything, searching for monoenergetic γ-rays which might reveal deeply bound nuclear states or four-quark states (Baryonium). (iv) Finally, we studied the $\bar{p}^4$He annihilation at rest searching for monoenergetic γ-rays with the aim to reveal any isospin dependence. A summery of the data can be seen in Figures 20 and 21.

(i) *The process* p̄p $\rightarrow$ π^0 (or η)+ *one other particle* was studied by the detection of one of the decay γ-rays from the π^0 or η. This enabled us to measure the annihilation channels p̄p $\rightarrow$ $\pi^0\omega, \pi^0\eta$ and $\pi^0\gamma$. Whereas the $\pi^0\gamma$ branching ratio is in accordance with the expectation of the vector dominance model, the large $\pi^0\omega$ branching ratio is surprising. Thus, the S-wave dominance in p̄p annihilation at rest does not seem to hold. This conclusion is also supported by the large $\pi^0\eta$ branching ratio and the mere existence of the $\pi^0\pi^0$ channel . It was not possible to distinguish neither p̄p $\rightarrow$ $\pi^0\omega$ from p̄p $\rightarrow$ $\eta\omega$, nor p̄p $\rightarrow$ $\pi^0\eta$ from p̄p $\rightarrow$ $\eta\eta$, and thus an overall ratio for η/π^0 had to be used. Our upper limit for this ratio (0.50) could possibly explain some of the $\pi^0\omega$ as coming from $\eta\omega$. However, it can only decrease the p̄p $\rightarrow$ $\pi^0\omega$ yield by 0.5 % and would then still be in disagreement with other experiments [55] on inclusive η production. One feature of our data analysis which has to be explained is the need for introducing the channel p̄p $\rightarrow$ π^0X^0 with $m_X = 680$ MeV. The omission of this channel would increase the $\pi^0\omega$ yield by a factor ≈ 1.5 which does not seem very plausible. It would be very tempting to

Figure 20

Summery of Barionium search in $\bar{p}p$ and $\bar{p}He$ annhilation

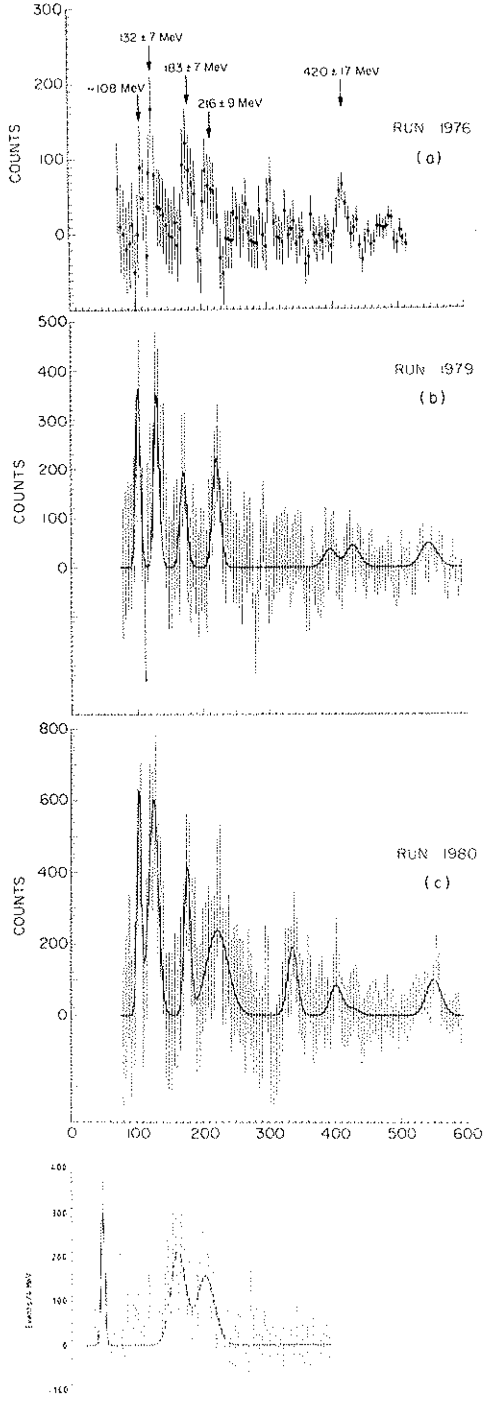

A comparison of experiments studying
γ-spectrum from $\bar{p}$ annihilation
a) ref [18]
b) this thesis 1979 run
c) this thesis 1980 run
and below this thesis $\bar{p}He$ annihilation

Figure 21
Summery of "box" channels (from paper II).

Uniform distributions, folded with the resolution as obtained from the fitting.

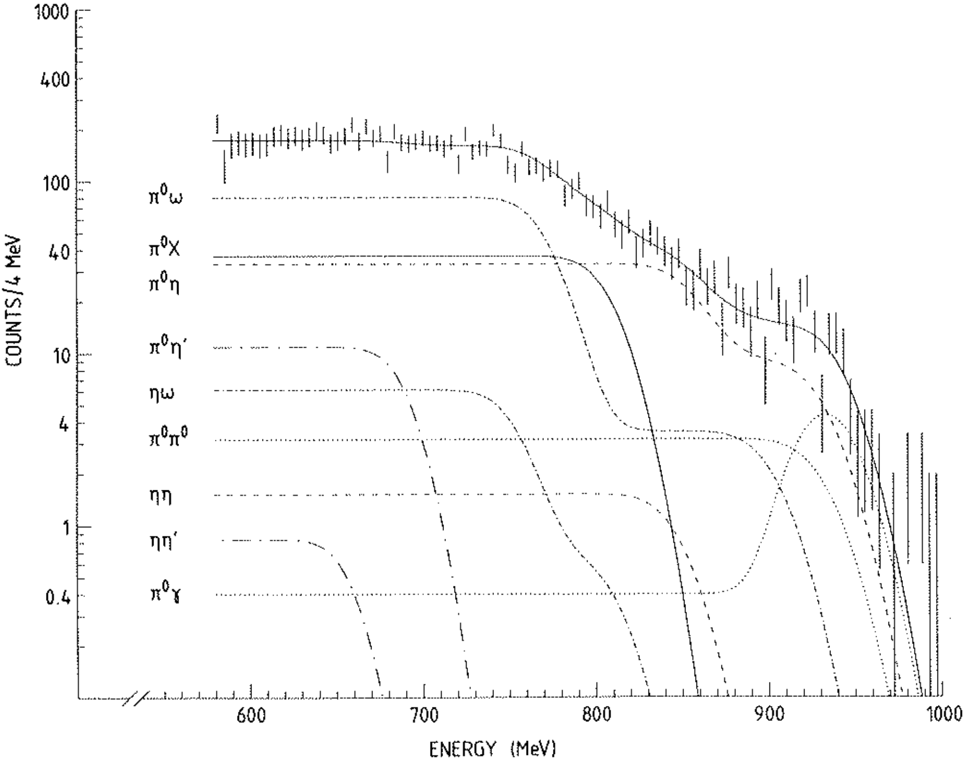

assign this effect to a particle in the Glueball ground state. However, at this stage we treat it rather as a correction of the background and other explanations have to await further studies at LEAR.

(ii) *The study of* π^0 *and* η *with coincidence techniques.* The count rate with this set-up was only enough to make it possible to detect about 1000 true π^0 and 275 true η. An upper limit for processes of the type $\bar{p}p \rightarrow \pi^0 + X^0$ (here X^0 is any neutral particle) of 8 % in the low energy region ($E_{\pi^0}^{tot} \leq 250$ MeV) could be obtained.

(iii) *The search for monoenergetic γ-rays from* $\bar{p}p$ *annihilation.* Although the resu of our experiment does not fully confirm the yields claimed by Pavlopoulos et a [18] for the processes $\bar{p}p \rightarrow \gamma$ + anything, where $E_\gamma \approx 180$, 220 and 420 MeV, w found structures in the γ-ray spectra at the same energies but with less yield. Ther could be several explanations for this observation. The main reason is probably tha the trigger conditions are different and the yields from the experiments describe here are normalized and with an unbiased trigger, whereas the old experiment b Pavlopoulos required at least two charged particle hits in a simple charged partic counter set-up around the target. Thus one has to conclude that the peaks at abou 180 MeV and 220 MeV appear in the spectrum but with lower yields than firs measured. For the 420 MeV peak the situation may be somewhat different du to the E/ι mesons, which should appear at 380–400 MeV. The structure in th 420 MeV region in Pavlopoulos' experiment could possibly be due to a recoil of on or both of these mesons because of the calibration uncertainties and trigger bia involved in the experiment. In our experiment the energy calibration is much bett but as the trigger is unbiased we cannot make a definite conclusion. It would no be possible to fit and resolve two broad structures in our data even if we knew i advance that they were present. In a future experiment one would have to detec other decay products in order to separate E and ι and other possible states.

(iv) *The search for monoenergetic γ-rays from* $\bar{p}$He *annihilation at rest.* We fin two prominent peaks in these data, both related to the previous findings in $\bar{p}$ annihilation data. The yield for these peaks is about 3 times higher than in the $\bar{p}$ case. This and a slightly larger width than the calculated one might indicate th presence of states with $I \geq 1$.

It should finally be concluded that the appearance of monoenergetic γ-rays of energie $\approx$ 180 MeV and $\approx$ 220 MeV in three different experiments on hydrogen and on experiment on helium can be interpreted as long-lived objects with masses $\approx$ 1690 an $\approx$ 1640 MeV. However, it must be admitted that so far it has not been possible t confirm these results in experiments of the type $\bar{p}p \rightarrow X^{\pm} + \pi^{\mp}$ and $\bar{p}p \rightarrow X^0 + \pi^0$. I can therefore not be excluded that the γ-ray peaks at 180 MeV and 220 MeV originat in processes which we have not been able to identify. Thus, it is still an open questio if Baryonium states are narrow objects or so wide that they disappear in the γ-ra continuum, if they exist at all.

APPENDIX A
SOME KINEMATICS FORMULAE

"A lord of wisdom throned he sat,
swift in anger, quick at laugh;
an old man in a battered hat
who leaned upon a thorny staff."

J. R. R. TOLKIEN *The Lord of the rings*

A.1 Notation and some basic formulas

The experimental methods used this thesis are based on a few very basic principles of physics, energy and momentum conservation and Lorentz invariance. Below follow a few results which are easily derived from those principles. For a detailed description see any basic textbook in elementary particle physics [56]. We use the four-vector X with components (E, **p**) where E is the energy of the particle and **p** the three-momenta and $|\mathbf{p}| = \mathrm{p}$. Also, we use the usual convention where $\hbar = c = 1$ (Planck's const./2π = speed of light = 1).

A.1.1 Conserved quantities

The total energy is conserved $E_{tot} = E_1 + ... + E_n$.

The total momentum is conserved $\mathbf{p}_{tot} = \mathbf{p}_1 + ... + \mathbf{p}_n$.

The rest mass is invariant $m_0^2 = E^2 - \mathbf{p}^2$ for one particle. Note also that E = p in all frames for a massless particle.

A.1.2 Lorentz transformations

A.1.2.1 Lorentz transformation of energy and momentum

If the four-vector X is seen from a second frame with relative velocity β in the z direction the components X′ in the second frame are

$$E' = \gamma E - \beta\gamma p_z \qquad p' = \gamma p_z - \beta\gamma E_z$$

$$p'_x = p_x \qquad p'_y = p_y$$

where

$$\gamma^2 = \frac{1}{1-\beta^2}$$

A.1.2.2 Lorentz transformations of angles

A.1.2.2.1 General

We can find the transformations for angles from the relation above. Suppose that a particle is moving with an angle α relative to the z-axis in frame A, and α' in frame A', and let * denote that a quantity is calculated in the primed frame. We see that the transverse component of the momenta is equal in both systems

$$p_T = \sqrt{p_x^2 + p_y^2} = p'_T$$

We get

$$\tan\alpha' = \frac{p_T}{p'_z} = \frac{1}{\gamma^*} \cdot \frac{p\sin\alpha}{p\cos\alpha + \beta^*\gamma^* E}$$

A.1.2.2.2 The Lorentz-transformation for a massless particle (photon)

For a massless particle where $E = p$ in both systems we can also get another relation used below.

Consider a photon propagating at an angle θ relative to the $\hat{z}$-axis in system A, and a angle θ' in system A'. Then we get the relations

$$\cos\theta' = \frac{p'_z}{p'} = \frac{p'_z}{E'} = \frac{\gamma \cdot (p_z + \beta p)}{\gamma \cdot (p + \beta p_z)} = \frac{\cos\theta + \beta}{1 + \beta\cos\theta}$$

A.1.3 The two-body decay kinematics

A.1.3.1 Introduction

The distinctive feature of the two-body decay is that if the total energy (and momentum of the initial particle is known, the decay is completely determined by measuring one o the decay particles. This important theorem in physics has been the ground for severa spectacular discoveries, e.g. the postulation of the neutrino [57] by Pauli when th e^--spectrum showed properties which could not be explained by two outgoing particles

A.1.3.2 Formulas

In the rest frame of the decaying particle, energy and momentum conservation and som algebra yield:

$$E_1 = \frac{M^2 + m_1^2 - m_2^2}{2M}$$

$$|\mathbf{p}_1| = p = \sqrt{\frac{[M^2 - (m_1 + m_2)^2][M^2 - (m_1 - m_2)^2]}{4M^2}}$$

Figure A.1

Recoil energies for $\bar{p}p \rightarrow \gamma$ or π^0 + one body (X).

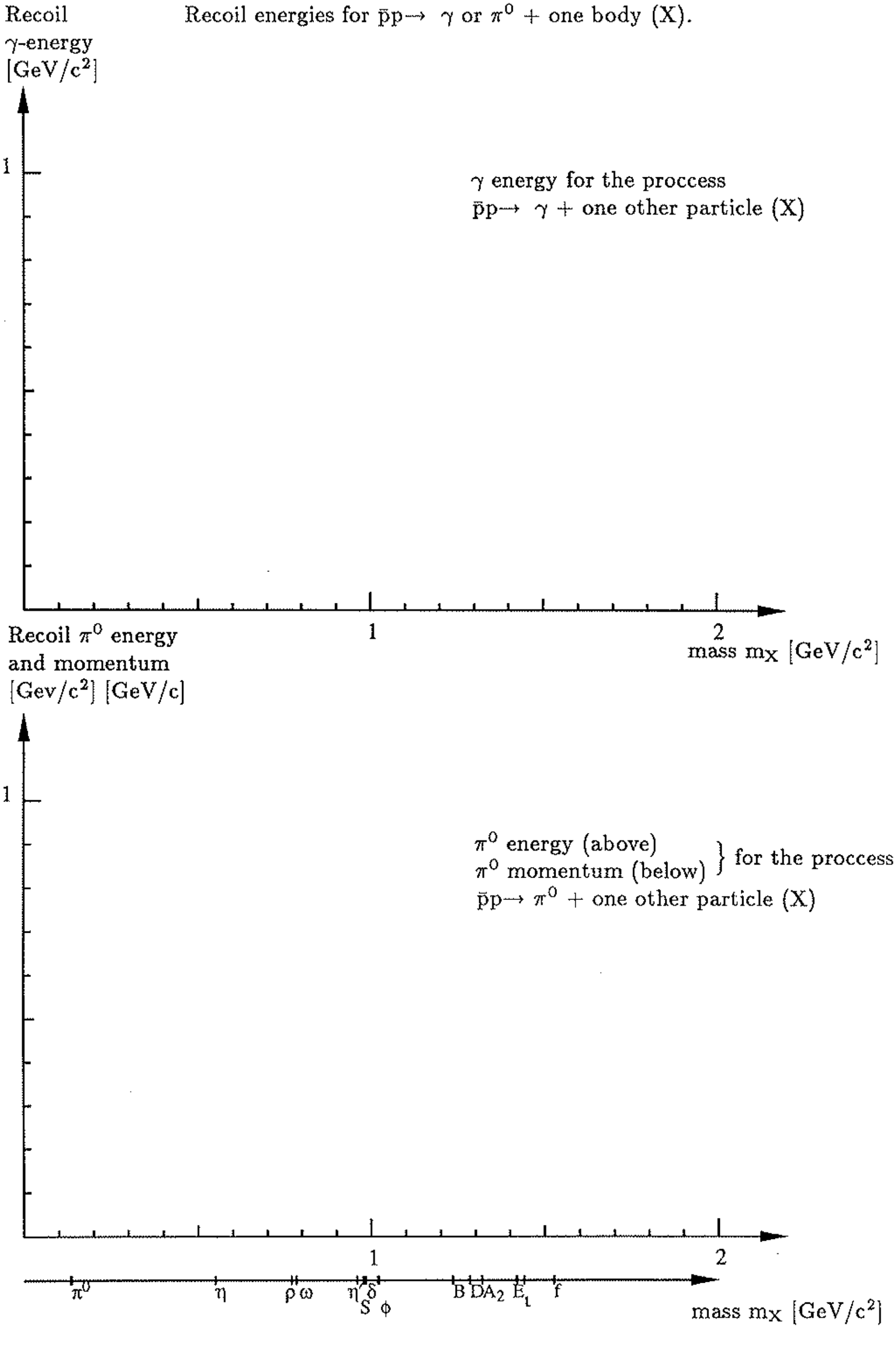

Thus, in our case, by detecting one outcoming particle from $\bar{p}p$ annihilation at rest we have an enhancement in the energy (or momentum) spectra whenever the energ corresponds to a two-body decay. Specializing to one massless particle (e. g. photon we have the mass and momentum for the recoiling particle

$$m_x = \sqrt{4m_p\,(m_p - p_\gamma)} \qquad\qquad p_x = p_\gamma = m_p - \frac{m_x^2}{4m_p}$$

in Figure A.1 this relation is shown graphically and with possible non-strange recoi particles indicated.

APPENDIX B

SOME DECAY PROPERTIES OF THE π^0 AND THE η

"Hunc mundum tipice laberinthus denotat ille"

"Intranti largus, redeunti sed nimis artus"

UMERTO, ECO *Il nome della rosa*

B.1 Decay properties for π^0 and η to $\gamma\gamma$

The π^0 and η decay to $\gamma\gamma$ with a branching ratio of 98.8 % and 39.0 %, respectively. The lifetimes and masses are $8 \cdot 10^{-17}$ s, $8 \cdot 10^{-19}$ s, 134.96 MeV and 549 MeV, respectively. Below are given some of the decay properties $\pi^0 \rightarrow \gamma\gamma$ used in this thesis. The figures consider π^0 but all formulas are also true for $\eta \rightarrow \gamma\gamma$.

For a π^0 decaying in the CM system with the parameters θ_1, θ_2, γ_1 and γ_2 where $\theta_1 + \theta_2 = 180\,^\circ$, the formulas in Appendix A give us $E_{\gamma 1} = E_{\gamma 2} = M_{\pi^0}/2$.

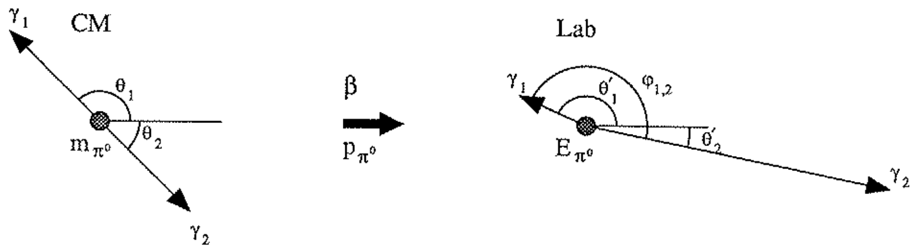

After calculating the quantities in the lab frame moving relative to the CMS with

$$\beta = \frac{p^{lab}_{\pi^0}}{E^{lab}_{\pi^0}}$$

they are denoted θ'_1, θ'_2, γ_1, γ_2 and $\theta'_1 + \theta'_2 = \varphi_{1,2}$. We want to calculate $E'_{\gamma 1}$, $E'_{\gamma 2}$ and $\varphi_{1,2}$. From Appendix A we know that

$$\cos\theta'_1 = \frac{\cos\theta + \beta}{1 + \cos\theta} \qquad \text{and thus} \qquad \cos\theta'_2 = \frac{\beta - \cos\theta}{1 + \beta\cos\theta}.$$

Now we can calculate

$$\cos\varphi_{1,2} = \frac{\beta^2(1+\sin^2\theta)-1}{1-\beta^2\cos^2\theta} \qquad \text{and} \qquad \cos\frac{\varphi_{1,2}}{2} = \frac{\beta\sin\theta}{\sqrt{1-\beta^2\cos^2\theta}}$$

Minimizing this we obtain

$$\cos\left(\frac{\varphi_{1,2}}{2}\right)_{\min} = \beta \qquad \text{or} \qquad \cos\varphi_{1,2\min} = 2\beta^2 - 1$$

and $\theta_{\max} = 180^\circ$.

The energy $E'_{\gamma 1}$ and $E'_{\gamma 2}$ for the extreme angles are (from Appendix B.2)

$$E'_{\gamma,\varphi_{1,2}\min} = \frac{E'_{\pi^0}}{2}$$

and

$$E'_{\gamma\max} = \frac{1}{2}(E'_{\pi^0} + p'_{\pi^0}) \qquad E'_{\gamma\min} = (E'_{\pi^0} - p'_{\pi^0})$$

The energy distribution is uniform between these extreme values and vanishes elsewher
(proof in Appendix B.2)

Finally, we give the probability for a decay to $\varphi_{1,2}$ from ref. [58].

$$W(\varphi_{1,2}) = \frac{1-\beta^2}{2\beta}\,\frac{\cos(\varphi_{1,2}/2)}{\sin^2(\varphi_{1,2}/2)}\,\frac{\Theta[\beta^2-\cos^2(\varphi_{1,2}/2)]}{\sqrt{\beta^2-\cos^2(\varphi_{1,2}/2)}}$$

with $\Theta(x) = 1$ for $(x > 0)$ and $= 0$ for $(x \leq 0)$.

Those parameters are summarized in Figure B.1.

B.2 THE BOX SHAPE OF THE (monoenergetic) π^0 DECAY SPECTRA

Theorem:

The energy distribution of a massless particle originating from the two-body deca
of a monoenergetic particle is flat between a maximum and a minimum value and
elsewhere.

The proof below considers $\pi^0 \to \gamma\gamma$ but it is of course true also for $\eta \to \gamma\gamma$. A sma
modification shows that the single γ from i.e. $\omega \to \pi^0\gamma$ is also getting the same bo
distribution.

Proof:

We consider the decay $\pi^0 \to \gamma\gamma$. In the π^0 rest frame (denoted by *) the emitte
gamma rays are monoenergetic with $E^*_\gamma = p^*_\gamma = m_{\pi^0}/2$, and collinear : $\mathbf{p}^*_{\gamma_1} = -\mathbf{p}^*_{\gamma}$
Their angular distribution is isotropic.

Figure B.1
The decay parameters for a π^0decay into 2γ's

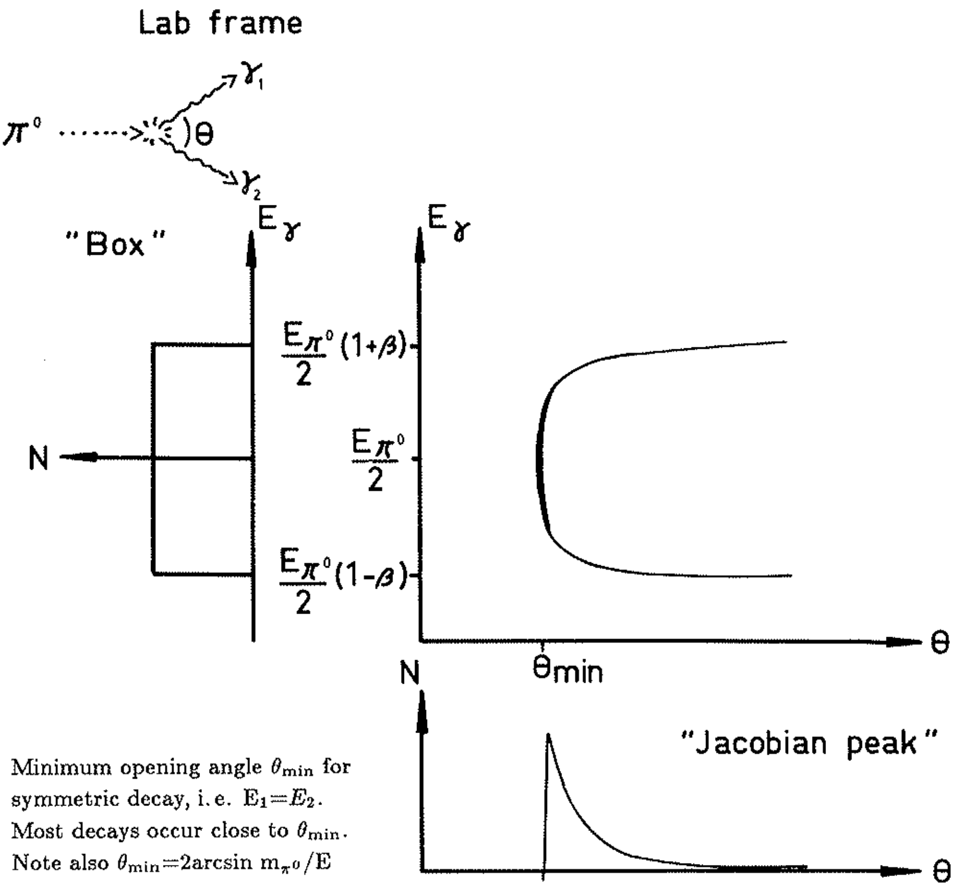

Minimum opening angle $\theta_{\min}$ for symmetric decay, i.e. $E_1 = E_2$. Most decays occur close to $\theta_{\min}$. Note also $\theta_{\min} = 2\arcsin m_{\pi^0}/E$

The number of gamma rays emitted into a CMS solid angle $d\Omega^*$ is

$$dN_\gamma = 2N_{\pi^0} \cdot \frac{d\Omega^*}{4\pi}$$

with the normalization $$\int dN_\gamma = 2N_{\pi^0} \frac{1}{4\pi} \int d\Omega^* = 2N_{\pi^0}.$$

In order to prove that the inclusive gamma spectrum has a rectangular shape, i. e. tha the number of gamma rays per energy bin is constant, we have to show that the rati of the CMS solid angle to the corresponding energy bin is constant. This is achieve by performing a Lorentz-transformation from the π^0 rest frame to the laboratory fram and by establishing the relations of the kinematical variables in both systems.

Assume the π^0 moves along the z-axis with a momentum p_{π^0}, carrying a total energ E_0. Its relativistic parameters of motion are

$$\beta = \frac{p_{\pi^0}}{E_{\pi^0}} \qquad \gamma = \frac{E_{\pi^0}}{m_{\pi^0}} \qquad \boldsymbol{\eta} = \frac{p_{\pi^0}}{m_{\pi^0}}$$

$$\text{Note that } \eta = \beta\gamma \qquad \gamma^2 = \frac{1}{1-\beta^2} \qquad \gamma^2 - 1 = (\gamma+1)(\gamma-1) = \beta^2\gamma^2 \qquad (1)$$

The Lorentz-transformation for the energy and the momentum of a gamma emitted int any direction is given by

$$E^* = \gamma E - \boldsymbol{\eta}\mathbf{p} \qquad \mathbf{p}^* = \mathbf{p} - \boldsymbol{\eta} \cdot \frac{E + E^*}{\gamma + 1} \qquad (\text{Lab} \rightarrow \text{CMS})$$

If δ denotes the emission angle formed with the z-axis we can write

$$E^* = \gamma E - \eta p \ \cos\delta = \gamma E - \eta E \ \cos\delta = \gamma E(1 - \beta \ \cos\delta)$$

$$E = \frac{E^*}{\gamma} \cdot \frac{1}{1 - \beta \ \cos\delta} = \frac{m_{\pi^0}}{2\gamma} \cdot \frac{1}{1 - \beta \ \cos\delta} \qquad (2$$

The gamma ray has a maximum energy if it is emitted in the forward direction (along th π^0 trajectory): $E_{max} = E(\delta = 0^\circ)$, while it achieves its lowest energy under backwar emission: $E_{min} = E(\delta = 180^\circ)$.

These energies are, respectively,

$$\underline{E_{max}} = \frac{m_{\pi^0}}{2\gamma}\frac{1}{1-\beta} = \frac{m_{\pi^0}}{2\gamma}\frac{1+\beta}{(1-\beta)(1+\beta)} = \frac{1}{2}m_{\pi^0}\gamma(1+\beta) = \underline{\frac{1}{2}(E_{\pi^0} + p_{\pi^0})}$$

$$\underline{E_{min} = \frac{1}{2}(E_{\pi^0} + p_{\pi^0}).}$$

One also obtains

$$\underline{\frac{dE}{d\cos\delta} = \frac{E^*}{\gamma}\frac{\beta}{(1-\beta\cos\delta)^2}} \qquad (3$$

The momentum components are transformed as

$$p_x^* = p_x \qquad p_y^* = p_y$$

$$p_z^* = p_z - \eta\frac{E+E^*}{\gamma+1} =$$

$$p\cos\delta - \frac{\eta}{\gamma+1}[E+\gamma E(1-\beta\cos\delta)] = E\cos\delta - \frac{\eta E}{\gamma+1}(1+\gamma-\beta\gamma\cos\delta) = .$$

$$E[\cos\delta - \eta(\frac{1+\gamma}{\gamma+1} - \frac{\beta\gamma}{\gamma+1}\cos\delta)] = E[\cos\delta - (\eta - \frac{\eta^2}{\gamma+1}\cos\delta)]$$

Using (1) we then get

$$p_z^* = E[\cos\delta - \{\eta - (\gamma-1)\cos\delta\}] = -E(\eta - \gamma\cos\delta)$$

$$\underline{p_z^* = -\gamma E(\beta - \cos\delta)}. \qquad (4)$$

The relation between δ^* and δ is obtained through

$$\cos\delta^* = \frac{p_z^*}{p^*} = \frac{p^*}{E^*} = -\frac{\gamma E}{\gamma E}\frac{(\beta-\cos\delta)}{(1-\beta\cos\delta)} =$$

$$-\frac{1}{\beta}\frac{\beta^2-\beta\cos}{(1-\beta\cos\delta)} = -\frac{1}{\beta}\frac{\beta^2-1+1-\beta\cos\delta}{(1-\beta\cos\delta)} = -\frac{1}{\beta}\left(\frac{\beta^2-1}{1-\beta\cos\delta}+1\right);$$

$$\underline{\cos\delta^* = \frac{1}{\beta\gamma^2}\left(\frac{1}{1-\beta\cos\delta} - \gamma^2\right)}. \qquad (5)$$

Now we can derive the relation between the solid angles in the laboratory and CM-system. Since

$$d\Omega = \sin\delta d\delta d\varphi \qquad d\Omega = d\cos\delta\ d\varphi \qquad \text{and} \qquad d\varphi = d\varphi^*$$

$$\frac{d\Omega^*}{d\Omega} = \frac{d\cos\delta^*}{d\cos\delta} = \frac{1}{\beta\gamma^2}\cdot\frac{\beta}{(1-\beta\cos\delta)^2}$$

$$\underline{\frac{d\Omega^*}{d\Omega} = \frac{1}{\gamma^2}\cdot\frac{1}{(1-\beta\cos\delta)^2}} \qquad (6)$$

By comparing eq. (6) with (3) we find the relation between the CM solid angle and the corresponding energy bin:

$$\frac{d\Omega^*}{d\Omega} = \frac{1}{\beta\gamma E^*}\frac{dE}{d\cos\delta} = \frac{1}{\beta\gamma E^*}\frac{dE}{d\Omega}d\varphi = \frac{2}{m_{\pi^0}\beta\gamma}\frac{dE}{d\Omega}d\varphi$$

$$\underline{d\Omega^* = \frac{2}{p_{\pi^0}}dE\,d\varphi}$$

Hence the number of gamma rays per energy bin dE is proportional to the corresponding solid angle $d\Omega^*$ but independent of the gamma energy in the laboratory frame. This was to be shown.

APPENDIX C

COINCIDENCE BACKGROUND

> ”Det är skönare att lyss till en sträng, som brast,
> än att aldrig spänna en båge.”
>
> HEIDENSTAM, *Åkallan och löfte*

The coincidence spectra did only yield in a weak upper limit for the process $\bar{p}p \rightarrow \pi^0 + X^0$ where $m_X \approx 1650$ MeV. This result is due to the low coincidence count rate and the fact that in most events the two γ-rays do not originate from the same π^0. In Figure C.1 we show a method [59] which visualize the π^0 in the coincidence spectrum with the following description: from the matrix of $\gamma - \gamma$ coincidences M_{ij} obtained under the assumption of no correlation between the γ-rays. The matrix of correlated events ΔN_{ij} is then constructed as

$$\Delta N = N_{ij} - M_{ij} = N_{ij} - \frac{\sum_l N_{il} \sum_k N_{kj}}{\sum_{lk} N_{kl}} \qquad (; \Delta N_{ij} \leq \text{ is put to 0 in the display})$$

Although this procedure is not entirely correct, since the N_{ij} matrix does contain correlated events, it is clearly showing in Figure C.1 that we are able to study π^0 spectra with this coincidence technic at LEAR.

Figure C.1
Coincidences before and after subtraction of statistical background

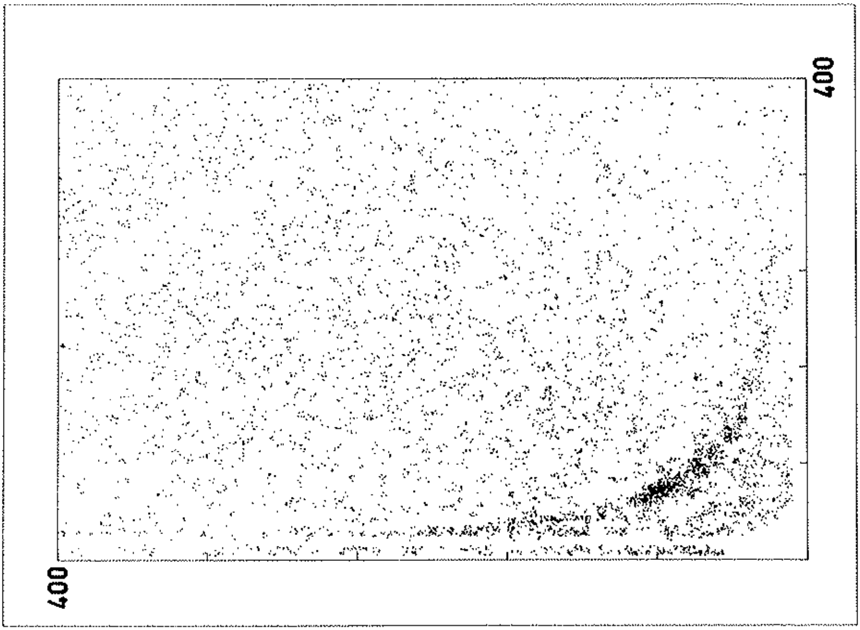

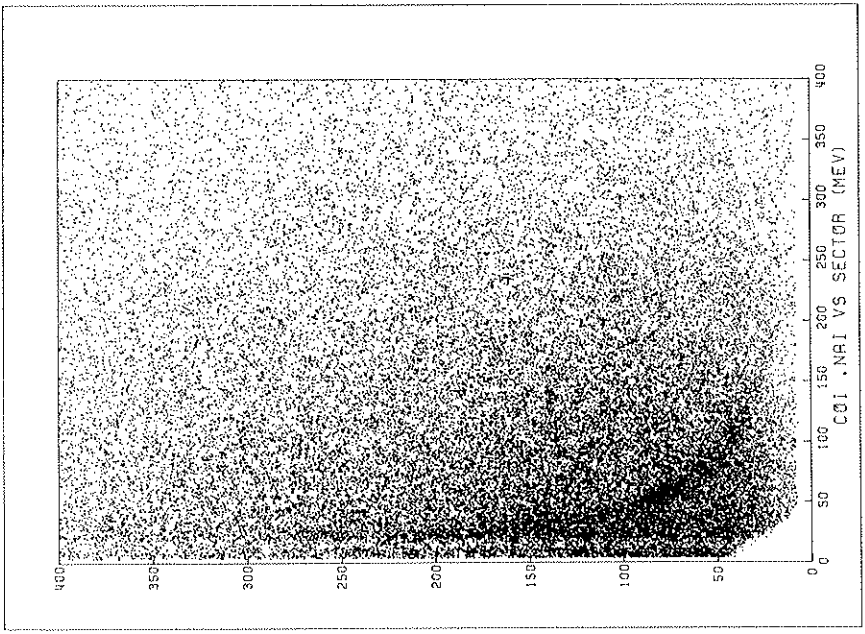

APPENDIX D

THE QUARK CONTENT OF THE ORDINARY MESONS

"He stood upon the bridge alone
and Fire and Shadow both defied;
his staff was broken on the stone
in Khazad-dûm his wisdom died."

J. R. R. TOLKIEN *The Lord of the rings*

THE SU(6) WAVE FUNCTIONS

$$\pi^{+} = \tfrac{1}{2}(u_\uparrow\bar{d}_\downarrow - u_\downarrow\bar{d}_\uparrow - \bar{d}_\uparrow u_\downarrow + \bar{d}_\downarrow u_\uparrow)\,,$$

$$\pi^{0} = \tfrac{1}{2}\sqrt{\tfrac{1}{2}}(-u_\uparrow\bar{u}_\downarrow + d_\uparrow\bar{d}_\downarrow + u_\downarrow\bar{u}_\uparrow - d_\downarrow\bar{d}_\uparrow - \bar{d}_\uparrow d_\downarrow + \bar{u}_\uparrow u_\downarrow - \bar{u}_\downarrow u_\uparrow + d_\downarrow\bar{d}_\uparrow)\,,$$

$$\pi^{-} = -\tfrac{1}{2}(d_\uparrow\bar{u}_\downarrow - d_\downarrow\bar{u}_\uparrow - \bar{u}_\uparrow d_\downarrow + \bar{u}_\downarrow d_\uparrow)\,,$$

$$\rho^{+}_{\uparrow} = \sqrt{\tfrac{1}{2}}(u_\uparrow\bar{d}_\uparrow + \bar{d}_\uparrow u_\uparrow)\,,$$

$$\rho^{+}_{\leftarrow} = \tfrac{1}{2}(u_\uparrow\bar{d}_\downarrow + u_\downarrow\bar{d}_\uparrow + \bar{d}_\uparrow u_\downarrow + \bar{d}_\downarrow u_\uparrow)\,,$$

$$\rho^{+}_{\downarrow} = \sqrt{\tfrac{1}{2}}(u_\downarrow\bar{d}_\downarrow + \bar{d}_\downarrow u_\downarrow)\,,$$

$$\rho^{0}_{\uparrow} = \tfrac{1}{2}(-u_\uparrow\bar{u}_\uparrow - u_\uparrow\bar{u}_\uparrow + \bar{d}_\uparrow d_\uparrow + \bar{d}_\uparrow d_\uparrow)\,,$$

$$\rho^{0}_{\leftarrow} = \tfrac{1}{2}\sqrt{\tfrac{1}{2}}(-u_\uparrow\bar{u}_\downarrow - u_\downarrow\bar{u}_\uparrow - \bar{u}_\uparrow u_\downarrow - \bar{u}_\downarrow u_\uparrow + d_\uparrow\bar{d}_\downarrow + d_\downarrow\bar{d}_\uparrow + \bar{d}_\uparrow d_\downarrow + \bar{d}_\downarrow d_\uparrow)\,,$$

$$\rho^{0}_{\downarrow} = \tfrac{1}{2}(-u_\downarrow\bar{u}_\downarrow - \bar{u}_\downarrow u_\downarrow + d_\downarrow\bar{d}_\downarrow + \bar{d}_\downarrow d_\downarrow)\,,$$

$$\rho^{-}_{\uparrow} = -\sqrt{\tfrac{1}{2}}(d_\uparrow\bar{u}_\uparrow + \bar{u}_\uparrow d_\uparrow)\,,$$

$$\rho^{-}_{\leftarrow} = -\tfrac{1}{2}(d_\uparrow\bar{u}_\downarrow + d_\downarrow\bar{u}_\uparrow + \bar{u}_\uparrow d_\downarrow + \bar{u}_\downarrow d_\uparrow)\,,$$

$$\rho^{-}_{\downarrow} = -\sqrt{\tfrac{1}{2}}(d_\downarrow\bar{u}_\downarrow + \bar{u}_\downarrow d_\downarrow)\,,$$

$$\omega^{0}_{\uparrow} = \tfrac{1}{2}(u_\uparrow\bar{u}_\uparrow + \bar{u}_\uparrow u_\uparrow + d_\uparrow\bar{d}_\uparrow + \bar{d}_\uparrow d_\uparrow)\,,$$

$$\omega^{0}_{\leftarrow} = \tfrac{1}{2}\sqrt{\tfrac{1}{2}}(u_\uparrow\bar{u}_\downarrow + u_\downarrow\bar{u}_\uparrow + \bar{u}_\uparrow u_\downarrow + \bar{u}_\downarrow u_\uparrow + d_\uparrow\bar{d}_\downarrow + d_\downarrow\bar{d}_\uparrow + \bar{d}_\uparrow d_\downarrow + \bar{d}_\downarrow d_\uparrow)\,,$$

$$\omega^{0}_{\downarrow} = \tfrac{1}{2}(u_\downarrow\bar{u}_\downarrow + \bar{u}_\downarrow u_\downarrow + d_\downarrow\bar{d}_\downarrow + \bar{d}_\downarrow d_\downarrow)\,,$$

$$\eta^{0} = \tfrac{1}{2}\sqrt{\tfrac{1}{2}}(u_\uparrow\bar{u}_\downarrow - u_\downarrow\bar{u}_\uparrow - \bar{u}_\uparrow u_\downarrow + \bar{u}_\downarrow u_\uparrow + d_\uparrow\bar{d}_\downarrow - d_\downarrow\bar{d}_\uparrow - \bar{d}_\uparrow d_\downarrow + \bar{d}_\downarrow d_\uparrow)\,,$$

$$\begin{aligned} p_\uparrow = \sqrt{\tfrac{1}{18}}\{&2(u_\uparrow d_\downarrow u_\uparrow + d_\downarrow u_\uparrow u_\uparrow + u_\uparrow u_\uparrow d_\downarrow) \\ &- (u_\downarrow d_\uparrow u_\uparrow + u_\downarrow u_\uparrow d_\uparrow + d_\uparrow u_\uparrow u_\downarrow + d_\uparrow u_\downarrow u_\uparrow + u_\uparrow d_\uparrow u_\downarrow + u_\uparrow u_\downarrow d_\uparrow)\}\,, \end{aligned}$$

$$\begin{aligned} p_\downarrow = \sqrt{\tfrac{1}{18}}\{&(u_\uparrow d_\downarrow u_\downarrow + u_\uparrow u_\downarrow d_\downarrow + d_\downarrow u_\uparrow u_\downarrow \\ &+ d_\downarrow u_\downarrow u_\uparrow + u_\downarrow d_\downarrow u_\uparrow + u_\downarrow u_\uparrow d_\downarrow) - 2(u_\downarrow d_\uparrow u_\downarrow + d_\uparrow u_\downarrow u_\downarrow + u_\downarrow u_\downarrow d_\uparrow)\}\,, \end{aligned}$$

$$\begin{aligned} n_\uparrow = \sqrt{\tfrac{1}{18}}\{&-2(d_\uparrow u_\downarrow d_\uparrow + u_\downarrow d_\uparrow d_\uparrow + d_\uparrow d_\uparrow u_\downarrow) \\ &+ (d_\downarrow u_\uparrow d_\uparrow + d_\downarrow d_\uparrow u_\uparrow + u_\uparrow d_\uparrow d_\downarrow + u_\uparrow d_\downarrow d_\uparrow + d_\uparrow u_\uparrow d_\downarrow + d_\uparrow d_\downarrow u_\uparrow)\}\,, \end{aligned}$$

$$\begin{aligned} n_\downarrow = \sqrt{\tfrac{1}{18}}\{&-(d_\uparrow u_\downarrow d_\downarrow + d_\uparrow d_\downarrow u_\downarrow + u_\downarrow d_\uparrow d_\downarrow + u_\downarrow d_\downarrow d_\uparrow + d_\downarrow u_\downarrow d_\uparrow + d_\downarrow d_\uparrow u_\downarrow) \\ &+ 2(d_\downarrow u_\uparrow d_\downarrow + u_\uparrow d_\downarrow d_\downarrow + d_\downarrow d_\downarrow u_\uparrow)\}\,. \end{aligned}$$

APPENDIX E

PAPERS I-V

"I like to work: it fascinates me. I can sit and look at it for hours. I love to keep it by me: the idea of getting rid of it nearly breaks my heart."

JEROME K. JEROME, *Three Men in a Boat*

This appendix contains a reprint of the following five papers which the thesis is based on.

I P. Blüm, R. Guigas, H. Koch, M. Meyer, H. Poth, U. Raich, B. Richter, G. Backenstoss, M. Hasinoff, P. Pavlopoulos, J. Repond, L. Tauscher, D. Tröster, L. Adiels, I. Bergström, K. Fransson, A. Kerek, M. Suffert and K. Zioutas

A modular NaI(Tℓ)) detector for 20-1000 MeV photons, Nuclear Instruments and Methods **213**(1983)251.

II G. Backenstoss, M. Hasinoff, P. Pavlopoulos, J. Repond, L. Tauscher, D. Tröster, P. Blüm, R. Guigas, H. Koch, M. Meyer, H. Poth, U. Raich, B. Richter, L. Adiels, I. Bergström, K. Fransson, A. Kerek, M. Suffert and K. Zioutas

Proton-antiproton annihilations at rest into $\pi^0\omega$, $\pi^0\eta$, $\pi^0\gamma$, $\pi^0\pi^0$, and $\pi^0\eta'$, Nuclear Physics **B228**(1983)424.

III B. Richter, L. Adiels, G. Backenstoss, I. Bergström, P. Blüm, K. Fransson, M. Glöckner, R. Guigas, M. Hasinoff, A. Kerek, H. Koch, T. Köhler, M. Meyer, P. Pavlopoulos, H. Poth, U. Raich, J. Repond, M. Suffert, L. Tauscher, D. Tröster and K. Zioutas

New results in the search for narrow states in the $p\bar{p}$ system below threshold, Physics Letters **126B**(1983)284.

IV L. Adiels, G. Backenstoss, P. Blüm, I. Bergström, K. Fransson, R. Guigas, H. Koch, A. Kerek, M. Meyer, P. Pavlopoulos, H. Poth, U. Raich, B. Richter, J. Repond, M. Suffert, L. Tauscher, D. Tröster and K. Zioutas

Search for narrow exotic states in $\bar{p}$ annihilations on ^{4}He, Physics etters 138B (1984)235.

V L. Adiels, G. Alberis, G. Backenstoss, P. Blüm, I. Bergström, K. Fransson, R. Guigas M. Hasinoff, H. Koch, A. Kerek, M. Meyer, P. Pavlopoulos, H. Poth, U. Raich, B. Richter J. Repond, M. Suffert, L. Tauscher, D. Tröster and K. Zioutas

π^0 and η spectra from $p\bar{p}$ annihilations at rest, Zeitschrift für Physik C - Particles an Fields **21**(1984)315.

Nuclear Instruments and Methods 213 (1983) 251–259
North-Holland Publishing Company

A MODULAR NaI(Tl) DETECTOR FOR 20–1000 MeV PHOTONS

P. BLÜM, R. GUIGAS *, H. KOCH, M. MEYER **, H. POTH, U. RAICH *** and B. RICHTER
Kernforschungzentrum Karlsruhe, Institut für Kernphysik, Institut für experimentelle Kernphysik, Universität Karlsruhe, Karlsruhe, Fed. Rep. Germany

G. BACKENSTOSS, M. HASINOFF †, P. PAVLOPOULOS, J. REPOND, L. TAUSCHER and D. TRÖSTER
Institute for Physics, University of Basle, Switzerland

L. ADIELS ***, I. BERGSTRÖM, K. FRANSSON and A. KEREK
Research Institute for Physics, Stockholm, Sweden

M. SUFFERT
Centre de recherches nucléaires and Université Louis Pasteur, Strasbourg, France

K. ZIOUTAS
Department of Nuclear Physics, University of Thessaloniki, Greece

Received 10 March 1983

A detector consisting of 54 NaI (Tl) modules is described. The detector has been optimized for the detection of 20–1000 MeV photons. An energy resolution (fwhm) of 5.5% at 130 MeV could be attained, and the stability has been better than 1% over several months.

1. Introduction

The detection of medium-energy (20–1000 MeV) photons with good energy resolution and high efficiency presents certain problems. As a matter of fact, lead–glass detectors are not suitable for the lower part of the energy domain, and the upper part requires big volumes in order to contain the photon shower. In the past, large monocrystals of NaI (Tl) were used with some success [1]. However, their main drawback is the lack of identification of multiple hits. Also, it is difficult to achieve a good uniformity of light output for very large crystals. A good solution consists in using a modular NaI detector such as the Stanford crystal ball [2].

For the measurement of γ-ray spectra produced by the $p\bar{p}$ system at rest, we used and optimized such a modular detector [3]. In addition to good energy resolution for the whole energy domain (20–1000 MeV) and good multiple-hit rejection, the detector had to present very good long term stability since the experiments lasted several months.

Good energy resolution was achieved in three ways: i) by having a large volume of NaI to contain the photon shower, and by the rejection of photons which did not hit the central part of the detector; ii) by very good uniformity of the light output for each module and a minimum of material between modules; iii) by very accurate energy calibration of each module (at 130 MeV) and control of its variation with time by use of a light pulser.

2. Experimental set-up

The photon spectrometer is composed of 54 modules (NaI and photomultiplier tube) assembled in a sealed housing, a light pulser for calibration and stabilization, and the associated electronics.

* Now at BBC, Mannheim, Fed. Rep. Germany.
** Now at ESO, Garching, Fed. Rep. Germany.
*** Now at CERN, Geneva, Switzerland.
† On leave of absence from the Department of Physics, University of British Columbia, Vancouver, Canada.

0167-5087/83/0000–0000/$03.00

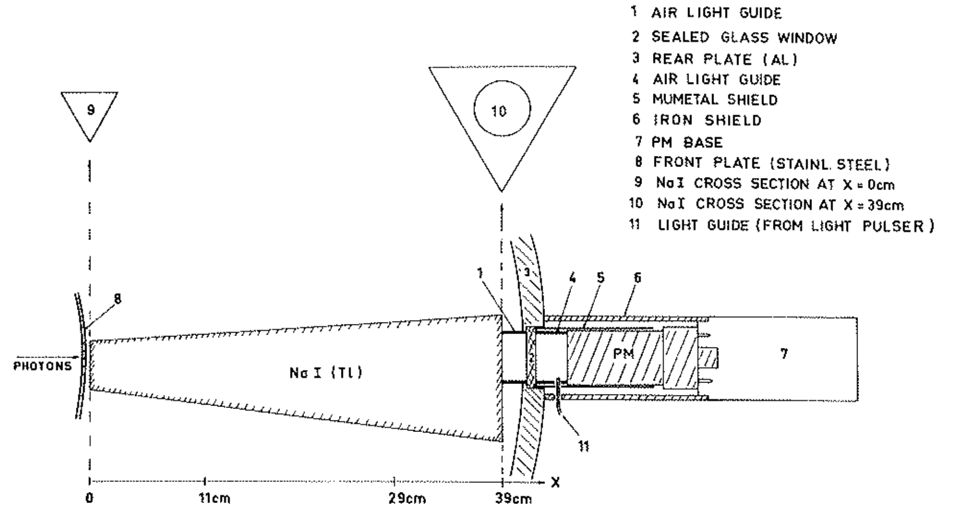

Fig. 1. Cross-section of a detector module.

2.1. The NaI modules

Fig. 1 shows the drawing of a typical module. Each module has the shape of a truncated triangular pyramid and is made of polycrystalline pieces of NaI (Tl) (polyscine) *. Owing to the geometrical arrangement of the 54 modules (see next subsection) there are differences up to 12% in the dimensions and thus in the volume of the crystals. They are wrapped in white paper and then in aluminized mylar (for optical separation) covering all faces, except for a 50 mm diameter hole in the large triangular face into which is fitted the first air light-guide between the crystal and the glass window of the housing. A second air light-guide connects the window and the photomultiplier (PM) tube. A small lateral hole in this light-guide allows injection of light pulses via a light fibre (see subsection 2.3).

The PMs were semi-fast, 50 mm diameter, 10-stage tubes of the type SRC L50B01 or RTC XP2202B, shielded magnetically by 1 mm μ-metal and about 5 mm of iron.

The specifications for the energy resolution and light collection uniformity of the NaI crystals were the following: 14.5% fwhm energy resolution for 661 keV photons irradiating the small (front) end of the module, and $\pm 2.5\%$ longitudinal light collection uniformity for collimated 661 keV photons irradiating the crystal laterally for $x = 0$ to 29 cm (see fig. 1), and $\pm 1.25\%$ fo $x = 0$ to 11 cm. Tests made before packing the module in the common housing showed that they all met th energy resolution specification, and all but nine mod ules met the uniformity specifications. Fig. 2 show typical variations of the 661 keV photopeak positio versus x. Module 44 was one of the nine modules whic did not meet the uniformity specifications for $x = 0$ t 29 cm. Since they were reasonably uniform for th important first 11 cm, they were accepted but placed o the outside of the assembly (see fig. 3). As a matter o fact, for the experiments, only those photons wer accepted which hit the inner 24 modules, so the oute modules (25 to 54) were used only to contain th shower, and thus their non-uniformity was much les detrimental.

Finally, it should be noted that the light output of module is only about 7% of that of a 2"×2" cylindrica NaI (Tl) crystal coupled directly to the PM. This loss i light output, mostly due to the use of the two ai light-guides, explains the modest energy resolution fo low-energy photons but is acceptable for the energ range (20–1000 MeV) for which the detector was de signed.

2.2. Arrangement of the modules

All 54 modules were tightly packed in a seale housing as shown in fig. 3. Each crystal was individuall

* Manufactured by Harshaw Chemical Co., Solon, Ohio, USA.

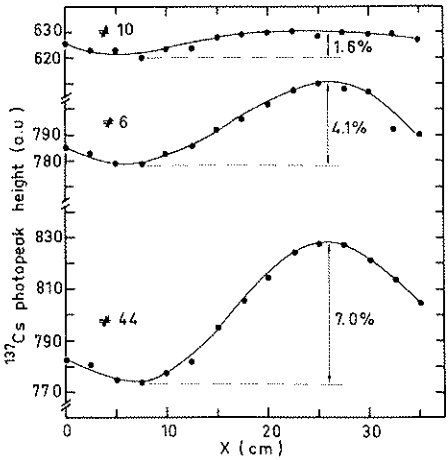

Fig. 2. Variation of the photopeak-height procuced by a collimated ^{137}Cs source (661 keV) placed at a distance x from the front end of the NaI crystal. Results for three module samples are shown. About two thirds of the modules had longitudinal uniformities similar to the one of module 6.

held by screws and pressure plates acting on the large (rear) end of the crystal.

Fig. 3 also shows the stacking scheme and the numbering of the modules. One can distinguish three concentric rings: modules 1 to 6, modules 7 to 24, and modules 25 to 54. Assembled in this way the detector constituted approximately 1 sr of the full sphere and was equivalent to 1/13 of the Stanford crystal ball [2]. In the following, the complete detector assembly will be called the "sector".

2.3. The light pulser

The light pulser is shown schematically in fig. 4. The light pulse was produced by a xenon flash-tube of the type FX280 *. The shape of the light pulse was tuned to be similar to that of the NaI (Tl) crystal. The intensity of the light was adjusted in a continuous manner by a diaphragm, and in steps by a set of six filters placed on a wheel. Both the diaphragm and the filter wheel could be positioned remotely.

The light then entered a white diffusion box and was distributed by 56 light guides of 1 mm diameter and 2 m length ** (fig. 5). The light pulses from 54 of these guides were injected into the air gap of the modules (fig. 1). One light guide was mounted in a similar way on a 2" × 2" NaI (Tl) PM assembly, but the intensity of the

* Manufactured by EGG Electro Optics Division, Salem, Mass., USA.

** Manufactured by Fiberoptik-Heim AG, CH 8707 Uetikon am See, Zurich, Switzerland.

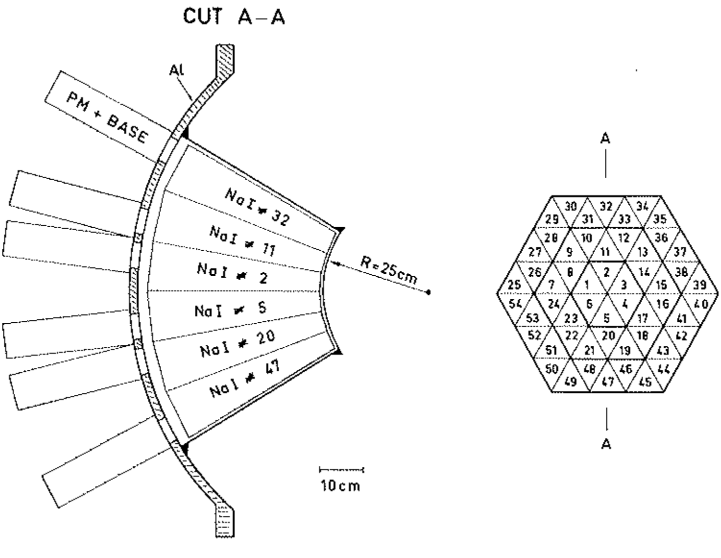

Fig. 3. The detector assembly: at right – stacking and numbering of the 54 modules; at left – cross-section A–A. For details of the coupling between the NaI and the PM, see fig. 1.

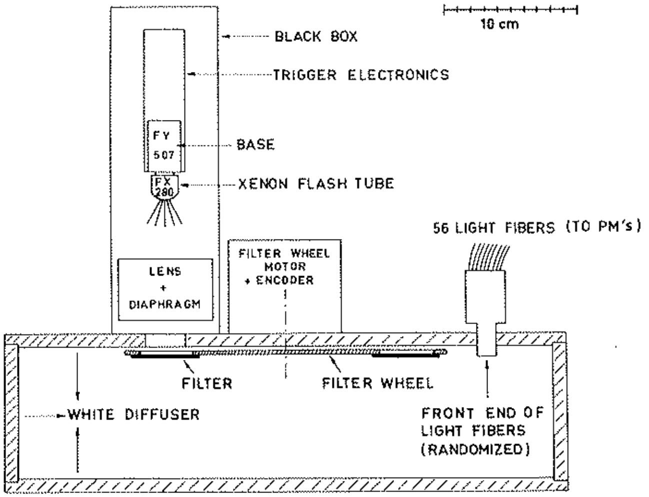

Fig. 4. The light pulser (schematic). Not shown are the motor and encoder for the diaphragm, and an additional retractable filte between the diaphragm and the filter wheel.

light pulse was strongly attenuated in order to be approximately the same as the light from the 2"×2" NaI crystal irradiated by a ^{22}Na γ-source (1.28 MeV). This assembly was placed in the same thermally isolated enclosure as the sector. The comparison of the light pulse intensity with the intensity of the light produced by the 1.28 MeV photons in the 2"×2" NaI crystal allowed a precise control of the light pulser stability, as explained later. Finally, the light of the last guide was seen directly by an RTC PM1910 photomultiplier (18 mm dia.) which produced a light-pulser trigger for the data acquisition.

The FX280 xenon bulb was driven at a rate of five flashes per second. At this rate the decrease in light output was about 1% per week. The fwhm of the peak produced by the light pulser was 2% to 4% depending on the bulb sample. Using different filters and diaphragm settings, the whole pulse-height range corresponding to 20–1000 MeV energy deposit in the NaI crystals could be covered. The light attenuation factors of the filters were calibrated using the 2"×2" NaI assembly, the linearity of which was checked with radioactive sources. In this way the linearity of the module PMs and the associated electronics was determined up to 1 GeV equivalent photon energy.

2.4. Electronics

Fig. 6a and 6b show the two types of electronic schemes which were used:

The arrangement of fig. 6a (d.c. coupling) is we suited for high counting rates but has two drawbacks: i the PM has to be operated with the high voltage at th photocathode, which induces irreversible gain losses (u to 5%/day) if the PM in the cathode region is nc extremely well shielded electrostatically; ii) the direc coupling may introduce ground loops and, in conse quence, noise which prevents the detection of low-er ergy (some MeV) events.

In order to avoid these two drawbacks, the arrange ment of fig. 6b (photocathode at ground potential an transformer coupling) was used during a later perioc However, in this case the transformer in the anod

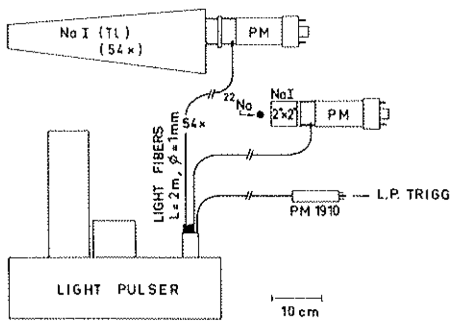

Fig. 5. Distribution of the light pulses to the different PMs.

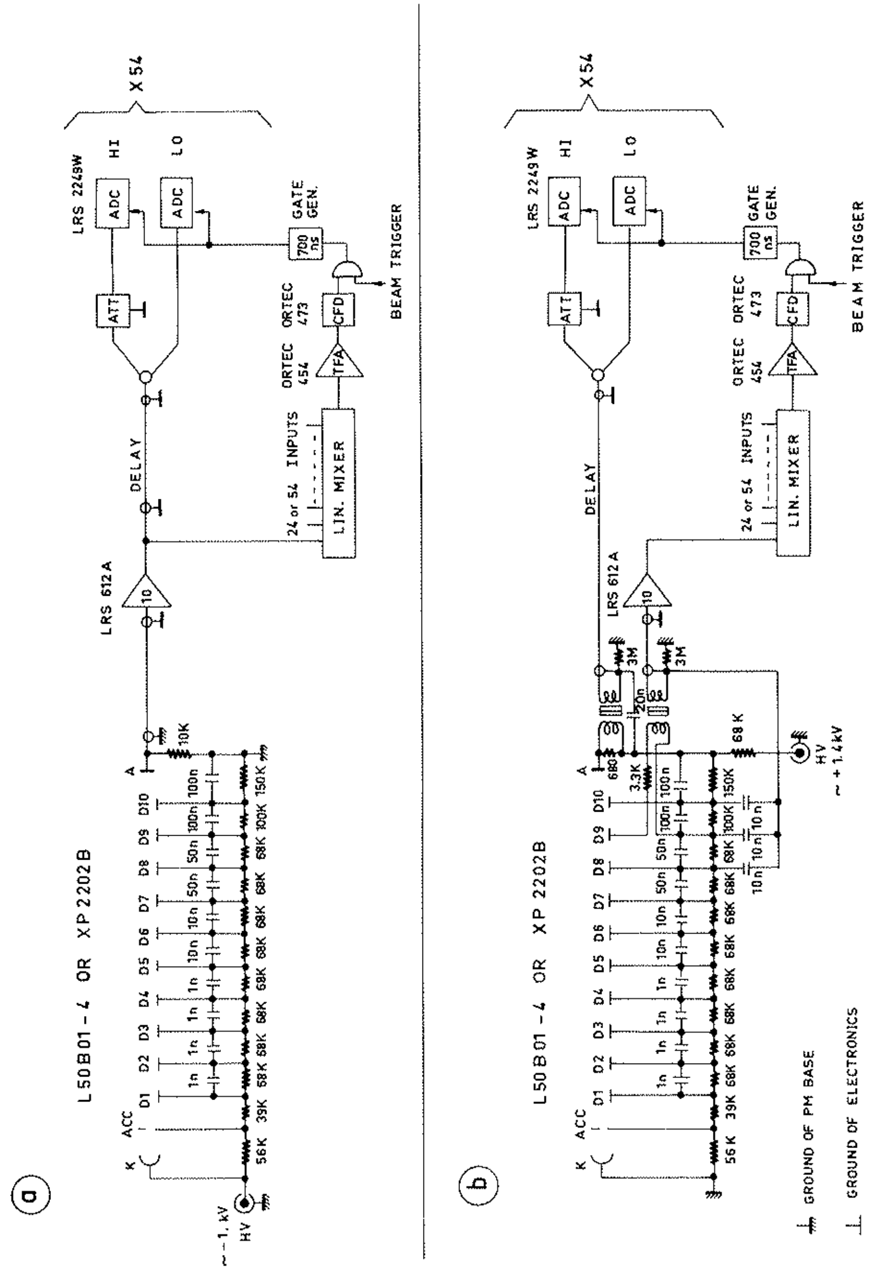

Fig. 6. The two electronic schemes used for the NaI-detector pulse processing.

circuit caused long (many microseconds) pulse overshoots which were particularly disturbing at high counting rates.

In both configurations the trigger was produced by a constant fraction discriminator (CFD) fed by the linearly added outputs of a certain number of modules (usually modules 1–24, fig. 3). For the pulse-height measurement, each module output was split (after amplification in the case of fig. 6a) and, after attenuation in one branch, fed a separate charge-sensitive ADC in order ot obtain two dynamic ranges. Usually, the low-range (LO) was chosen to cover 0–100 MeV and the high-range (HI) 0–1000 MeV.

The contents of the 108 ADCs as well as the one of the ADC belonging to the 2"×2" NaI assembly were read out in the usual way via CAMAC and written on magnetic tape via a PDP 11-34 computer. This computer also served to perform regular on-line checks on photon and light-pulser spectra produced by the detector modules.

3. Energy calibration

The modular structure of the system was conceived in such a way that a high-energy γ shower extends over several modules. Proper reconstruction of the event thus required a precise intercalibration of the modules and then an absolute calibration. The usual standards for calibrating γ spectrometers, such as γ radiation from radioactive sources or nuclear reactions, are not higher than 25 MeV and hence not relevant for the energ range up to 1000 MeV. Therefore a special method wa developed in order to intercalibrate the different modules and to obtain an absolute energy calibration.

3.1. Intercalibration of the modules

3.1.1. Rough intercalibration

A rough calibration of the modules relative to eac other was obtained by irradiating the spectrometer wit the 660 keV γ-rays from a ^{137}Cs source and the 2.6 Me γ-radiation from a Th source. The signals had to b additionally amplified in order to obtain pulse height falling into the dynamic range of 10–1000 MeV. Th signals were multiplexed to an amplifier, and the hig voltage for the PMs of each module was adjusted so a to give the same outputs for all.

Owing to the limited resolution at these energie ($\Delta E/E \approx 15\%$ fwhm) the precision of this type of intercalibration was not better than 5%, and the resolutio finally obtained at 130 MeV when using the even reconstruction described later was ≈ 12% FWHM. Thi is demonstrated in fig. 7a.

3.1.2. Intercalibration at higher energies

The final intercalibration was obtained from γ-radiation of ≈ 130 MeV. The low-energy secondary bean k_{23} of the CERN Proton Synchrotron (PS) was tuned t slow π^- (200 MeV/c) which were then stopped in liquid-hydrogen target. The π^- then underwent the reac

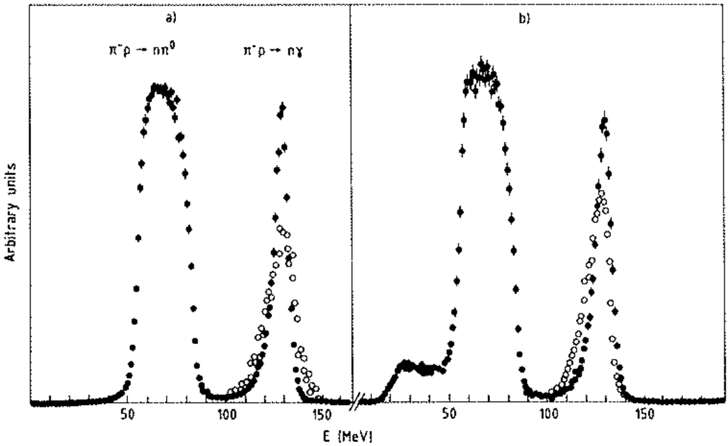

Fig. 7. The spectra from the reaction $\pi^- p \to n\pi^0$ and $\pi^- p \to n\gamma$ [(a) as obtained from the calibration run, (b) 2 months later]. Ope dots (O) in (a) show the 129.4 MeV peak as obtained from the source calibration alone. Open dots (O) in (b) show the 129.4 Me peak as obtained without light-pulser correction.

tion

$$\pi^- p \to n + \gamma \qquad (E_\gamma = 129.4\ \text{MeV}), \tag{1}$$

$$\pi^- p \to n + \pi^0 \qquad (55 \leqslant E_\gamma \leqslant 83\ \text{MeV}). \tag{2}$$

Since the initial state is a pionic atom at rest, the final-state energies were extremely well determine. Reaction (1) resulted in a monoenergetic peak, reaction (2) in a uniform distribution.

The procedure of finding the calibration factors for the single modules was the following. The 129.4 MeV peak of reaction (1) was assigned to the module ν if at least 60% of the energy was deposited in that module (central module of the shower). The remaining 40% or less of the total energy being spread over the twelve neighbouring modules was added to the energy in the central module in order to obtain the full energy of 129.4 MeV. This procedure of γ reconstruction needs, of course, the rough intercalibration described above. It worked well for the 24 inner modules. Reconstruction of the energy for the 30 outer modules suffered somewhat from uncontrolled energy escapes. This was estimated by Monte Carlo simulations of the showers using EGS [4], and then corrected accordingly.

In a first step of several iterations, the peak positions c_ν for each module were obtained with the intercalibration from the source calibration, i.e. with intercalibration factors $a_\nu^{(1)} = 1$. The deviation of these peak positions from the average peak position $\langle c \rangle$ determines the correction for the a_ν's. The new intercalibration factors are thus

$$a_\nu^{(2)} = 1 + \left(\frac{\langle c \rangle - c_\nu}{c_\nu} \right).$$

In the second iteration the new intercalibration ($a_\nu^{(2)}$'s) was taken to obtain more accurate factors $a_\nu^{(3)}$. Not more than three iterations were necessary until stability was reached. The accuracy obtained for each a_ν was limited by statistics but was always better than 5%. The improvement in total energy resolution after the first step of iterations was approximately 50%. The final energy resolution was 5.5% FWHM at 130 MeV, if only the inner 24 modules were used as trigger modules. Fig. 7a shows the improved γ spectrum after this intercalibration procedure.

It should be noticed that the calibration factors determined in such a way were applied only in the off-line analysis.

3.2. The absolute energy calibration

The energy scale for the modular γ spectrometer was defined by the peak position of the 129.4 MeV line, the two edges of the γ distribution of reaction (2), and the source peak positions. This still required an extrapolation when measuring energies higher than 130 MeV. Two more calibration points (774 MeV and 938 MeV) were available in the final experiment [5]. The linearity could be influenced by energy dependent shower escapes through the rear face of the detector. EGS-calculations show, however, that such non-linearities amount to 0.5% at most in the energy range from 100 MeV to 1 GeV.

3.3. Stabilization

As the calibration, once established, had to be maintained over periods of several months, a light-pulser system was developed as described above. The light-pulser information (i.e. the PM signals from the 54 modules measured by the same ADCs as those used for the actual data, and the signals from the reference module) was stored on magnetic tape and evaluated off-line. The stabilization, hence, was done only off-line.

In order to stabilize the light-pulser bulb, it first had to be ensured that the reference module PM and its electronics were stable. This was done by adjusting the amplification of the reference module off-line by a time-dependent correction factor A_{ref} so that the ^{22}Na peak (P_{source}) stayed at its defined ($t = 0$) position

$$A_{\text{ref}} = \frac{P_{\text{source}}(0)}{P_{\text{source}}(t)}.$$

The stability of the light-pulser bulb was then obtained by maintaining (correction factor A_{lp}) its peak position in the stabilized reference module ($P_{\text{lp}}^{\text{ref.}}$) at the position it had at $t = 0$ with respect to the ^{22}Na peak

$$A_{l\text{p}} = \frac{P_{l\text{p}}^{\text{ref}}(0)}{A_{\text{ref}} \cdot P_{l\text{p}}^{\text{ref}}(t)}.$$

Once the light pulser was stabilized, it could be used for correcting the instabilities of the single modules of the system. The calibration factors a_ν were corrected off-line so as to maintain the light-pulser peaks (P_{lp}^ν) at the positions define at $t = 0$

$$a_\nu(t) = \frac{P_{l\text{p}}^\nu(0)}{A_{l\text{p}} P_{l\text{p}}^\nu(t)}.$$

The light pulser was measured in the experiment every four hours. In between the four-hourly measurements, the $a_\nu(t)$'s were interpolated. This was possible because the real time was recorded for each individual event during the experiment.

This stabilization controlled only the PMs and the subsequent electronics, but did not control stability of the light output of the NaI module directly. Thus temperature shifts could still take place. However, by housing the reference module and the system of 54 modules in the same heat isolated cabinet, the temperature shifts were minimized.

The quality of the stabilization is demonstated in fig. 7b: using unstabilized calibration factors $\{a_\nu(0)\}$, the instabilities of the system led to a resolution of 11% after a period of 2 months. The absolute energy calibration also changed by ≈ 2%. Switching on the stabilization resulted in a resolution of 7%, as compared to the initial 5.5%. The absolute calibration did not shift more than 1%.

4. Response to pions and electrons

The system's response to pions and electrons of well-defined momenta was investigated separately. The detector was placed in the beam in such a way that its virtual centre was in the focus of the beam. A specially designed support allowed the system to be positioned so that particles could be shot into single modules along their axes. A small plastic scintillator served as the trigger for impinging particles.

Pions (and muons) are expected to lose their energy by ionization only. If their energy is low enough for them to be stopped in the module, part of their rest mass is seen in the detector through their decay or reaction products.

Positive and negative pions are expected to react differently if they stop in the detector. A stopped π^+ can only decay, thus releasing a slow muon (5 MeV), which will stop again but whose decay positron will not be recognized by the system because of the long times involved. A π^-, on the other hand, when stopped will be totally absorbed by nuclear reactions whose decay products will partly be seen by the detector.

In consequence, fast through going pions release energy mostly in the module into which they are shot. Slow stopping pions release all of their kinetic energy in the trigger module. For stopping π^-'s, in addition, some of their rest mass energy is also seen by neighbouring modules. This is demonstrated in fig. 8, where the ratio of the energy deposited in the trigger module to the totally observed energy is displayed for different incident energies.

In the same figure this ratio is displayed also for electrons. The electron being almost massless, it releases its energy like a γ-ray through an electromagnetic shower. Consequently a much larger fraction of its energy is deposited in modules adjacent to the trigger module. The "error bars" in fig. 8 indicate the width of the distribution at half maximum.

The energy dependence of the energy resolution of the detector was measured with electrons in the energy range from 150 MeV to 800 MeV. The nominal momentum resolution of the beam being $\Delta p/p = \pm 2\%$, the resolution showed a weak energy dependence, which can be described by

$$\frac{\Delta E}{E}(\text{fwhm}) = \frac{3.3\%}{\sqrt[4]{E(\text{GeV})}}.$$

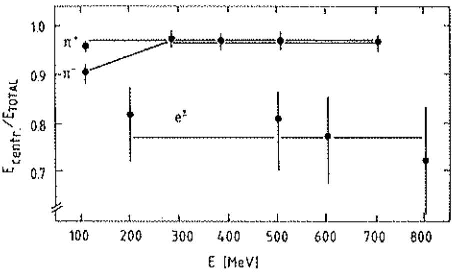

Fig. 8. Response of the detector to π^+, π^- and $e^\pm$. The fractio of energy released in the trigger module ($E_{central}/E_{total}$) plotted as function of particle energy. The error bars indicat the width at half maximum.

5. Shower identification for γ-rays

The conditions leading to an acceptable γ-event hav been defined in such a way as not to introduce an energy dependence of the efficiency nor to reject to many events:

–One of the 24 inner modules was required to con tain at least 40% of the totally registered energy.

–The trigger module together with its 12 direc neighbours was required to contain more than $90[1 - e^{-E(\text{MeV})/58}]\%$ of the total energy. This condition wa imposed in order to reject double events, but was em pirically weakened at lower energies in order to mair tain a constant cut-efficiency.

–The γ-to-pion selection as discussed above wa finally not applied, as the efficiency losses would hav been severe. Instead, a large plastic scintillator in fror of the detector was used to reject charged particles.

6. Conclusions

A 54-module NaI (Tl) detector of spherical geometr (1/13th of the full sphere) was optimized to dete γ-rays from 20 MeV to 1000 MeV. A resolution c $3.3\%/\sqrt[4]{E(\text{GeV})}$ FWHM was obtained. A gain stabi ity of ±0.5% could be maintained over periods c several weeks. The reconstruction efficiency for γ's wa energy independent for energies higher than 70 MeV The response to charged pions and electrons was mea sured.

This work was supported by the Ministry of Re search and Technology of the Federal Republic c Germany and the Swiss National Science foundatio One of us (M.S.) gratefully acknowledges the suppo from CERN. We also thank CERN for its hospitality.

References

[1] M. Suffert, P. Pavlopoulos, K. Zioutas and A. Hegerath, preprint CERN-EP/83-22 (1983), Nucl. Instr. and Meth., to be published.

[2] Y. Chan et al., IEEE Trans. Nucl. Sci. NS 25 (1978) 333.

[3] B. Richter et al., preprint CERN-EP/83-07, to be published in Phys. Letters.

[4] R.L. Ford and W.R. Nelson, report SLAC-210 (1978).

[5] G. Backenstoss et al., preprint CERN-EP/83–58, submitted to Nucl. Phys.

II

Nuclear Physics B228 (1983) 424–438

PROTON–ANTIPROTON ANNIHILATIONS AT REST INTO $\pi^0\omega, \pi^0\eta, \pi^0\gamma, \pi^0\pi^0$, AND $\pi^0\eta'$

G. BACKENSTOSS, M. HASINOFF[1], P. PAVLOPOULOS, J. REPOND, L. TAUSCHER and D. TRÖSTER

Institute for Physics, University of Basle, Switzerland

P. BLÜM, R. GUIGAS[2], H. KOCH, M. MEYER[3], H. POTH, U. RAICH[4] and B. RICHTER

Kernforschungszentrum, Institut für Kernphysik, Institut für experimentelle Kernphysik, Universität Karlsruhe, Karlsruhe, Fed. Rep. Germany

L. ADIELS[4], I. BERGSTRÖM, K. FRANSSON and A. KEREK

Research Institute for Physics, Stockholm, Sweden

M. SUFFERT

Centre de recherches nucléaires and Université Louis Pasteur, Strasbourg, France

K. ZIOUTAS

Department of Nuclear Physics, University of Thessaloniki, Greece

Received 2 May 1983
(Revised 8 July 1983)

Proton–antiproton annihilations at rest in liquid hydrogen were investigated through the inclusive γ spectrum, related to the annihilation. The high-energy part of the spectrum was used to deduce branching ratios for the so far unobserved annihilation channels: $R(p\bar{p}\to\pi^0\omega) = (2.38\pm0.65)\%$, $R(p\bar{p}\to\pi^0\eta) = (0.82\pm0.10)\%$, $R(p\bar{p}\to\pi^0\gamma) = (0.015\pm0.007)\%$, and $R(p\bar{p}\to\pi^0\pi^0) = (0.06\pm0.04)\%$. An upper limit for the $\pi^0\eta'$ channel was deduced to be $R(p\bar{p}\to\pi^0\eta') < 1.1\%$.

1. Introduction

Investigations of $p\bar{p}$ annihilations at rest have so far been done mostly using bubble-chamber techniques, and the most comprehensive review of these works is still the one by Armenteros and French [1]. Updates may be found elsewhere [2].

[1] On leave of absence from the Dept. of Physics, University of British Columbia, Vancouver, Canada.
[2] Present address: BBC, Mannheim, Fed. Rep. Germany.
[3] Now at ESO, Garching, Fed. Rep. Germany.
[4] Now at CERN, Geneva, Switzerland.

From these earlier works it appears that multipionic final states in $p\bar{p}$ annihilation are frequently reached via intermediate resonance production, e.g.

$$p\bar{p} \to \rho^0 \pi^0 = \pi^+\pi^-\pi^0 .$$
$$\hookrightarrow \pi^+\pi^-$$

Only those intermediate states could have been identified there for which the final states contain at most one π^0. Final states with more than one π^0 or purely neutral channels are very difficult to determine in bubble-chamber experiments owing to their poor sensitivity to γ radiation.

New information on annihilation channels involving more than one π^0 in the final state (or simple, purely neutral channels) can be expected from experiments using γ spectrometers of sufficient resolution.

In an experiment on the inclusive γ spectrum after $p\bar{p}$ annihilation at rest, we were able to measure branching ratios for the so far unobserved multi-π^0 channels $\pi^0\omega$, $\pi^0\eta$, and the channel $\pi^0\gamma$. A new value for the $\pi^0\pi^0$ and an upper limit for the $\pi^0\eta'$ channel were deduced as well.

2. The experiment

2.1. EXPERIMENTAL SET-UP

The experiment was set up at the low-energy electrostatically separated k_{23} beam at the CERN proton synchrotron (PS). A detailed description of the layout is given elsewhere [3] and only the essentials will be described here.

A low-energy $\bar{p}$ beam (600 MeV/c) of $\Delta p/p \approx \pm 2\%$ was slowed down in a graphite moderator and then stopped in a 25 cm long liquid-hydrogen (LH_2) target. The moderation was adjusted such that the maximum of the range distribution was in the centre of the target; the longitudinal width of this distribution (FWHM) was equivalent to about 14 cm of LH_2.

The target was viewed by a large modular NaI γ spectrometer placed perpendicularly to the beam. The properties of this spectrometer have been described elsewhere [4]. Events where charged particles entered the γ spectrometer were rejected, using plastic scintillators in front and at the sides of the NaI spectrometer. Double γ events were recognized by topology cuts and were rejected as well. These rejections lead to a reduction of the order of 5% each.

2.2. DATA-TAKING AND RESULTS

The γ radiation emerging after $p\bar{p}$ annihilation was measured for 33×10^6 $\bar{p}$'s entering the target. The effective running time was about two weeks in total. During this time, the system could be stabilized off line to better than 1%. The resulting

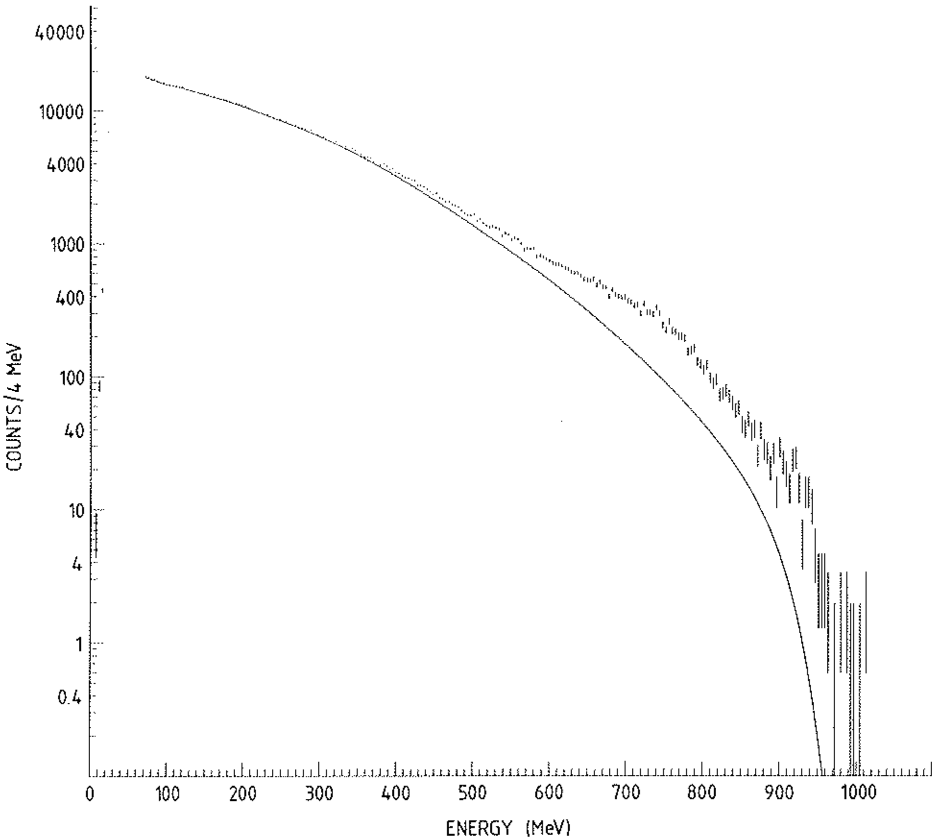

Fig. 1. Inclusive γ spectrum as obtained from 33×10^6 $\bar{p}$'s. The solid line represents the continuous background as defined by eq. (2) and scaled to the data.

spectrum is shown in fig. 1 in logarithmic scale. It exhibits a smooth behaviour and ends sharply, as it should, at ~950 MeV.

3. Analysis

3.1. METHOD

Proton–antiproton annihilation at rest leading to two-body final states, where one particle decays into two γ's, such as

$$p\bar{p} \to \pi^0 X, \quad \pi^0 \to \gamma\gamma$$

may be studied via the γ spectrum of the decaying particle. Owing to the fact that

TABLE 1
Limits of the uniform distributions of the γ spectra for some two-body channels in $p\bar{p}$ annihilation at rest

Channel	Decaying particle	E^{γ}_{min} (MeV)	E^{γ}_{max} (MeV)
$p\bar{p} \to \pi^0\omega$	$\pi^0 \to \gamma\gamma$	5.88	774.15
	$\omega \to \pi^0\gamma$	159.25	904.65
$p\bar{p} \to \pi^0\eta$	$\pi^0 \to \gamma\gamma$	5.31	857.57
	$\eta \to \gamma\gamma$	80.71	932.97
$p\bar{p} \to \eta\omega$	$\eta \to \gamma\gamma$	99.62	755.80
	$\omega \to \pi^0\gamma$	177.05	813.70
$p\bar{p} \to \eta\eta$	$\eta \to \gamma\gamma$	88.62	849.66
$p\bar{p} \to \pi^0\pi^0$	$\pi^0 \to \gamma\gamma$	4.88	933.40
$p\bar{p} \to \pi^0\gamma$	$\pi^0 \to \gamma\gamma$	4.85	938.28
			($E_\gamma = 933.43$)
$p\bar{p} \to \pi^0\eta'$	$\pi^0 \to \gamma\gamma$	6.58	692.24
$p\bar{p} \to \eta\eta'$	$\eta \to \gamma\gamma$	114.05	660.16

the particles are monoenergetic, the γ spectrum exhibits a uniform shape between the limits

$$E^{\gamma}_{max/min} = \tfrac{1}{2}E(1 \pm \beta)\,, \tag{1}$$

where E is the total energy of the decaying particle and β is its velocity. The edges of these distributions are sharp if the particles involved have narrow widths, and thus may show up in the inclusive γ spectrum from $p\bar{p}$ annihilation at rest. The lower the background and the better the resolution, the higher are the chances of observing these edges. Thus at the high-energy end of the spectrum (fig. 1) such edges are most likely to be observed.

Table 1 shows the limits of the uniform γ distribution for some relevant annihilation channels. From the table one may conclude that the lower edges are of no use, as they are either below the experimental energy threshold (~20 MeV) or just fall into regions where the background is highest.

3.2. MONTE CARLO SIMULATION

3.2.1. Construction of the γ spectrum. The crucial point in extracting the uniform distributions from the experimental γ spectrum is the proper subtraction of the continuous background which comes from annihilations into more than two particles. To this end, the γ spectrum was simulated by Monte Carlo calculations, using the annihilation channels of table 2 and ignoring any influence of the apparatus. This spectrum is shown in fig. 2. It was used to extract the shape of the continuous background. The assumption has to be made that the purely neutral channels, which are not contained in the simulated spectrum, produce the same spectral shape.

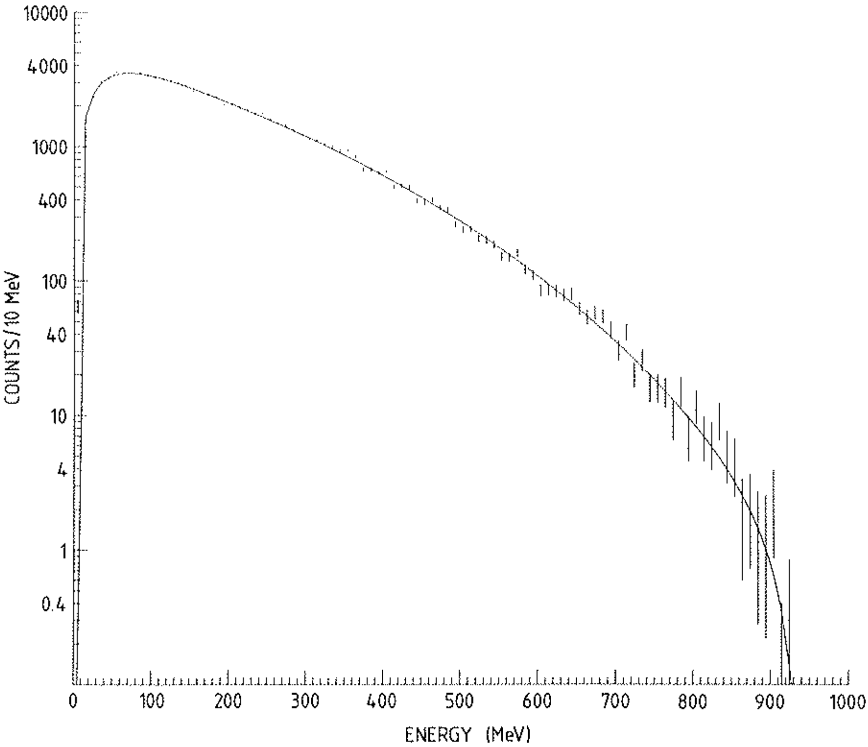

Fig. 2. γ spectrum from a Monte Carlo simulation using the annihilation channels from table 2. The solid line represents the fit to it.

The simulated spectrum was then approximated by an analytical function. This shape function has the form

$$F(E_\gamma) = N[(E_0 - E_\gamma)^{\alpha_1}\,e^{\beta_1} + (E_0 - E_\gamma)^{\alpha_2}\,e^{\beta_2} + \beta_3\,e^{\alpha_3 E_\gamma}]\,, \tag{2}$$

with

$$\begin{aligned} &E_0 = 938.28\,[\mathrm{MeV}]\,, && \beta_2 = -19.9818\,, \\ &\alpha_1 = 4.1548\,, && \alpha_3 = -0.03273\,[\mathrm{MeV}^{-1}]\,, \\ &\beta_1 = -33.4948\,, && \beta_3 = -0.006921\,. \\ &\alpha_2 = 1.6732\,, && \end{aligned}$$

With these constants, which (except E_0 and N) were fit parameters, the expression in the brackets of eq. (2) is normalized to one. The constant N being the average number of γ's per annihilation, the shape function $F(E_\gamma)$ represents the average number of γ's per MeV and per annihilation. The constant N has to be determined appropriately, as will be described in sect. 4. Inspection of $F(E_\gamma)$ shows that at high energies the term $(E_0 - E_\gamma)^{\alpha_2}\,e^{\beta_2}$ is dominant.

Fig. 2 demonstrates the quality of the fit. The spectrum can be reproduced from 20 MeV to 1000 MeV with only six free parameters and a χ^2/DF of only 1.33.

It is assumed that the spectral shape given by eq. (2) represents well the continuous part of the real spectrum. This might not fully correspond to reality since the intermediate resonances in the channels with more than one π^0 are not known. Double hit rejection essentially leads to reduction of high-multiplicity annihilation channels and thus affects mostly the lower energies.

3.2.2. Normalization of the simulated spectrum. In order to relate the shape function (1) to the number of annihilations, the number of γ's per annihilation has to be evaluated. This number is defined by

$$N_\gamma = \frac{\sum_\nu R_\nu N_\gamma^\nu}{\sum_\nu R_\nu},$$

where R_ν is the branching ratio of the channel ν, and N_γ^ν is the average number of γ's for this channel, as indicated in table 2. The number of γ's from the decay of ω's and η's was taken to be 2.06 and 3.20, respectively.

From table 2 the average number of γ's per annihilation is derived to be

$$N_\gamma = 3.93 \pm 0.24 . \tag{3}$$

The error stems mostly from the uncertainties of the branching ratios, i.e. N_γ may be wrong by $\pm 6\%$. A further source of error might be found in the average multiplicity of π^0's in the purely neutral channels, leading to an estimated error of $\pm 0.06\gamma$'s per annihilation.

Since the Monte Carlo simulated spectrum does not account for the uniform distributions of two-body annihilations, their contributions have to be subtracted from the above number. Anticipating the final results for these uniform distributions (see sect. 4), 0.11 γ's per annihilation have to be deduced. Thus the average number of γ's for the continuous part of the spectrum is 3.82 per annihilation, and the factor N in eq. (2) is

$$N = 3.82 . \tag{4}$$

3.3. NORMALIZATION AND BACKGROUND SUBTRACTION FOR THE EXPERIMENTAL SPECTRUM

The total γ-spectrum emerging from $\mathrm{p\bar{p}}$ annihilation at rest is assumed to be composed of the continuous part discussed in the previous subsections 3.2.1 and 3.2.2 and a superposition of distributions from two-body annihilation channels of table 1. The measured spectrum may therefore be approximated by a function of the form

$$S(E_\gamma) = S_0 \left[F(E_\gamma) + \sum_\nu R_\nu B_\nu(E_\gamma) \right], \tag{5}$$

TABLE 2

Branching ratios and relative number of γ's from $p\bar{p}$ annihilation at rest

Channel	Branching ratio R (%)	Number of γ's $=R(\%)\times N_\gamma$	Comment	Ref.
$\pi^+\pi^-\pi^0$	3.7	7.4	MC	[1]
$\pi^+\pi^-\pi^0(\rho^\mp\pi^\pm)$	2.7	5.4	MC	[1]
$\pi^+\pi^-2\pi^0$	9.3	37.2	MC	[2b]
$\pi^+\pi^-3\pi^0$	23.3	139.8	MC	[2b]
$\pi^+\pi^-4\pi^0$	2.8	22.4	MC	[1]
$2\pi^+2\pi^-\pi^0(\omega\pi^+\pi^-)$	3.8	7.83	MC	[1]
$2\pi^+2\pi^-\pi^0(\rho^0\pi^0\pi^+\pi^-)$	7.3	14.60	MC	[1]
$2\pi^+2\pi^-\pi^0(\rho^\pm\pi^\mp\pi^+\pi^-)$	6.4	12.80	MC	[1]
$2\pi^+2\pi^-2\pi^0$	16.6	66.40	MC	[2b]
$2\pi^+2\pi^-3\pi^0$	4.2	25.20	MC	[2b]
$3\pi^+3\pi^-\pi^0$	1.3	2.60	MC	[1]
$\pi^+\pi^-\eta$	1.2	3.84	MC	[1]
$2\pi^+2\pi^-\eta$	0.6	1.92	MC	[1]
$\pi^0\rho$	1.4	2.80		[1]
$\eta\rho$	0.22	0.64		[1]
$n\pi^0$	3.2	31.90 [a])		[1]
$\pi^+\pi^-$	0.4	0		[2a]
$2\pi^+2\pi^-$	6.9	0		[2a]
$3\pi^+3\pi^-$	2.1	0		[2a]
$K\bar{K}n\pi(n\geq 0)$	6.82	26.95 [b])		[1]
total	104.24	409.72		

[a]) Obtained with an average number of π^0's of 4.99.
[b]) Assuming 0.95 π^0's on the average.

Channels used for Monte Carlo simulation are marked MC. Branching ratios are taken from refs. [1] and [2]. The values from ref. [2b] are not measured but obtained from a model-dependent evaluation.

where $F(E_\gamma)$ is defined by eqs. (2) and (4), R_ν is the branching ratio of the annihilation channel ν, and S_0 is a scaling factor.

The $B_\nu(E_\gamma)$ in eq. (5) is the function describing the γ-energy distribution for the channel ν,

$$B_{p\bar{p}\to ab}=\frac{\Gamma_{a\to\gamma's}}{\Gamma_a^{tot}}B^a(E_\gamma)+\frac{\Gamma_{b\to\gamma's}}{\Gamma_b^{tot}}B^b(E_\gamma)\,,$$

with $\Gamma_{a,b\to\gamma's}$ being the partial widths of the particle a or b decaying into γ's (e.g. $\Gamma_{\eta\to\gamma\gamma}/\Gamma_\eta^{tot}\approx 0.3$). The $B^{a,b}(E_\gamma)$ are the uniform distributions defined by

$$B^{a,b}(E_\gamma)=\frac{N_\gamma^{a,b}}{E_{max}^{a,b}-E_{min}^{a,b}}\ \text{for}\ E_{min}^{a,b}\leq E_\gamma\leq E_{max}^{a,b}$$

$$=0\ \text{otherwise}\,.$$

E_{max} and E_{min} are defined by eq. (1) and table 1; $N_\gamma^{a,b}$ is the number of monoenergetic γ's into which particle a or b decay at rest.

With these definitions the integral of the expression in brackets of eq. (5), i.e. $\int_0^\infty S(E_\gamma)/S_0\,dE_\gamma$ equals the average number of γ's per annihilation. Hence S_0 represents the number of $p\bar{p}$ annihilations which contributed to the measured spectrum.

The scaling factor S_0 is determined by a fit of eq. (5) to the measured spectrum. In order to reduce the number of parameters to a minimum, a fit region has to be selected where none of the boxes starts or ends. Then eq. (5) has only two free parameters, namely S_0 and a constant $C=\sum R_\nu B_\nu$, i.e.

$$S(E_\gamma)=S_0[F(E_\gamma)+C]\,. \tag{6}$$

After folding this function with the experimental energy-resolution, it was fitted to the measured spectrum in the energy range from 400 to 600 MeV. The accuracy of this determination of S_0 is ±5%.

The advantage of such a normalization procedure is obviously its independence of errors in solid angle, stop-rates, dead-time of the electronics, etc. Fig. 3 shows the measured spectrum after subtraction of the continuous background $S_0F(E_\gamma)$ and the distributions of the known $\pi^0\rho^0$ and $\eta\rho^0$ contributions as specified in table 2. This reduced spectrum is then approximated by the function

$$S^{\text{red}}(E_\gamma)=S_0\sum_\nu R_\nu B_\nu(E_\gamma)\,,$$

folded with the detector resolution. The branching ratios R_ν are the fitting parameters.

3.4. FITTING PROCEDURES

3.4.1. Energy calibration, resolution, and continuous background. The parameters to be verified before entering into the detailed analysis of the spectrum are the energy calibration and the resolution of the γ spectrometer.

The energy calibration was obtained from the reactions $\pi^-p\rightarrow n\gamma$ and $n\pi^0$ at rest, as described in ref. [4]. A final adjustment was done using the end point of the spectrum E_0 [eq. (2)] and the edge of the $\pi^0\omega$ distribution at $E=774.15$ MeV.

The resolution, as determined in ref. [4] from the reaction $\pi^-p\rightarrow n\gamma$ at rest, does not have to be the same as in the $\bar{p}$ experiment since the detector load is different. In fact there is no way of checking the energy resolution on-line. It is therefore a parameter to be determined. The resolution turned out to be not entirely independent of the composition of channels contributing to the spectrum, particularly the $\pi^0\rho^0$ channel (see sect. 4) and hence was not treated independently.

The analysis is based on the assumption that the continuous background is properly described in eq. (2). Variation of the parameter α_2 in eq. (2) when fitting the spectrum showed correlations between α_2 and $\pi^0\omega$ and $\pi^0\eta$ and less or no correlation for the other channels. In the further analysis, α_2 is, however, kept fixed.

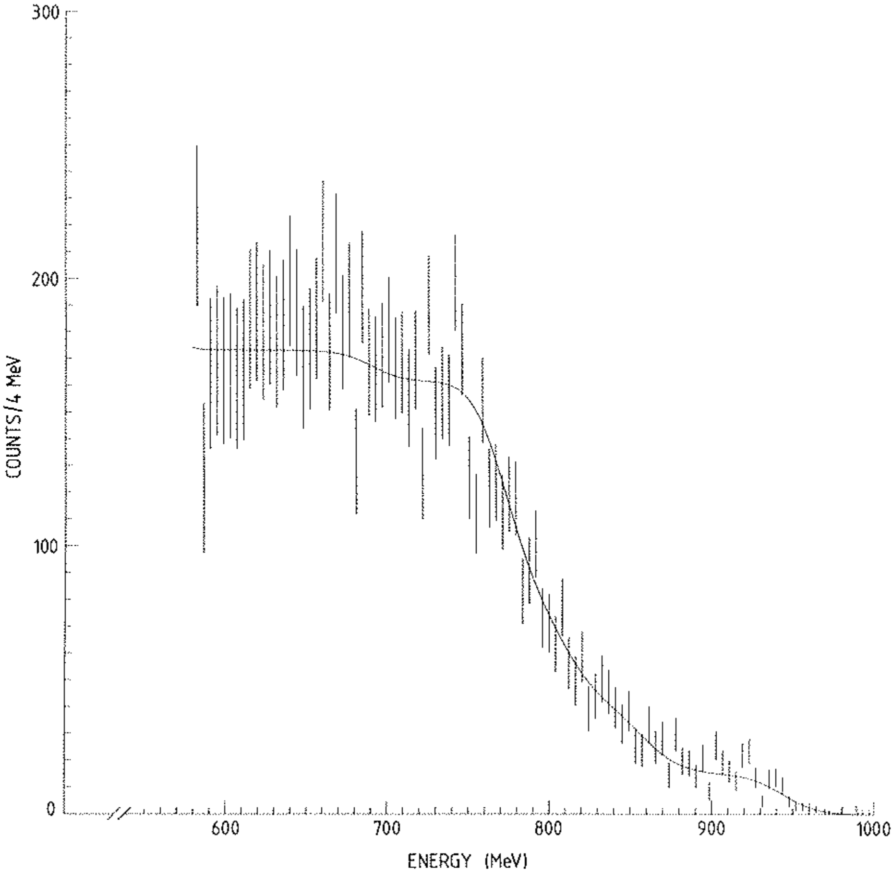

Fig. 3. Experimental spectrum after subtraction of the continuous background and the $\pi^0\rho^0$ and $\eta\rho^0$ contributions. The solid line shows the fit.

3.4.2. Procedures for the different annihilation channels. From the channels listed in table 1, those whose uniform distributions ("boxes") end at different energies are quite independent of each other. However, the channels where the box-edges are not resolved are correlated to a great extent. The latter case holds particularly for the channels $\pi^0\omega$, $\eta\omega$ and $\pi^0\eta$, $\eta\eta$. It was thus impossible to disentangle their individual contributions. Instead, an over-all η/π^0 ratio of 0.16 was adopted when fitting the spectrum. This value is suggested by the ratio of the measured branching ratios (see table 2) of $\eta\rho^0/\pi^0\rho^0 = 0.16 \pm 0.10$. The η/π^0 ratio was also varied stepwise within the limits $0 \leq \eta/\pi^0 \leq 0.33$ in order to estimate systematic errors.

The $\pi^0\omega$ and $\pi^0\rho^0$ channels obviously interfere, as the masses of ρ and ω are almost identical. The $\pi^0\rho^0$ channel leads, however, to a smeared-out edge owing to the width of the ρ. This in consequence leads also to some correlation with the detector resolution. The fits were therefore done for different $\pi^0\rho^0$ contributions, varying between 1.4 and 1.8%, and for different values for the detector resolution, varying between $3.5\%/\sqrt[4]{E}$ and $5.5\%/\sqrt[4]{E}$ (where E is measured in GeV). The data favour a $\pi^0\rho^0$ contribution of 1.6%, which is somewhat higher than that listed in table 2, but still compatible with it. This value was adopted for the final fits. The resolution was found to be with large errors around $5\%/\sqrt[4]{E}$, and was fixed at this value for the further fits.

The $\pi^0\eta$ channel has a box-edge energy which renders its contribution extremely uncorrelated and thus obtainable with the least amount of ambiguities.

Both channels, *$\pi^0\eta'$ and $\eta\eta'$*, have their box-edges at energies below the $\pi^0\omega$ edge. They are thus showing up in regions of the spectrum where the background is already high. The determination of their branching ratios is correspondingly difficult, and values between 0 and 0.5% for $\pi^0\eta'$ were obtained under the different fit conditions.

The edges of both the *$\pi^0\pi^0$ and the $\gamma\pi^0$ channel* and the γ peak of the $\pi^0\gamma$ channel fall with 5 MeV (see table 1) and are thus not resolved. The correlation between the two channels is, however, not very high. A simultaneous fit of both parameters resulted in a branching ratio of $(0.06\pm0.04)\%$ for $\pi^0\pi^0$. Since the $\pi^0\pi^0$ channel had been measured before [5, 6], it was kept fixed at values between $0.01 \leqslant \pi^0\pi^0 \leqslant 0.08\%$ when fitting, thus allowing for estimates of systematic errors. In the final fits a value of 0.04% was adopted for $\pi^0\pi^0$, a value which is close to that of ref. [5] and which is slightly favoured by our data with respect to the lower value of 0.014% quoted in ref. [6].

The edges of the distributions from $\pi^0\omega$, $\pi^0\eta$, and $\pi^0\pi^0$ show up at energy intervals of ~80 MeV, and thus are well resolved. The data require an additional distribution ending at 811 MeV, coming from a hypothetical process $p\bar{p}\rightarrow\pi^0X$. This assumption is arbitrary, and a process $p\bar{p}\rightarrow\gamma X$ would, from the fitting point of view, work equivalently. One may, nevertheless, obtain a reasonably good fit without π^0X by increasing the resolution to $6.7\%/\sqrt[4]{E[\mathrm{GeV}]}$. Such a high value is, however, unjustified in view of the high performance of the γ detection system [4].

3.4.3. Parameter variations, errors, and results. When fitting the spectrum, the branching ratios R [see eq. (5)] of the channels $\pi^0\eta'$, $\pi^0\omega$, π^0X, $\pi^0\eta$, and $\pi^0\gamma$ were always varied simultaneously, but under different conditions for $\pi^0\pi^0$, $\pi^0\rho^0$, η/π^0, resolution, and α_2, as described in subsects. 3.4.1 and 3.4.2. The results are listed in table 3. The branching ratios R have statistical errors as obtained from a MINOS error analysis [7]. In addition, systematic errors are quoted which reflect the maximum and minimum values obtained for R under the different fit conditions.

Furthermore, all branching ratios have an uncertainty of ±6% of their value originating from the error of N_γ (eq. (3)) and of ±5% from the scaling factor S_0 of the function (eq. (6)).

The fit quality is demonstrated by the solid line in fig. 3. The single distributions as used for the final fit are displayed in fig. 4.

TABLE 3

Results for branching ratios of different channels in $p\bar{p}$ annihilation at rest

Channel	Yield	Error (stat.)	Error (syst.)	Yield
$\pi^0\eta'$	0.30	± 0.53	$+0.58$ -0.30	0.30
$\pi^0\omega$	2.38	± 0.27	$+0.32$ -0.52	3.45
$\pi^0\eta$	0.82	± 0.07	± 0.06	0.84
π^0X	1.19	± 0.25	± 0.44	0.00
$\pi^0\gamma$	0.015	± 0.004	± 0.003	0.015
$\pi^0\pi^0$	0.06	± 0.03	± 0.01	0.06
χ^2/DF		1.16		1.29

Yields are given in per cent of all annihilations. The $\pi^0\rho^0$ yield was assumed to be 1.6%, and an η/π^0 ratio of 0.16 was used. The last column shows the results for $R_{\pi^0 X} = 0$. In this case the resolution had to be increased to $6.7\%/\sqrt[4]{E}$ [GeV].

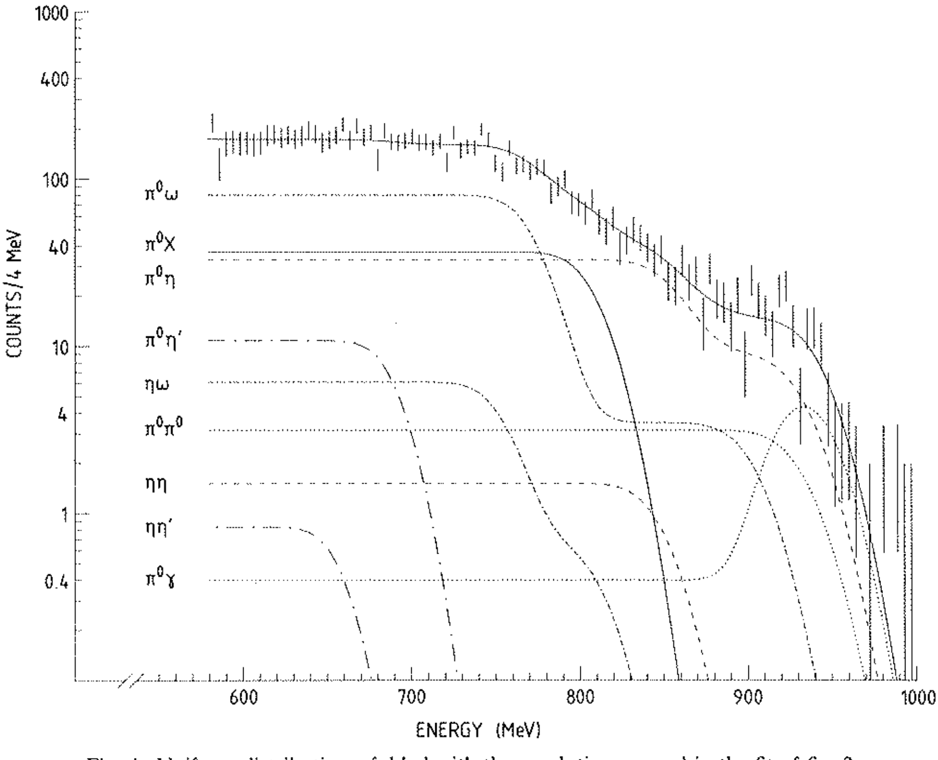

Fig. 4. Uniform distributions, folded with the resolution as used in the fit of fig. 3.

For comparison the results are also listed in table 3 for the case where the hypothetical channel π^0X is omitted.

It should be noted that the π^0 annihilation channels of table 3 together with the corresponding η-channels yield 0.11 γ's per annihilation which contribute to uniform distributions. This result was used already in subsect. 3.2.2.

4. Discussion of results

4.1. $p\bar{p} \to \pi^0\omega$

The branching ratio of this state is found to be 2.38%. This value is surprisingly high if we compare it with the result for the equivalent reaction in $\bar{p}n$ annihilation at rest, whose branching ratio is $R(\bar{p}n \to \omega\pi^-) = (0.41 \pm 0.08)\%$ [8]. The initial state for both reactions, $p\bar{p} \to \pi^0\omega$ and $\bar{p}n \to \pi^-\omega$, could be an $l = 1$ state but in liquid hydrogen most likely is a $^3S_1$ state. Assuming only atomic S-states, the $^3S_1$ state population in the $p\bar{p}$ atom is 75%, but in the $\bar{p}n$ case, which is formed from a $\bar{p}d$ atom, it is only 66%. Moreover, the $\bar{p}n$ is a pure $I = 1$ state, but the $p\bar{p}$ state is an isospin mixture, whereas the final $\pi\omega$ state is in both cases pure $I = 1$. We therefore expect

$$\frac{\Gamma(p\bar{p} \to \pi^0\omega)}{\Gamma(\bar{p}n \to \pi^-\omega)} = \frac{1}{2} \times \frac{0.75}{0.66} = 0.52\,,$$

and thus $\pi^0\omega = 0.2\%$, assuming pure S-wave absorption. The latter condition seems to be controlled by the observation of the recoil proton in the deuterium bubble chamber, when the $\bar{p}$ is absorbed on the neutron of the deuterium. A momentum cut at 250 MeV/c should largely eliminate P-wave annihilation [8]. In our experiment a similar control was not possible, and P-wave annihilation from interactions in flight may occur in a few per cent of all $p\bar{p}$ annihilations, as discussed in the next subsection, but by no means could it account for 2% of the extra $\pi^0\omega$ final states.

On the other hand, the inclusive ω production in $p\bar{p}$ annihilation at rest was found in a bubble-chamber experiment to be comparable with inclusive ρ^0 production [9].

4.2. THE CHANNEL $p\bar{p} \to \pi^0\eta$

The $\pi^0\eta$ channel is found to be 0.82%. This is unexpectedly high in view of the fact that this annihilation channel has to come from an initial p-state. The generally believed S-wave dominance in annihilations of $\bar{p}$'s in liquid targets, caused by Stark mixing in the initial atomic states, seems to be at variance with this finding. P-wave annihilation could, however, occur in reactions in flight. Our experiment has no control over whether or not a $\bar{p}$, entering the 25 cm long H_2 target, really stops before annihilating. In fact the momentum spectrum of $\bar{p}$'s when entering the target extends up to 360 MeV/c. Since the beam keeps its direction when slowing down in the target, and since our detector sees only γ radiation perpendicular to the beam axis, the γ-energy distortions are of the order of $\beta^2_{\bar{p}p} \approx 1\%$. Thus in this experiment interactions in flight are indistinguishable from interactions at rest. On the other hand, of all $\bar{p}$'s entering the target, at most $\sim 4\%$ would annihilate in flight, and thus cannot alone lead to the above branching ratio for $\pi^0\eta$.

A sizeable P-wave annihilation has already been seen in the channel $\bar{p}p \to \pi^0\pi^0$. There it was concluded that it amounts to as much as 38% of the annihilations going to $\pi\pi$ [5].

4.3. $p\bar{p} \to \pi^0\pi^0$

The $2\pi^0$ final state can only be reached from initial $^3P_0$ and $^3P_2$ states. Its branching ratio had been determined by two experiments to be $(0.048 \pm 0.010)\%$ [5] and $(0.014 \pm 0.003)\%$ [6], respectively. Our result of $(0.06 \pm 0.04)\%$ favours the higher value.

4.4. $p\bar{p} \to \pi^0\gamma$

This channel is formed from initial $^3S_1$ and $^1P_1$ states and was never observed before. The branching ratio was determined to be 0.015%. In the frame of vector dominance the $\pi^0\gamma$ channel is linked to the channels involving vector mesons such as $\pi^0\rho^0$, $\pi^0\omega$, etc. Assuming pure s-wave annihilation (hence p-wave in the final state) we obtain in a straightforward calculation

$$R_{\pi^0\gamma} = \frac{4\pi}{f^2_{\rho\gamma}}\alpha\left[R_{\pi^0\rho} + 2\frac{f_{\rho\gamma}}{f_{\omega\gamma}}\sqrt{R_{\pi^0\rho}R_{\pi^0\omega}}\cos(\phi_{\pi^0\rho} - \phi_{\pi^0\omega}) + \frac{f^2_{\rho\gamma}}{f^2_{\omega\gamma}}R_{\pi^0\omega}\right]\left(\frac{P_\gamma}{P_\rho}\right)^3 .$$

Here α is the fine-structure constant, f is the vector meson-photon coupling constant, ϕ is the strong phase and $(P_\gamma/P_\rho)^3$ is the p-wave phase-space factor, the P's being the momenta and $P_\rho \approx P_\omega$. Using the measured value of table 3 for $R_{\pi^0\omega}$, the value of table 2 for $R_{\pi^0\rho}$, $f^2_{\rho\gamma}/4\pi = 2.26$ and $f^2_{\omega\gamma}/4\pi = 18.4$, and assuming $\cos(\phi_{\pi^0\rho} - \phi_{\pi^0\omega}) \approx 1$ we obtain

$$R_{\pi^0\gamma} = 0.017\% ,$$

in agreement with our measurement.

4.5. $p\bar{p} \to \pi^0X$

The fact that reproducing the spectrum properly requires a reaction involving a particle X is puzzling. Although the spectrum could be fitted by using a reaction of the type $p\bar{p} \to \gamma X'$, the reaction π^0X was considered to be the more likely one in $p\bar{p}$ annihilation, if the process is considered as a physical process at all rather than as a particular way of correcting the background. The particles mass would be

$m_X = 680$ MeV and its width narrow, thus falling into a domain which is reserved for the ground states of the light quark $q\bar{q}$, or more exotic configurations. The nature of the phenomenon has to await a final clarification in forthcoming experiments on dedicated π^0 spectroscopy.

4.6. $p\bar{p} \to \pi^0\eta'$

Owing to reasons already discussed in subsect. 3.4.2, this channel was not seen clearly. The upper limit for it with 1σ confidence is

$$\pi^0\eta' < 1.1\% .$$

4.7. THE CHANNELS $p\bar{p} \to \eta\omega, \eta\eta$, ETC.

These channels were not determined separately since they interfere too much with the corresponding channels $\pi^0\omega$, $\pi^0\eta$, etc. Instead, an over-all ratio $\eta\omega/\pi^0\omega = \eta\eta/\pi^0\eta = \eta\rho^0/\pi^0\rho^0 = \eta\eta'/\pi^0\eta'$ was assumed. This ratio could still not be determined uniquely, and fits usually converged to values between 0 and 0.28 with a statistical uncertainty of ± 0.22. We conclude from our data that with 1σ confidence

$$\eta/\pi^0 < 0.50 .$$

In inclusive η production in low-energy $p\bar{p}$ annihilation the η/π^0 ratio was found [9] to be $\eta/\pi^0 < 0.11$ with 90% confidence.

5. Summary and conclusions

By analysing the high-energy portion of the inclusive γ spectrum after $p\bar{p}$ annihilation at rest, it was possible to obtain branching ratios for the so far unobserved annihilation channels $p\bar{p} \to \pi^0\omega$, $\pi^0\eta$, and $\pi^0\gamma$. Whereas the $\pi^0\gamma$ branching ratio is in accordance with vector dominance, the large $\pi^0\omega$ contribution to annihilation cannot be explained easily. The S-wave dominance in $p\bar{p}$ annihilation at rest seems not to hold generally, as is indicated by the large $\pi^0\eta$ branching ratio. Upper limits could be obtained for the channel $\pi^0\eta'$ and for the η/π^0 ratio in the reactions $p\bar{p} \to \pi^0\omega/\eta\omega$, $\pi^0\eta/\eta\eta$.

Pure single γ spectroscopy, provided the spectrometer resolution is sufficiently good, has thus proved to be a useful method of investigating annihilation channels involving more than one π^0 in the final state or purely two-body neutral channels. Direct π^0 spectroscopy by $\gamma\gamma$ coincidence measurements seems therefore to be the next step in further studies of $p\bar{p}$ annihilations at rest.

We are grateful to the CERN Data Handling Division for providing us with the data-acquisition systems, and to L. Mazzone for the hydrogen target. The help of G. Raffi, H. Johanson, Th. Köhler and A. Lundin is gratefully acknowledged.

This work was supported by the Swiss National Science Foundation and by the Federal Ministry for Research and Technology of Germany.

References

[1] R. Armenteros and B. French, Antinucleon–nucleon interactions in high-energy physics, ed. E.H.S. Burhop (Academic Press, New York, 1969), vol. IV, p. 237

[2a] R. Armenteros, CERN PS proposal CERN/PSCC/80-101 (1980)

[2b] C. Ghesquière, Proc. Symp. Antinucleon–nucleon interactions, ed. L. Montanet (Liblice-Prague), CERN, Geneva, CERN 74-18, 1974, p. 436

[3] L. Adiels, I. Bergström, K. Fransson, A. Kerek, G. Backenstoss, M. Hasinoff, J. Repond, P. Pavlopoulos, L. Tauscher, D. Tröster, P. Blüm, R. Guigas, H. Koch, M. Meyer, H. Poth, U. Raich, B. Richter, M. Suffert and K. Zioutas, New results in the search for narrow states in the $p\bar{p}$ system below threshold, in preparation;
B. Richter, L. Adiels, G. Backenstoss, I. Bergström, P. Blüm, K. Fransson, M. Glöckner, R. Guigas, M. Hasinoff, A. Kerek, H. Koch, T. Köhler, M. Meyer, P. Pavlopoulos, H. Poth, U. Raich, J. Repond, M. Suffert, L. Tauscher, D. Tröster and K. Zioutas, Phys. Lett. 126B (1983) 284

[4] P. Blüm, R. Guigas, H. Koch, M. Meyer, H. Poth, U. Raich, B. Richter, G. Backenstoss, M. Hasinoff, P. Pavlopoulos, J. Repond, L. Tauscher, D. Tröster, L. Adiels, I. Bergström, K. Fransson, A. Kerek, M. Suffert and K. Zioutas, Nucl. Instr. Meth. 213 (1983) 251
CERN-EP/83-37 (1983), Nucl. Instr. Meth., to be published

[5] S. Devons, T. Kozlowski, P. Nemethy, S. Shapiro, N. Horowitz, T. Kalogeropoulos, J. Skelley, R. Smith and H. Uto, Phys. Rev. Lett. 27 (1971) 1614

[6] G. Bassompierre, G. Binder, P. Dalpiaz, P.F. Dalpiaz, G. Gissinger, S. Jacquey, G. Maderni, C. Peroni, M.A. Schneegans and L. Tecchio, Proc. 4th European Antiproton Symp. Barr (Strasbourg), ed. A. Freidman (CNRS, Paris, 1979), vol. I, p. 139

[7] F. James and M. Roos, Comp. Phys. Comm. 10 (1975) 343

[8] A. Bettini, M. Cresti, S. Limentani, L. Peruzzo, S. Santangelo, S. Sartori, L. Bertanza, A. Bigi, R. Carrara, R. Casali and P. Lariccia, Nuovo Cim. A47 (1967) 642

[9] G. Levman, R. Singer and T. Fields, Phys. Rev. D21 (1980) 1

NEW RESULTS IN THE SEARCH FOR NARROW STATES IN THE $p\bar{p}$ SYSTEM BELOW THRESHOLD

Basle–Karlsruhe–Stockholm–Strasbourg–Thessaloniki Collaboration

B. RICHTER [b], L. ADIELS [c,1], G. BACKENSTOSS [a], I. BERGSTRÖM [c], P. BLÜM [b], K. FRANSSON [c], M. GLÖCKNER [b], R. GUIGAS [b,2], M. HASINOFF [a,3], A. KEREK [c], H. KOCH [b], T. KÖHLER [b], M. MEYER [b,4], P. PAVLOPOULOS [a], H. POTH [b], U. RAICH [b,1], J. REPOND [a], M. SUFFERT [d], L. TAUSCHER [a], D. TRÖSTER [a] and K. ZIOUTAS [e]

[a] *Institut for Physics, University of Basle, Switzerland*

[b] *Kernforschungszentrum und Universität Karlsruhe, Institut für Kernphysik, Karlsruhe, Germany*

[c] *Research Institute for Physics, Stockholm, Sweden*

[d] *Centre de Recherches Nucléaires and Université Louis Pasteur, Strasbourg, France*

[e] *Department of Nuclear Physics, University of Thessaloniki, Greece*

Received 19 January 1983

The γ-ray spectrum after $p\bar{p}$ annihilation at rest was measured in two independent high-statistics runs. Both spectra show narrow peaks, corresponding to masses of 1210, 1638, 1694 and 1771 MeV.

More than five years ago, two experiments were carried out to look for discrete γ-rays from stopped antiprotons. One, performed by the Syracuse group [1] at BNL, gave only an upper limit of ~3% on the yield of monoenergetic gammas. The other, performed by the Basle–Karlsruhe–Stockholm Collaboration at CERN [2], claimed three monoenergetic gamma rays with a yield of a few per mille (fig. 1a), reflecting the existence of narrow states strongly related to the $p\bar{p}$ system.

Various theoretical ideas [3] based on nuclear physics arguments, quark models, and the dual topological unitarization led to the expectation of massive mesons, called baryonium, coupled strongly to the $p\bar{p}$ channel but weakly to ordinary mesons, thus resulting in a virtually high stability, particularly for states below the $p\bar{p}$ threshold. If there exist bound states of $N\bar{N}$, a highly characteristic way of revealing them would be by the observation of γ transitions between them or from the atomic $p\bar{p}$ state to bound states. A discrete spectrum would be a clear signature. With the experiment of the Basle–Karlsruhe–Stockholm Collaboration the search for discrete γ-rays had reached, at that time, just the region of relevant branching ratios.

We now report on a new experiment with higher statistics and a considerably improved γ detection system. The experiment (fig. 2) took place at the k_{23} low-momentum electrostatically separated beam of the CERN Proton Synchrotron (PS). We found the optimum conditions at 600 MeV/c and, with a momentum spread of ±2%, about 250 $\bar{p}$'s per burst were stopped, after passing through a graphite moderator, in our 2 g/cm^2 thick liquid-hydrogen target. A configuration of scintillation and Čerenkov counters and of MWPCs, the so-called telescope, typical for stop experiments, identified the incoming particles. A time-of-flight (TOF) counter system worked parallel to the telescope so that we finally obtained a pure $\bar{p}$ trigger, the remaining contamination of $\sim 10^{-4}$ being only fast pions.

[1] Now at CERN, Geneva, Switzerland.
[2] Present address: BBC, Mannheim, Fed. Rep. Germany.
[3] On leave of absence from the Dept. of Physics, University of British Columbia, Vancouver, Canada.
[4] Now at ESO, Garching, Fed. Rep. Germany.

Table 1
Results of the two experimental runs (cols. 2, 4 and 5) in comparison with the results of ref. [2] (col. 3). Yields (cols. 2, 4 and 5) have an additional systematic error of ± 11%, γ-energies (cols. 4 and 5) have an additional systematic error of ± 5%.

		1976	1979	1980
mass (MeV)	1770.78 ± 1.06			
position (MeV)		~108	102.0 ± 1.9	103.1 ± 1.2
yield (‰)	1.8 ± 0.36		2.7 ± 0.9	1.6 ± 0.4
stat. significance			3.0 σ	3.6 σ
width (MeV)			<6.2	<8.0
	$\pi^- p \rightarrow \eta\gamma$			
position (MeV)		132 ± 6	129.4 ± 2.3	125.0 ± 2.1
yield (‰)		5.1 ± 2.7	3.0 ± 1.0	3.5 ± 0.8
stat. significance		1.9 σ	3.0 σ	4.4 σ
width (MeV)		<16	<7.5	17.4 ± 4.3
mass (MeV)	1693.53 ± 1.99			
position (MeV)		183 ± 7	170.4 ± 2.9	176.2 ± 2.2
yield (‰)	1.6 ± 0.44	7.2 ± 1.7	1.8 ± 1.0	1.6 ± 0.5
stat. significance		3.0 σ	1.8 σ	3.1 σ
width (MeV)		<19	<9.3	<12.0
mass (MeV)	1637.77 ± 2.52			
position (MeV)		216 ± 9	224.1 ± 2.3	222.0 ± 6.3
yield (‰)	3.0 ± 0.8	6.0 ± 1.9	3.0 ± 1.2	3.0 ± 1.1
stat. significance		2.6 σ	2.5 σ	2.7 σ
width (MeV)		<21	18.1 ± 7.8	38.4 ± 18.6
position (MeV)				294.2 ± 2.5
yield (‰)				1.2 ± 0.5
stat. significance				2.7 σ
width (MeV)				<18.2
position (MeV)				336.0 ± 3.8
yield (‰)				1.1 ± 0.5
stat. significance				2.2 σ
width (MeV)				17.3 ± 10
mass (MeV)	1420.69 ± 6.08			
position (MeV)		420 ± 17	395.9 ± 9.0	402.1 ± 5.4
yield (‰)	0.64 ± 0.35	8.5 ± 2.0	0.8 ± 0.7	0.6 ± 0.4
stat. significance		2.8 σ	1.1 σ	1.5 σ
width (MeV)		<34	<17.6	<22.6
mass (MeV)	1383.21 ± 2.04			
position (MeV)		420 ± 17	428.3 ± 11	428.6 ± 1.5
yield (‰)	<1.0	8.5 ± 12.0	1.0 ± 0.7	$0.1^{+0.4}_{-0.0}$
stat. significance		2.8 σ	1.4 σ	0.3 σ
width (MeV)		<34	<17.9	<23.0
mass (MeV)	1209.81 ± 5.12			
position (MeV)			545.5 ± 7.1	549.4 ± 3.7
yield (‰)	0.98 ± 0.26	?	1.2 ± 0.5	0.9 ± 0.3
stat. significance			2.4 σ	3.0 σ
width (MeV)			<22.4	<29.0

Gamma-rays in the energy range between 20 and 1000 MeV were detected in a modular NaI(Tl) detector [4] with good energy resolution and high efficiency for the rejection of background events (neutrons, double hits, charged particles, γ-rays entering from the side, etc.). The shape of the detector is a sector cut out of a hollow sphere and subtending a solid angle of ~7%. It consists of 54 modules of polycrystalline pieces of NaI(Tl) shaped as truncated pyramids. Each of the 54 modules is 16 radiation lengths long and is equipped with its own photomultiplier, amplifier, and two ADCs allowing for two different dynamical ranges. The topology of the shower was reconstructed to achieve an energy-independent efficiency. Only events where the shower was safely located inside the detector were accepted, and the light output of the neighbouring modules was added. In this way a good energy resolution was achieved. This required an energy calibration of each module in the relevant energy region (few hundred MeV) with a precision of about 1%. For this purpose, pions of 200 MeV/c momentum, coming out of the same beam line, were stopped in the hydrogen target, giving rise to the reactions $\pi^- p \to n\gamma$ or $n\pi^0$. The monoenergetic γ line at 129.4 MeV was used as the calibration standard, and the relative calibration of each module was performed in an iterative procedure [4]. This calibration method for a modular high-energy gamma detector was never applied before, and has led to the (so far) best resolution of $\sim 4\%/E^{1/4}$ (GeV) for a large NaI(Tl) system. As energy reference at high energies, the upper edge (774 MeV) of the uniform γ-distribution from the annihilation channel $p\bar{p} \to \pi^0\omega^0$ and the end point of the spectrum were used. The data-taking extended over periods of several months and required the stabilization of the γ-detection system, which was achieved by using a Xe bulb light-pulser system. This resulted in a stability of better than 1% for the 129.4 MeV γ-line, which was regularly checked in short pion runs.

With this experimental set-up, two major runs were performed, one in 1979 and one in 1980, with 40×10^6 and 110×10^6 stopped antiprotons, respectively. Between these two runs, major components of the experiment were modified:

(a) Two targets, different in diameter and container material, were used.

(b) Positive photomultiplier high voltage was used in the second run, involving the replacement of photomultipliers and their electronics for the gamma spectrometer.

Hence these two running periods can be considere as two independent experiments. The resulting two sets of γ spectra show the same high background fro annihilation π^0's, so that small structures can hardly be seen. In order to subtract this background, the γ spectra originating from all known annihilation chan nels were simulated by Monte Carlo and resulted in a spectrum with equivalent shape. Scaling the shape function with a proper factor and subtracting it from the data, we found a good agreement in the high-energ part (above 400 MeV) of the spectrum, only below 400 MeV some background remained. It corresponds to only 3% of the whole spectrum and is perhaps due to annihilation processes not being considered in the Monte Carlo calculations. The resulting spectra, afte the subtraction of these backgrounds, show small bu very similar structures (figs. 1b and 1c). A computer fit to the peaks yields the results of table 1.

In comparison with the old spectrum (fig. 1a), we conclude that two of the previous lines (183, 216 MeV) reappear in the present spectra at the same ene gies within the limits of the energy error, whereas th evidence for the 420 MeV line has become weak. Th confidence level for the structures at 175 and 220 MeV varies for each individual spectrum between 1.8 and 3.1 σ. In the present experiment the 220 MeV li shows a width slightly larger than the instrumental re olution (table 1). With a similar confidence level, two more peaks appear in the spectra: structures around 102 MeV (3.0–3.6 σ) and round 550 MeV (2.4–3.0 The appearance of these peaks does not contradict th old results because: (i) the line at 102 MeV appeared also in the old spectrum (fig. 1a), but owing to the high background and the worse resolution of the 10″ × 12″ spectrometer at this energy, in connectio with the adjacent 129.4 MeV line the evaluation was difficult and thus we hesitated at that time to presen it as a peak; (ii) the statistics at energies above 500 MeV were so marginal as to prevent the appearance o low intensity lines. The recent yields seem to be systematically lower as compared to the old experimen However, we are more confident of our present resul owing to the following fact:

(1) The experimental energy resolution is improv by a factor of two.

(2) The lateral size, the depth and the modularity

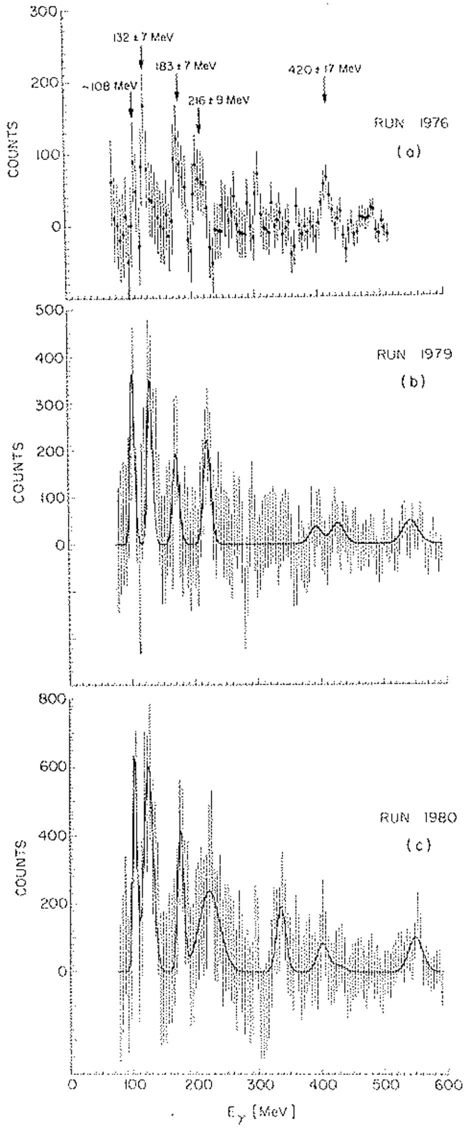

Fig. 1. The spectrum of the first Basle–Karlsruhe–Stockholm experiment (1976) (a) and the spectra of the 1979 (b) and 1980 (c) runs after subtraction of the background. Two point smoothing was applied in all three spectra.

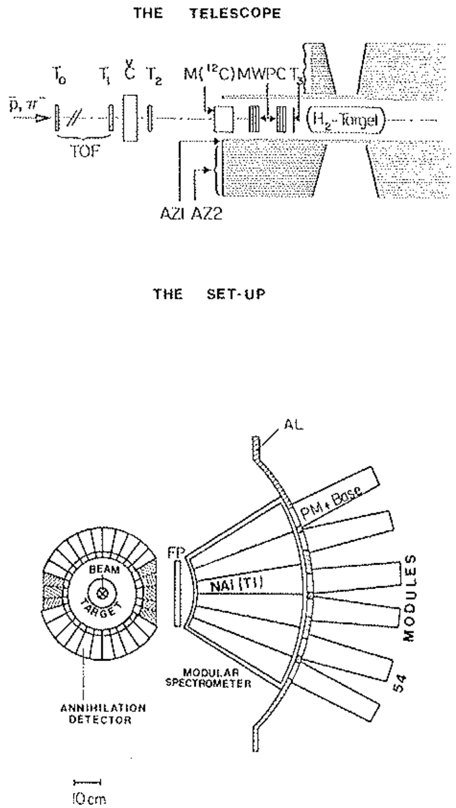

Fig. 2. The experimental set-up. The annihilation detector (AZ1, AZ2) was not used in this experiment.

of the new γ spectrometer allowed an energy-independent γ detection efficiency over the whole energy range of interest.

(3) The exact studies of the Monte Carlo simulated annihilation reactions allowed, in the present experiment, a normalization which is rather independent of further assumptions. This was not possible in the old experiment.

More details will be given in a forthcoming paper.

Summarizing the results of the former experiment and the present one, it is concluded that three independent measurements have found tiny narrow structures with an individual significance of up to three standard deviations, and yields of several per mille per formed $p\bar{p}$ system are visible. Their simultaneous appearance in all three spectra (except the peak at 550 MeV) at energies identical within the errors quoted and with similar yields seems to rule out any statistical fluctuation as their source. The above γ transitions correspond to states with masses of 1771 ± 1 MeV, 1694 ± 2 MeV, 1638 ± 3 MeV, and 1210 ± 5 MeV, assuming atomic states as initial states (table 1).

We would like to express our thanks to L. Mazzone and his group for technical support. This work was supported in part by the Swiss National Science Foundation, the German Bundesministerium für Forschung und Technologie (BMFT), and the Bank of Sweden Tercentenary Foundation. One of us (K.Z.) would like to thank the Greek Administration for Research and Technology (YEET) for financial support.

We gratefully acknowledge CERN's hospitality and support.

References

[1] T. Kalogeropoulos et al., Phys. Rev. Lett. 35 (1975) 824.
[2] P. Pavlopoulos et al., Phys. Lett. 72B (1978) 415.
[3] For a review, see L. Montanet, G.C. Rossi and G. Veneziano, Phys. Rep. 63 (1980) 149.
[4] P. Blüm et al., A modular NaI(Tl) detector for 20–1000 MeV photons (in preparation).

IV

SEARCH FOR NARROW EXOTIC STATES IN $\bar{p}$ ANNIHILATIONS ON ^{4}He

Basle–Kralsruhe–Stockholm–Strasbourg–Thessaloniki Collaboration
at CERN, Geneva, Switzerland

L. ADIELS [c], G. BACKENSTOSS [a], P. BLÜM [b], I. BERGSTRÖM [c], K. FRANSSON [c], R. GUIGAS [b,1], H. KOCH [b], A. KEREK [c], M. MEYER [b,2], P. PAVLOPOULOS [a,3], H. POTH [b], U. RAICH [b,3], B. RICHTER [b], J. REPOND [a], M. SUFFERT [d], L. TAUSCHER [a], D. TRÖSTER [a] and K. ZIOUTAS [e]

[a] *Institute for Physics, University of Basle, Switzerland*
[b] *Kernforschungszentrum, Institut für Kernphysik and Institut für Experimentelle Kernphysik, Universität Karlsruhe, Karsruhe, Fed. Rep. Germany*
[c] *Research Institute for Physics, Stockholm, Sweden*
[d] *Centre de recherches nucléaires and Université Louis Pasteur, Strasbourg, France*
[e] *Department of Nuclear Physics, University of Thessaloniki, Greece*

Received 11 January 1984

After having found evidence for narrow exotic states in $\bar{p}p$ annihilation, the production of such states on a nuclear target was studied with similar techniques. The γ spectrum associated with $\bar{p}$ annihilation on ^{4}He at rest was measured. The spectrum shows two peaks, at energies of 161.9 and 203.0 MeV, corresponding to intermediate narrow states of masses which seem to be related to states found in $\bar{p}p$ annihilations. The confidence is better than 4σ.

Several independent experiments on $\bar{p}p$ annihilation at rest have shown indications for monoenergetic γ-rays [1,2], which may be discussed in the context of exotic objects such as baryonium or glueballs. It is of great interest to know whether such objects, if existing, are also produced in $\bar{p}$ annihilations on nuclear targets. If so, also charged states could become observable through the γ-ray spectrum. We studied the reaction

$$\bar{p}\ ^4\mathrm{He} \to \gamma + X + \text{nucleons},$$

by measuring the γ spectrum associated with the $\bar{p}$ annihilation on an α particle.

The experimental method and the set-up are described in detail in ref. [2] and correspond to our 1979 run. The low-energy $\bar{p}$'s were stopped in liquid ^{4}He, contained in a target of 25 cm length and 12.5 cm diameter. A modular NaI(Tl) γ spectrometer [3] was used to measure the γ-ray spectrum. The experiment was performed at the separated beam k_{23} of the CERN PS.

In a run of 10 days about 10^7 $\bar{p}$'s were stopped. The resulting γ-ray spectrum is shown in fig. 1. As in the annihilation on hydrogen it consists of a large background produced by π^0's from the annihilation, and exhibits a uniform shape very similar to that of $\bar{p}p$ annihilation at rest [2], with the exception, however, that it extends up to energies of 1150 MeV instead of 940 MeV and that it monotonically increases also below 70 MeV.

In order to reveal possible structures in this spectrum the background has to be understood quantitatively and eventually subtracted. For this purpose we adopt the hypothesis that the annihilation in ^{4}He occurs on a single nucleon, so that the background may be related quantitatively to the one produced by $\bar{p}p$ annihilation at rest. The latter has been explained quantitatively [2,4].

For normalization purposes we first estimate the number of γ's per $\bar{p}$ annihilation on ^{4}He. In $\bar{p}p$ annihi-

[1] Present address: BBC, Mannheim, Fed. Rep. Germany.
[2] Now at ESO, Garching, Fed. Rep. Germany.
[3] Now at CERN, Geneva, Switzerland.

0.370-2693/84/$ 03.00 © Elsevier Science Publishers B.V.
(North-Holland Physics Publishing Division)

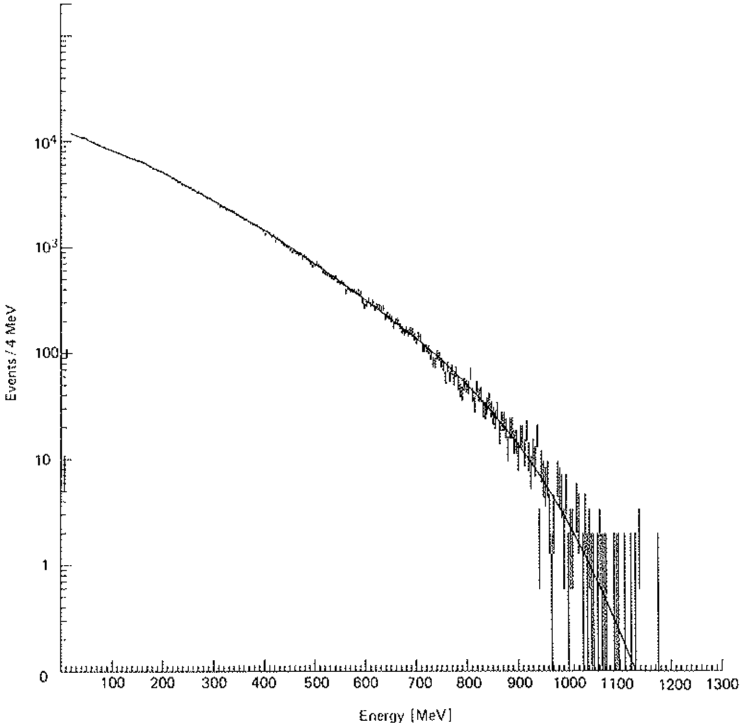

Fig. 1. The γ spectrum from $\bar{p}$ annihilation on ^{4}He at rest. The solid line represents the background fit.

lation, on average, there are 1.7 π^0, 1.7 π^+, and 1.7 π^-, and in $\bar{p}$n annihilation, assuming only charge conservation, there are 1.7 π^0, 0.7 π^+, and 2.7 π^- per annihilation. Therefore the number of γ's per $\bar{p}$ annihilation on ^{4}He is roughly the same as for $\bar{p}$p annihilation.

Furthermore, assuming the same branching ratios of the multipionic final states in $\bar{p}$n annihilation as in $\bar{p}$p annihilation, the shape function found for the continuous background from p$\bar{p}$ annihilation at rest [4] may be applied to the $\bar{p}$ ^{4}He annihilation.

In addition to the continuous background there is a superposition of uniform γ-energy distributions from two-body final states where at least one of the particles decays into two γ's as found in p$\bar{p}$ annihilation at rest [4]. The branching ratios found in ref. [4] or quoted therein were adapted to the mixed annihilations on neutrons and protons. The resulting branching ratios for $\bar{p}$ ^{4}He annihilation are listed in table 1.

The continuous background (taken from $\bar{p}$p annihilation) and the two-body annihilations from table 1 lead to a γ spectrum in the $\bar{p}$N rest frame. Owing to the Fermi motion of the nucleons in the α particle, however, the annihilation occurs on a system which is in motion, thus leading to a Doppler smearing of the γ energies. Moreover, the $\bar{p}$ in its atomic orbit, when annihilating, is localized at the nuclear surface. Hence it has acquired kinetic energy in the Coulomb potential, which corresponds to a momentum in the lab system of

$$k_{\bar{p}} \approx (2M_{\bar{p}}^{\mathrm{red}}\, \alpha Z/R)^{1/2}. \qquad (1)$$

Here $M_{\bar{p}}^{\mathrm{red}}$ is the reduced $\bar{p}$ mass, α is the fine struc-

Table 1
Branching ratios for the relevant two-body final states for $\bar{p}\,^4$He annihilation as a percentage of all annihilations.

Channel	Scaled from ref. [4]	Fitted
$\pi^0\rho^0 + \pi^0\rho^-$	1.2	} 2.08 ± 0.19 [a]
$\pi^0\omega$	1.2	
$\pi^0\pi^0 + \pi^0\pi^-$	0.195	0.144 ± 0.037
$\pi^0\gamma + \pi^-\gamma$	0.011	0.011
$\pi^0\eta + \pi^-\eta$	0.41	0.39 ± 0.09

[a] The two channels cannot be disentangled when fitting.

ture constant, $Z = 2$, and $R = 1.676$ fm is the r.m.s. radius of the α particle [5]. This yields $k_{\bar{p}} = 51$ MeV/c. The α particle carries the opposite momentum. In evaluating the energy smearing, the Fermi-momentum distribution of the nucleons in ^{4}He is given by the Fourier transform of the nuclear density distribution, resulting in the momentum density

$$\rho(\boldsymbol{k}_{\rm F}) = \exp[-(k_{\rm F}/k_0)^2]/(\pi\sqrt{\pi}\,k_0^3), \tag{2}$$

where $k_{\rm F}$ is the nucleon's momentum relative to the α particle and $k_0 = 126.3$ MeV/c [6]. Because only one of the four nucleons of the α particle interacts with the $\bar{p}$, the total momentum of the annihilating $\bar{p}$N system is in the lab system

$$\boldsymbol{p}_{\bar{p}N} = \boldsymbol{k}_{\rm F} + \tfrac{3}{4}\,\boldsymbol{k}_{\bar{p}}$$

and the unnormalized momentum density distribution is

$$\rho(\boldsymbol{p}_{\bar{p}N}) = \exp[-|(\boldsymbol{p}_{\bar{p}N} - \tfrac{3}{4}\,\boldsymbol{k}_{\bar{p}})/k_0|^2]. \tag{3}$$

Monoenergetic γ-rays of energy $E_\gamma^{\rm cm}$, isotropically emitted from the $\bar{p}$N rest frame, experience a Lorentz boost when emitted from a moving system of momentum $p_{\bar{p}N}$ and energy E, and hence result in the normalized uniform distribution

$$B(p_{\bar{p}N}) = M_{\bar{p}N}/2E_\gamma^{\rm cm}\,p_{\bar{p}N},$$

$$\text{for}\quad (E - p_{\bar{p}N})/M_{\bar{p}N} \leqslant E_\gamma^{\rm lab}/E_\gamma^{\rm cm} \leqslant (E + p_{\bar{p}N})/M_{\bar{p}N},$$

$$= 0 \quad \text{otherwise}, \tag{4}$$

where $M_{\bar{p}N}$ is the effective mass of the annihilating system and $E_\gamma^{\rm lab}$ is the γ energy observed in the laboratory system. Note that since the nucleons are bound, $M_{\bar{p}N}$ becomes smaller with increasing $p_{\bar{p}N}$.

Since the γ background in the rest frame is continuous, integration over all available γ energies $E_\gamma^{\rm cm}$ has to be performed. Furthermore, integration has to be done over all available momenta. Hence the shape function $F_{\bar{p}\alpha}$ for the γ background from $\bar{p}\,^4$He in the lab system is

$$F_{\bar{p}\alpha}(E_\gamma^{\rm lab}) = \int_0^{938\,\rm MeV} {\rm d}E_\gamma^{\rm cm}\,F_{\bar{p}p}(E_\gamma^{\rm cm})\cdot N\int {\rm d}^3p_{\bar{p}N}$$

$$\times\,\rho(\boldsymbol{p}_{\bar{p}N})\,B(|p_{\bar{p}N}|), \tag{5}$$

where $F_{p\bar{p}}$ is the shape function of ref. [4] for p$\bar{p}$ annihilation at rest, and N is a normalization constant. Integration over the angles may be performed by assuming that the momenta of the $\bar{p}$ and the nucleon are randomly oriented with respect to each other.

In order to reconstruct the background consistently a similar procedure has to be applied for the uniform distributions of table 1. In a procedure identical to that applied in ref. [4] the spectral shape function [eq. (5)] and the uniform contributions were folded with the detector resolution and scaled to the experimental spectrum, where the scaling factor (the number of $\bar{p}$ annihilations) and the total height of the uniform distributions were varied in the fitting procedure. The spectrum corresponds to $N_{\bar{p}p} = 144000 \pm 1240$ annihilation $\bar{p}$'s giving a trigger in the γ spectrometer. The solid line in fig. 1 represents the fit. It is worth while noting, that with only one non-trivial parameter (the total height of the uniform distributions), the $\bar{p}\,^4$He γ spectrum could be related to the $\bar{p}$p spectrum in an energy range from 200 to 1150 MeV.

A fine-tune on the two-body annihilation channels of table 1 yields the branching ratios in the third column of table 1. The yields do not differ drastically from the scaled ones. The errors are statistical ones only. There is an additional systematic error of 10%, coming from uncertainties in the normalization.

The background shape [eq. (5)] accounts only for energies above ~200 MeV. As in the case of $\bar{p}$p annihilation [2] the background at low energies requires an additional correction. For energies below 200 MeV an arbitrary smooth function had therefore to be added. After subtraction of the continuous background and the uniform distributions of table 1, the residual spectrum is obtained (see fig 2). Between 100 MeV

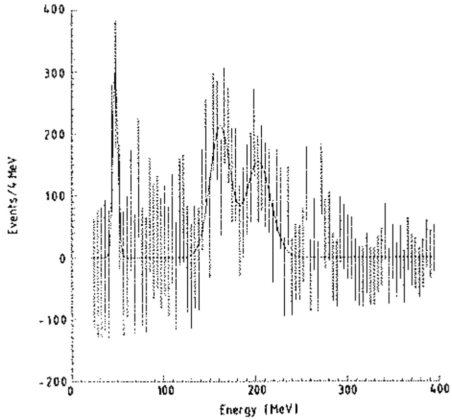

Fig. 2. The residual spectrum after subtraction of the background. Note that the peak at 135 MeV formerly seen in p̄p annihilation [1,2], which is due to the secondary reaction $\pi^- p \to n\gamma$, is not visible as expected.

and 300 MeV the spectrum exhibits clearly two peaks. They are broader than expected from the resolution, which was taken to be $5\%/\sqrt[4]{E(\mathrm{GeV})}$ (c.f. ref [4]). Assuming that narrow structures coming from the process

$$\bar{p}N \to \gamma + X,$$

are smeared by the Fermi motion, analogously to eq. (5) and folded with the detector resolution, the two peaks were fitted with only the peak positions and the peak intensities as free parameters A third but narrower peak was found at a lower energy. Fits were also done where the width of each peak was a free parameter. The results are listed in table 2. The statistical errors are for fixed line shape. For the case where als the line widths were varied the errors are obtained by adding the fit systematic errors in quadrature to the statistical ones There are additional systematic errors for calibration and normalization (c.f ref. [4]). The fitted line widths tend to be somewhat larger than expected from the Fermi-motion induced line shape. The yields are on the level of 1% per annihilation, thu more than three times higher than those of the peaks from p̄p annihilation [2].

The two peaks are compatible with narrow states X. Assuming the same origin as in pp̄ annihilation, i.e pN → X + γ, two possible reactions have to be considered:

$$\bar{p}\,{}^4\mathrm{He} \to \bar{p}N + 3 \text{ free nucleons}, \quad \hookrightarrow \gamma + X \qquad (6a$$

$$\bar{p}\,{}^4\mathrm{He} \to \bar{p}N + t \text{ or } {}^3\mathrm{He}, \quad \hookrightarrow \gamma + X \qquad (6b$$

In the first reaction the annihilating p̄N system is at least 28.3 MeV (binding energy of the α particle) below threshold; in the case of tritium or ^{3}He being in the final state, the system is at least 19.8 and 20.6 MeV, respectively, below threshold. Carrying out the correct kinematical calculations we expect the "160 MeV" peak to be shifted with respect to p̄p by 28.8 MeV and 22.3 MeV for reactions (6a) and 6b), respec tively. For the "200 MeV" peak the corresponding shifts are 31.9 MeV and 25.5 MeV, respectively. Sinc the absolute calibration might be wrong by about ±5 as indicated in table 2, we prefer not to discuss absolute energies for the moment, but instead compare th

Table 2
Energies and intensities of the γ peaks. Intensities are given as a percentage of all annihilations. For comparison the γ energies found in hydrogen are listed as well (1979 run of ref. [2]).

E (MeV)	Error (MeV)			Yield (%)	Error			Width (FWHM) (MeV)	E from p̄p (MeV)
	stat.	fit	calibr.		stat.	fit	norm.		
47.5	±1.4	–		0.38	±0.14	–		6.80 ± 2.5	–
161.9	±3.3	$^{+2.1}_{-3.0}$	±5%	0.93	±0.16	$^{+0.48}_{-0.00}$	±10%	30^{+10}_{-7}	170.4 ± 2.9
203.0	±3.6	$^{+5.5}_{-3.4}$		0.89	±0.17	$^{+0.47}_{-0.10}$		34 ± 12	224.1 ± 2.3

Table 3
Masses of the particles X. For comparison the masses found in hydrogen [2] are listed in column 2.

M (MeV)	Error (MeV)	Final state	M from $\bar{p}p$ (MeV)
1687.1	$^{+5.0}_{-4.3}$	t or ^{3}He	1693.5 ± 2.0
1644.0		t or ^{3}He	
or	$^{+5.6}_{-7.3}$		1637.8 ± 2.5
1637.1		3N	

measured energy difference of the two peaks with the energy differences expected in $\bar{p}$ ^{4}He, assuming the intermediate states X of reactions (6) to be the same as in $\bar{p}p$ [2]. In the case where both states are produced by reaction (6a) the expected energy difference is 50.6 ± 3.7 MeV (case A); for reaction (6b) it is 50.5 ± 3.7 MeV (case B), and in the case where the "160 MeV" state is related to reaction (6b) whereas the "200 MeV" state is related to reaction (6a), the energy difference is 44.1 ± 3.7 MeV (case C). The error of 3.7 MeV is deduced from the last column of table 2. The measured energy difference of $41.1^{+6.6}_{-5.0}$ MeV is fully compatible with case C and overlaps within 1σ with cases A and B. The measured energy difference hence is compatible with expectation. The absolute energies of the two peaks become consistent with cases B and C if an energy shift of −5% (as possible from the systematic calibration errors) is applied. Case A is not compatible with our measurement. The masses after applying this correction to the energies of table 2 are listed in table 3. For the "200 MeV" peak two masses are given since we cannot distinguish between cases B and C. The significance is on the level of 4σ. Comparison with the masses found from $\bar{p}p$ annihilation [2] shows good agreement.

The peak at 47.8 MeV cannot originate through the same processes as the others, since it is too narrow. It shows up on a confidence level of 2.7σ and therefore is not significant enough to exclude it as being due to a statistical fluctuation.

Two obvious questions have to be discussed: why are the yields of the peaks so high in ^{4}He as compared to hydrogen, and why are the peaks corresponding to 100 and 550 MeV in hydrogen [2] not observed?

One difference between annihilation of $\bar{p}$'s in liquid hydrogen and liquid He is the initial atomic state from which the annihilation occurs For hydrogen it is most likely an s state, whereas for helium it is almost certainly an $l \neq 0$ state [7]. Hence we expect for peripheral reactions and sufficiently high relative momenta some enhancement of p state annihilation. States which can only be reached from p states of a $\bar{p}p$ system such as 1^{-+}, 2^{-+} (via dipole-radiation) or 0^{+-}, 2^{+-} (via quadrupole-radiation), would thus be strengthened in helium.

A second difference is the additional annihilation on neutrons in helium, which implies formation of negative states ($I \neq 0$). Reactions of the type $\bar{p}n \to X^- + \gamma$ are not subject to restrictions imposed by C-parity. The relevant symmetry instead is G-parity, which, however, is only restrictive in the frame of vector dominance. This is the reason why states such as 0^{+-} or 2^{+-}, which cannot be reached from s-states in hydrogen, can be reached from the $^3S_1$ state of the $\bar{p}n$ system. The consequence is that the yields of such states are stronger in helium than in hydrogen. A further enhancement of yields due to $\bar{p}n$ annihilations concerns 1^{+-} states which in hydrogen are formed from initial $^1S_0$ atomic states only, whereas in $\bar{p}n$ annihilation both $^1S_0$ and $^3S_1$ states contribute.

Assuming dominant s-wave annihilation also in helium we therefore may conclude that the states observed in helium are also due to $\bar{p}n$ annihilations and thus have $I \geqslant 1$. The somewhat larger width, as discussed above, could be an indication of a charge splitting. Such charged states have previously not been observed [8].

The non-observation of the lines corresponding to 100 MeV and 550 MeV in hydrogen could indicate that they are related to $I = 0$ particles. The consequence would be that their yields in ^{4}He are two times lower than in hydrogen (< 0.3% [2]). The additional Fermi-motion induced broadening would render them unobservable with the present statistics.

A more detailed study of the phenomenon, e.g. an experiment on deuterium, is required before giving a conclusive answer to the above questions.

This experiment has provided evidence that exotic states associated with $\bar{p}$ annihilation may also be produced in nuclei, with yields larger than in hydrogen. Moreover, by these observations the confidence in the states of mass 1693 MeV and 1638 MeV which have been observed in three independent measurements on hydrogen [1,2], has further been strengthened. We also conclude that nuclear targets are complementary to hydrogen in the sense that, by comparing yields of reactions in hydrogen ($\bar{p}p \to X + \gamma$ or π) with yields from the nuclear target ($\bar{p}n \to X + \gamma$ or π), quantum numbers for the states X may be deduced. Therefore nuclear targets may be successfully used in the search for exotic states in the $\bar{p}N$ system.

We would like to thank CERN for its hospitality. This work was supported by the Swiss National Science Foundation, the Ministry for Research and Technology of the Federal Republic of Germany, and the Swedish Science Research Council.

References

[1] P. Pavlopoulos et al., Phys. Lett. 72B (1978) 415.
[2] B. Richter et al., Phys. Lett. 126B (1983) 284.
[3] P. Blüm et al., Nucl. Instrum. Methods 213 (1983) 251.
[4] G. Backenstoss et al., Nucl. Phys. B228 (1983) 424.
[5] I. Sick, Phys. Lett. 116B (1982) 212.
[6] I. Sick, private communication.
[7] H. Poth et al., Phys. Lett. 76B (1978) 523.
[8] R. Bertini et al., Nucl. Phys. B209 (1982) 269.

V

Z. Phys. C – Particles and Fields 21, 315–319 (1984)

Zeitschrift für Physik C Particles and Fields

π^0 and η Spectra from $p\bar{p}$ Annihilations at Rest

Basle[1]-Karlsruhe[2]-Stockholm[3]-Strasbourg[4]-Thessaloniki[5] Collaboration at CERN, Geneva, Switzerland

L. Adiels[3], G. Alberis[5], G. Backenstoss[1], P. Blüm[2], I. Bergström[3], K. Fransson[3], R. Guigas[2a], M. Hasinoff[1b], H. Koch[2], A. Kerek[3], M. Meyer[2c], P. Pavlopoulos[1], H. Poth[2], U. Raich[2d], B. Richter[2], J. Repond[1], M. Suffert[4], L. Tauscher[1], D. Tröster[1], K. Zioutas[5]

1 Institute for Physics, University, CH-4056 Basle, Switzerland
2 Kernforschungszentrum, Institut für Kernphysik and Institut für Experimentelle Kernphysik, Universität, D-7500 Karlsruhe, Federal Republic of Germany
3 Research Institute for Physics, S-11346 Stockholm, Sweden
4 Centre de recherches nucléaires and University Louis Pasteur, F-67100 Strasbourg, France
5 Dept. of Nuclear Physics, University of Thessaloniki, Greece

Received 7 September 1983

Abstract. The low-energy part of the π^0 spectrum associated with $p\bar{p}$ annihilation at rest was measured in order to search for bound baryonium-like states. The upper limit for reaching such states via the emission of monochromatic π^0's was found to be 8% per annihilation in the mass region of 1650 MeV. The low-energy part of the η spectrum from $p\bar{p}$ annihilations at rest was also observed.

The search for bound baryonium states has so far been done mainly by investigating the γ spectra associated with $p\bar{p}$ annihilation at rest [1–3]. Owing to the relative weakness of the electromagnetic vertex involved in reactions of the type $p\bar{p}\rightarrow\gamma X$ it seems probable that, for sufficiently deeply bound states X, reactions involving a π^0 instead of a γ ($p\bar{p}\rightarrow\pi^0 X$) have higher probability. Annihilations of this type have so far never been searched for experimentally.

Here we shall describe an experiment where the reaction $p\bar{p}\rightarrow\pi^0 X$ was studied in liquid hydrogen for a limited range of π^0 energy. Results are also presented for the low-energy part of the η spectrum.

The experimental set-up has been described earlier [3] and will therefore only be sketched briefly here. A $\bar{p}$ beam was stopped in a 25 cm long liquid-hydrogen target of 10 cm diameter. The beam diameter at the maximum of its stop distribution was about 7 cm. The target was viewed by two NaI γ detectors, a modular NaI system described by Blüm et al. [4], and a 10 in. × 12 in. NaI crystal described by Suffert et al. [5]. The target was surrounded by an annihilation multiplicity counter (charged particles and photons), which, however, was not used in the following evaluation owing to the limited statistics. The two γ detectors were placed opposite to each other such that two γ's could be measured in coincidence when the angle $\phi_{\gamma_1\gamma_2}$ between them was larger than 155°. The solid angle of the 10 in. × 12 in. detector was defined by a 10 cm thick lead collimator of 15 cm diameter. The acceptance of the modular system was limited by the requirement that the shower centre should not be located in the peripheral modules [4]. Assuming a point-like source, the fractional solid angle of the 10 in. × 12 in. crystal was $\Omega_1 = 0.69\%$ and that of the modular system was $\Omega_2 = 1.74\%$. Charged particles were vetoed by plastic scintillators in front of the detectors. The apparatus is shown schematically in Fig. 1. Whenever one of the γ detectors gave a trigger both systems were read out. Cuts were only applied in the off-line analysis.

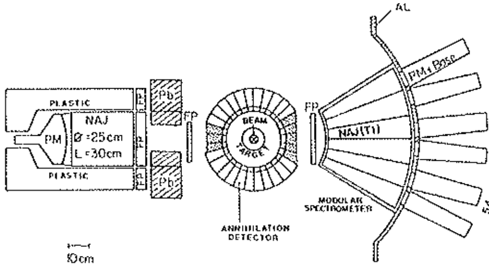

Fig. 1. Experimental set-up. Cross-section perpendicular to the beam

[a] Present address: BBC, D-6800 Mannheim, FRG
[b] On sabbatical leave from the Dept. of Physics, University of British Columbia, Vancouver, Canada
[c] Now at ESO, D-8046 Garching, FRG
[d] Now at CERN, CH-1211 Geneva, Switzerland

With the above-mentioned solid angles and assuming $N_\gamma = 3.93$ γ's per annihilation on the average [6], the probability for a single trigger is $N_\gamma(\Omega_1 + \Omega_2)$, and for the coincidences we expect in first approximation $N_\gamma(N_\gamma - 1)\,\Omega_1\,\Omega_2 = 1.38 \times 10^{-3}$ $\gamma\gamma$'s per annihilation. With a total of $N_{p\bar{p}} = 46 \times 10^6$ stopped $\bar{p}$'s this gives $\sim 63{,}500\,\gamma\gamma$ coincidences. This number is reduced by those events where a charged particle hits the same detector as one of the γ's. The total solid angle $\bar{\Omega}$ for the veto counters being about five times that of the γ-sensitive central region of the detector, and assuming 3.4 charged pions per annihilation, we roughly estimate a total of $40{,}000\,\gamma\gamma$ coincidences.

Most of these coincident γ's are, however, uncorrelated, i.e. not originating from the same particle, e.g. π^0 or η. Therefore their invariant mass

$$m_{\gamma_1\gamma_2} = \sqrt{2E_{\gamma_1}E_{\gamma_2}(1-\cos\phi_{\gamma_1\gamma_2})} \tag{1}$$

is usually not the π^0 mass or η mass, but covers a continuous spectrum. When reconstructing the invariant $\gamma\gamma$ mass from the data it was assumed that $\phi_{\gamma_1\gamma_2}$ was 180°. The error introduced by the finite angular acceptance of the system of

$$155° \leqq \phi_{\gamma_1\gamma_2} \leqq 180°$$

is only of the order of $\pm 2.5\%$ in the mass, hence much less than the energy resolution of the coincidence system ($\sim 15\%$). The spectrum of the invariant $\gamma\gamma$ mass is shown in Fig. 2. It contains 27,500 events, thus 31% lower than expected from the above estimate. The reduction is compatible with an energy cut at 25 MeV in the single γ energies, which was introduced in order to reduce low-energy neutron-induced and bremsstrahlung background. This cut affects mostly the uncorrelated background. As expected, the spectrum is essentially continuous. The π^0 peak at 135 MeV is quite prominent and contains 1000 ± 55 events. A second peak at ~ 550 MeV, originating from η's which decay into two γ's, contains 272 ± 48 events.

The kinematics for π^0 decay in flight lead to a probability for the emission angle $\phi_{\gamma_1\gamma_2}$ of the form [7]:

$$W(\phi_{\gamma_1\gamma_2}) = \frac{1-\beta^2}{2\beta}\,\frac{\cos(\phi_{\gamma_1\gamma_2}/2)}{\sin^2(\phi_{\gamma_1\gamma_2}/2)}\,\frac{\Theta[\beta^2 - \cos^2(\phi_{\gamma_1\gamma_2}/2)]}{\sqrt{\beta^2 - \cos^2(\phi_{\gamma_1\gamma_2}/2)}}, \tag{2}$$

where β is the velocity of the π^0 and Θ is a step function defining the minimum angle

$$\cos^2\left(\frac{\phi^{\min}_{\gamma_1\gamma_2}}{2}\right) = \beta^2.$$

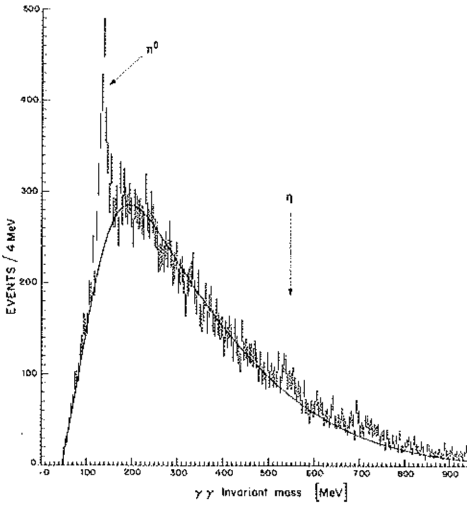

Fig. 2. Spectrum of the invariant $\gamma\gamma$ mass. The solid line re sents the background from uncorrelated γ's. The structure aro 700 MeV is due to the decay of ω's into $\pi^0\gamma$. As expected confirmed by Monte Carlo simulations, this decay mode lead such a structure in the $\gamma\gamma$ mass spectrum

From these formulae we deduce that the minim angle is also the most probable one, and that 180 quite improbable for fast π^0's. Hence our set-up expected to provide only reduced efficiency for ergies higher than $E_{\pi^0} \geqq 138$ MeV and $E_\eta \geqq 562$ M Figure 3 shows the efficiency of our apparatus calculated for π^0 and η detection. It exhibits a sh plateau, then drops down owing to the acceptan limitations, and finally is cut off owing to the ene cuts in the single γ energies.

When evaluating the $\gamma\gamma$ coincidences further, greatest problem is obviously the very large correlated background underneath the π^0 or η m peaks in the invariant mass spectrum. In order reduce this background the γ spectra in each tector were considered separately and approxima by smooth functions $F(E_\gamma)$. For each point in the $-E_{\gamma_2}$ plane the background is then given $F_1(E_{\gamma_1})F_2(E_{\gamma_2})$. The quality of this background proximation is demonstrated by the solid line Fig. 2. Obviously the correlated events in the π^0 c peak are barely affected by this procedure, althou the single γ spectra also contain correlated γ's.

In order to reconstruct the π^0 or η energy sp tra, appropriate cuts were applied to the invari mass $m_{\gamma_1\gamma_2}$ and the energies of the two γ's w added to give $E_{\pi^0,\eta} = E_{\gamma_1} + E_{\gamma_2}$. The spectra shown in Figs. 4a and 5a for the π^0 and η m

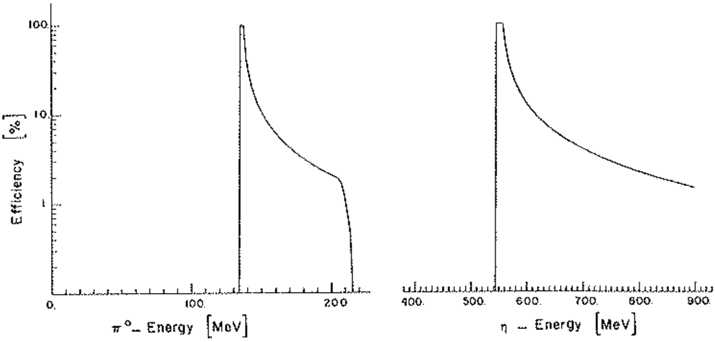

Fig. 3. Detection efficiency for π^0's and η's as a function of the total energy of the particle

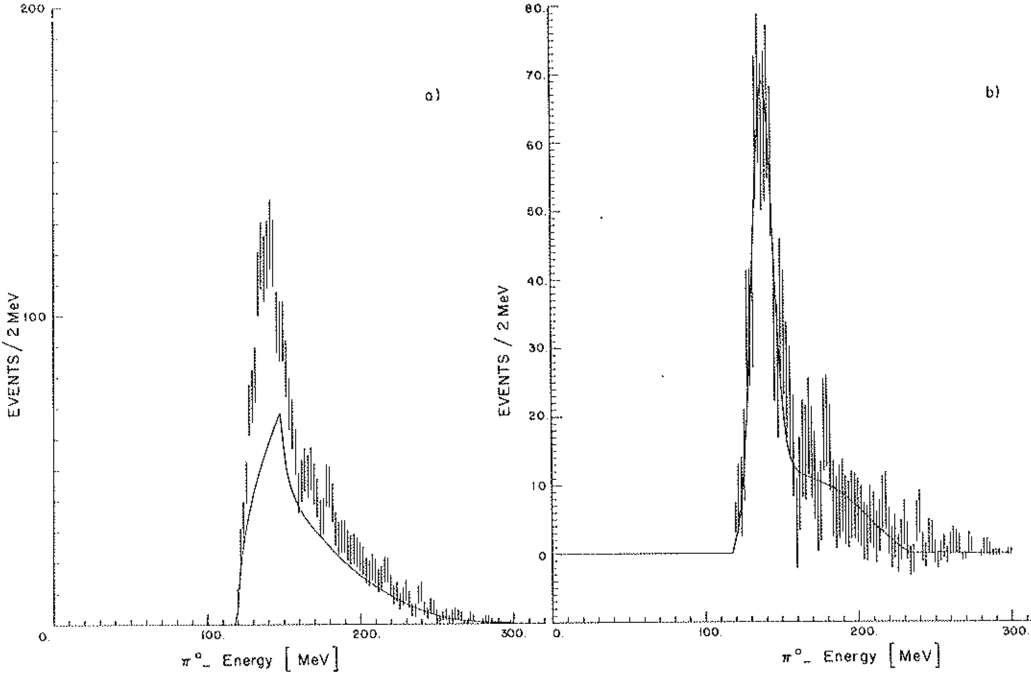

Fig. 4. a π^0 energy spectrum. The solid line represents the uncorrelated background. **b** π^0 energy spectrum after subtraction of the uncorrelated background. The solid line represents the peak from π^0 charge exchange at rest and the Monte Carlo simulated π^0 spectrum

cuts, respectively. These spectra still contain uncorrelated background. By subtracting it, using again the functions F_1 and F_2 for the single γ-spectra, the "pure" π^0 and η energy spectra shown in Figs. 4b and 5b are obtained.

The π^0 spectrum exhibits a peak at $E_{\pi^0} = 138$ MeV and a tail towards higher energies. The peak at 138 MeV is due to reactions of slow π^-'s from $p\bar{p}$ annihilations, which stop in the target and undergo charge exchange ($\pi^- p \to \pi^0 n$), whereas the tail is due to primary π^0's from annihilation.

First we analyse the peak at 138 MeV in order to obtain an estimate of the total number of primary π^0's. This peak contains 500 ± 10 events. The peak width at half maximum corresponds to 11.5%. From [3] we know that the corresponding radiative cap-

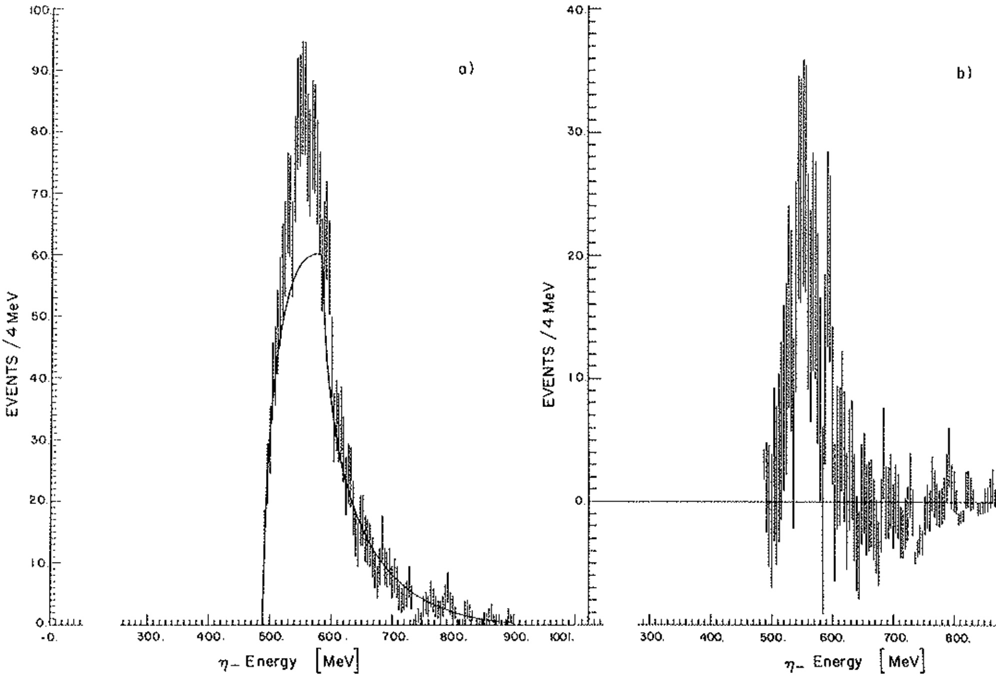

Fig. 5. a η energy spectrum. The solid line represents the uncorrelated background. b η energy spectrum after background subtraction

ture $(p\pi^- \to n\gamma)$ amounts to $Y_{n\gamma} = (3 \pm 1) \times 10^{-3}$ per annihilation for our set-up. Using the Panofsky ratio

$$R = \frac{\Gamma_{p\pi^- \to n\pi^0}}{\Gamma_{p\pi^- \to n\gamma}} = 1.546 \pm 0.009 \ [8],$$

and taking into account the reduction due to charged particles as discussed above, we expect the number of π^0's from charge exchange to be

$$N_{\pi^- p \to n\pi^0} = N_{p\bar{p}} Y_{n\gamma} R \Omega_{\text{coinc}} (1 - \bar{\Omega})^{N_{\pi^+} + N_{\pi^-} - 1},$$

where Ω_{coinc} is the average effective fractional solid angle for coincidences of correlated γ's, i.e. the cone defined by the condition $155° < \phi_{\gamma_1\gamma_2} < 180°$ and the solid angles of the two detectors. With $\Omega_{\text{coinc}} = 0.66\%$ and $N_{\pi^+} = N_{\pi^-} = 1.7$ per annihilation, the expected number of π^0's from charge exchange is $N_{\pi^- p \to n\pi^0} = 1000 \pm 340$. This number is higher than the measured one, hence indicating that we have overestimated the detection efficiency, but it is a safe upper limit to be used for normalization, i.e. a redefinition of the effective number of stopped $\bar{p}$'s which becomes $N_{p\bar{p}}^{\text{eff}} = (23 \pm 8) \times 10^6$. The number of primary π^0's from annihilation which we expect to observe is therefore $(1.6 \pm 0.5) \times 10^5$, when assuming 1.7 π^0's annihilation on an average.

The number of primary π^0's from annihilat may also be obtained directly from the spectrum. this end the remaining tail of the spectrum has to explained by the spectral shape of π^0's from annihilations at rest. A Monte Carlo simulat using the same annihilation channels as used in was performed. This simulated spectrum normali to one π^0 was folded with the assumed resolution $7\%/\sqrt[4]{E_{\pi^0}[\text{GeV}]}$ (which reproduces the peak 138 MeV) and the efficiency as displayed in Fi The number of π^0's was adjusted to the measu spectrum and corresponds to $(1.0 \pm 0.1) \times 10^5$, he lower than, but not in disagreement with, the exp tation as derived from the π^0 peak at 138 MeV. solid line in Fig. 4b represents the peak at 138 M and the simulated π^0 spectrum.

Obviously there is no structure left over wh could be attributed to a sharp baryonium-like st With an efficiency of 3.1% at 180 MeV (Fig. 3) limit at 3σ confidence for baryonium formation $E_{\pi^0} = 180$ MeV is 8% per annihilation when nor lized to the fitted number of π^0's and assuming

π^0's per annihilation in average. This limit would not change when normalization had been carried out with respect to the expected number of π^0's.

The η spectrum, Fig. 5a, may also be reduced by the uncorrelated background. The remainder is displayed in Fig. 5b. This spectrum seems to contain only low-energetic η's. Comparison with a Monte Carlo simulated η spectrum is not possible since only very little is known about annihilation channels involving η's. Therefore a determination of the number of η's from the low-energy part of the spectrum is not possible. In the energy range of our acceptance (Fig. 2), i.e. for $m_\eta < E_\eta < 600$ MeV, there are $270 \pm 50\,\gamma\gamma$ events or, using the branching ratio $R_{\eta\to\gamma\gamma} = 0.39$, a total of 700 ± 125 η's. The number of η's produced in this energy range is thus $N_\eta \geqq 0.46\%$ per annihilation. If only annihilation into $\eta\pi\pi\pi$ is assumed to contribute to our spectrum, this channel would have to have a yield of $(18 \pm 7)\%$ per annihilation. In view of the upper limit for η production in low-energy $p\bar{p}$ annihilation of $\eta/\pi^0 \leqq 0.11$ [9] or $N_\eta \leqq 19\%$ (assuming 1.7 π^0's per annihilation) this indicates a fairly large amount of four-body or more complicated final states associated with η production in $p\bar{p}$ annihilation at rest.

We conclude that this measurement, although very sensitive to low-energetic π^0's and η's, could not acquire sufficient statistics to reveal narrow baryonium-like states. The upper limit for baryonium production through π^0 emission is 8% in the mass region of ~ 1650 MeV. Search for baryonium states in $\bar{p}$-interactions in flight by observing a π^- instead of a π^0 [10] have resulted in a limit of 8 μb/sr for a 4 MeV wide signal. It is difficult to compare this result with ours since it is not a branching ratio and since the (intrinsic) initial state selection in interactions at rest (s- or p-states) is not possible in an experiment in flight. The number of η's produced per annihilation with kinetic energies below 50 MeV was found to be at least 0.46%.

Acknowledgements. We would like to thank CERN for its hospitality. This work was supported by the Swiss National Science Foundation, the Ministry for Research and Technology of the Federal Republic of Germany and the Swedish Science Research Council.

References

1. L. Tauscher: Bound baryonium states, Proc. 5th European Symposium on Nucleon-Antinucleon Interactions, Bressanone, 1980 p. 575. (Ed. Istituto Nazionale di Fisica Nucleare, Sezione di Padova), Padova CLEUP, 1980
2. P. Pavlopoulos et al.: Phys. Lett. **72B**, 415 (1978)
3. B. Richter et al.: Phys. Lett. **126B**, 284 (1983)
4. P. Blüm et al.: Nucl. Instrum. Methods **213**, 251 (1983)
5. M. Suffert, P. Pavlopoulos, K. Zioutas, A. Hegerath: Nucl. Instrum. Methods **215**, 107 (1983)
6. H. Backenstoss et al.: Nucl. Phys. B **228**, 424 (1983)
7. G. Källén: Elementary particle physics. Reading: Addison-Wesley 1964
8. J. Spuller et al.: Phys. Lett. **67B**, 479 (1977)
9. G. Levman, R. Singer, T. Fields: Phys. Rev. **D21**, 1 (1980)
10. R. Bertini et al.: Nucl. Phys. **B209**, 269 (1982)

APPENDIX F
PROPOSAL FOR EXPERIMENT PS182

"One Ring to rule them all, One Ring to find them"

J. R. R. TOLKIEN *The Lord of the rings*

EUROPEAN ORGANIZATION FOR NUCLEAR RESEARCH

CERN/PSCC/80-142
PSCC/P 36
9 January 1981

PROPOSAL

INVESTIGATIONS ON BARYONIUM AND OTHER RARE $\bar{p}p$ ANNIHILATION MODES USING HIGH-RESOLUTION π^0 SPECTROMETERS

Basel[1]-Stockholm[2]-Thessaloniki[3] Collaboration

L. Adiels[2], G. Backenstoss[1], I. Bergström[2],
K. Fransson[2], A. Kerek[2], P. Pavlopoulos[1],
J. Repond[1], L. Tauscher[1], D. Tröster[1] and K. Zioutas[3]

G E N E V A
1981

1. INTRODUCTION

In the search for baryonium carried out so far, various methods were used (high-energy production and low-energy formation in $\bar{p}$ and e^+e^- reactions). The results of all these measurements suffer from poor statistics[1-3]. Search for baryonium states below threshold ($m_B < m_{\bar{p}p}$) has given evidence for a few states[4], and the situation for bound states is perhaps less conflicting than for baryonium resonances in the continuum[3].

Among the methods applied in the baryonium bound state research, we consider the study of the following reactions at rest as most promising:

$$\bar{p}p \rightarrow \begin{cases} B + \gamma & \text{(1a)} \\ B + \pi^0 & \text{(1b)} \end{cases}$$

The reason is that in a stop-experiment the initial state is already a well-defined bound $\bar{p}p$ state (protonium atom). The transition from this state to a baryonium state by emission of a neutral particle populates both isospin 0 and isospin 1 baryonia (this is in contrast to charged pion emission, where only charged baryonia are formed).

The study of the γ-ray spectrum associated with the $\bar{p}p$ annihilation at rest seems, however, to have reached its limits at conventional beams[5], and improvements are only possible with much larger detectors or much better definitions of the annihilation channels[6].

The previous studies of the reaction $\bar{p}p \rightarrow B + \pi^0$ by measuring the two γ's from the π^0 under backward conditions, as was done in the experiment S161 (Ref. 5), must be considered as exploratory only. The reason is twofold:

i) the angular acceptance was restricted to $150^\circ \leq \theta_{\gamma_1\gamma_2} \leq 180^\circ$, thus limiting the range for the total energy of the π^0 to $E_{\pi^0} < 150$ MeV; for higher energies the detection efficiency dropped down to a few %;

ii) the total number of stopped $\bar{p}$'s obtained by S161 during 1980 was just sufficient to obtain, at $E_{\pi^0} = 200$ MeV and at a significance of 4σ, a sensitivity of $\Gamma_{\bar{p}p\rightarrow B\pi^0}/\Gamma_{tot} < 0.3$.

An experiment of this type must thus be done at different angular positions of the two γ detectors and at a beam of much higher intensity than has been available so far. The high potential of LEAR allows such an experiment to be carried out without using large and costly apparatus. We intend to study π^0 reactions by means of a simple detector system, allowing for both angular distribution measurements and high-resolution π^0 spectroscopy.

2. PROPOSED PHYSICS

2.1 π^0 spectroscopy

We propose to search for baryonium states below threshold by studying the $\bar{p}p$ reaction at rest:

$$\bar{p}p \rightarrow B + \pi^0 \ . \tag{2}$$

The monoenergetic π^0's will be measured in a set-up especially tailored for measuring π^0's. The apparatus will also give information about monoenergetic γ's.

2.2 Direct γ production

We further propose to study the direct (i.e. not via intermediate vector meson) production of γ's in $\bar{p}p$ annihilations at rest, which comes from the $\bar{p}p$ annihilation into the radiative channels $\pi^0\gamma$, $\omega\gamma$, $\rho^0\gamma$, and $\gamma\gamma$. These channels can to a large extent be derived from the channels $\pi^0\rho^0$, $\omega\rho^0$, and $\rho^0\rho^0$, assuming vector dominance. The branching ratios of the latter channels are known[7)], and any excess compared to what would be expected from vector dominance may then be attributed to direct γ production in the $\bar{p}p$ annihilation.

The branching ratio for the rarest of these channels ($\bar{p}p \rightarrow \gamma\gamma$) may be estimated from an early measurement of this reaction[8)] done at 1.5 GeV/c $\bar{p}$ momentum, and should be larger than 10^{-6} for a reaction at rest.

2.3 Baryonium decays

Search for baryonium by looking at its decay products in formation experiments becomes feasible at LEAR intensities. Our apparatus will be suitable for measuring some particular decays. We propose to study the reactions

$$\bar{p}p \rightarrow \ldots + B$$
$$\hookrightarrow \gamma\gamma \tag{3a}$$
$$\hookrightarrow e^+e^- \tag{3b}$$
$$\hookrightarrow \pi^+\pi^- \tag{3c}$$

These reactions will show up in kinematical regions where the background is expected to be very small. The decay of baryonium into γ's or leptons depends on the baryonium internal structure and the quark dynamics involved. A heuristic estimate of the branching ratio $\Gamma_{B\rightarrow\gamma\gamma \text{ or } e^+e^-}/\Gamma_{B\rightarrow\text{hadrons}}$ may be of the order of α^2. Too little is known, however, to make any reliable prediction[9)]. We intend to study these reactions at a later stage when LEAR will be operated at low extraction energies.

3. EXPERIMENTAL SET-UP

In order to investigate the proposed items, we will use high-resolution γ-ray detection methods and so-called Jacobian peak spectroscopy. The experiment will be designed such as to make full use of the LEAR beams right from the beginning.

Before discussing the experimental set-up in detail, we shall give a description of the γ-ray detectors to be used in the experiment and make some general comments about π^0 spectroscopy.

3.1 High-resolution γ-ray detectors

High-resolution γ-ray detectors of high efficiency are usually made from NaI. This material has the disadvantage of having relatively low density and of being highly hygroscopic. Such detectors have therefore to be housed in vacuum-tight vessels and are thus rather clumsy.

The availability of large crystals of BGO ($Bi_4Ge_3O_{12}$) now makes possible the construction of high-energy γ-ray detectors. This material is ideally suited to γ-ray spectroscopy owing to its particular properties:

- high density (7.13 g/cm^3),
- short radiation length (ℓ_{rad} = 1.12 cm),
- high intrinsic resolution ($\sim$ 15% at 600 keV),
- low afterglow characteristics,
- non-hygroscopic and chemically inert,
- mechanically robust.

One detector unit will consist of seven modules of hexagonal cross-section (see Fig. 1). The modules will have a diameter of 5 cm and a length of 15 cm. Each module will be equipped with its own photomultiplier. The spatial resolution in one direction for the central trigger-module will be achieved by a hodoscope consisting of five BGO crystals of 1 × 5 × 2.5 cm^3 (see Fig. 1), each one viewed with two photomultipliers.

The whole detector will have a weight of 15 kg, a diameter of 15 cm, and a length of 17.5 cm, without photomultipliers. This compactness together with its chemical and mechanical insensibility makes it very versatile and easy to handle.

The performance of one BGO crystal was tested at CERN in an electron beam (150-700 MeV/c) and with a ^{137}Cs source. The homogeneity and resolution turned out to be equivalent to those of NaI [10]. From these measurements we expect a resolution of $\Delta E/E \lesssim 5\%/\sqrt{E}$ for the total system of seven modules.

If the baryonium states are considerably narrower than 10 MeV there could be a need for much higher resolution without losses in efficiency. Liquid xenon may offer such a possibility, but so far such a detector has not been tested at the high γ energies involved in our experiment. A 4 ℓ prototype is under construction in Stockholm. If the tests of this detector are successful, it would be attractive to introduce at a later stage a much bigger liquid-xenon detector in the experiment.

3.2 π^0 spectroscopy

The two γ's from the decay of a particle of mass m and total energy E are strictly correlated by their kinematics:

$$m^2 = 2E_{\gamma_1}E_{\gamma_2}(1 - \cos\theta_{\gamma_1\gamma_2}) . \tag{4}$$

Sufficiently accurate measurements of all three quantities (E_{γ_1}, E_{γ_2}, $\theta_{\gamma_1\gamma_2}$) define the particle uniquely ($E = E_{\gamma_1} + E_{\gamma_2}$, $\vec{p} = \vec{p}_{\gamma_1} + \vec{p}_{\gamma_2}$). We call this method 'high-resolution π^0 spectroscopy'.

However, even if the energies E_γ of the γ's are not measured but only their relative angles $\theta_{\gamma_1\gamma_2}$, there is still a very pronounced angular correlation since most of the γ's are emitted into a narrow angular interval $\Delta\theta$ above the most probable angle θ^{minimum} (Jacobian peak); θ^{min} is a function of m/E only:

$$\sin\left(\frac{\theta^{\text{min}}}{2}\right) = \frac{m}{E} . \tag{5}$$

In Fig. 2 we display, as a function of the total π^0 energy E, the angular interval $\Delta\theta$, which is necessary to collect 40% of all decay events. The energy resolution $\Delta E/E$ obtained for the same condition is displayed in the same figure. It is 9% at 500 MeV and improves for smaller energies.

The narrowness of the Jacobian peak is demonstrated by the fact that 40% of all events fall within an angular interval of $\Delta\theta \leq 5.5°$.

The attractive feature of Jacobian spectroscopy is thus that the kinematics of the decay process offer a relatively good energy definition even if the intrinsic energy resolution of the γ detector itself is modest. The disadvantage of the method is, however, that it does not distinguish between correlated (from one π^0) and uncorrelated (from two different π^0's) γ's. It is thus well suited for a survey measurement; the final identification of a possible peak has, however, to be done with the high-resolution method.

3.3 The target

We intend to use a liquid-hydrogen target, which is matched in length to the range distribution of a 600 MeV/c $\bar{p}$ beam of a momentum resolution of $\Delta p/p \approx 10^{-3}$. The range distribution is then entirely determined by range straggling ($\sim$ 1% of the total range). The target diameter will correspond to the actual beam size. The total size will thus be: $\ell = 5$ cm, $\emptyset = 5$ cm. In order to enhance p-wave annihilation we will operate the target also with gaseous hydrogen at boiling point, thus reducing the density by almost a factor of 100. This mode of operation is, however, only possible at beam momentum of less than 400 MeV/c, where range straggling is accordingly smaller.

3.4 The beam telescope and moderation

The beam will have to be moderated in a moderator down to momenta of around 100 MeV/c. If moderation occurs from 600 MeV/c on, about 70% of the $\bar{p}$'s will be lost by interaction in flight. A plastic scintillation telescope will be used to identify slow $\bar{p}$'s entering the target.

3.5 Set-up for high-resolution π^0 spectroscopy

Two γ-ray detectors of the above-described type will be used to measure the γ's from the π^0 decay. The set-up is sketched in Fig. 3. Charged particles entering the two BGO crystals will be identified by plastic scintillation counters.

From the above discussion it is evident that the highest acceptance for a monoenergetic π^0 is at the most probable angle θ^{min}. However, this monoenergetic π^0 appears strongest in the π^0 energy spectrum at exactly the same position where the detection efficiency, for π^0's of a continuous energy distribution, peaks. Therefore the angular setting of the detectors must always be at somewhat smaller angles than would correspond to the π^0 energy searched for. It proves that the simultaneous measurement of precise energies ($\Delta E/E \sim 5\%/\sqrt{E}$) and angles ($\Delta\theta = 2.3°$) allows for very sharp $\gamma\gamma$ correlation conditions.

In order to demonstrate this property of our detector systems and to estimate the sensitivity of the apparatus for monoenergetic π^0's, Monte Carlo calculations were performed for various angles θ_{12} between the two detectors. The π^0 energy spectrum as expected from $\bar{p}p$ annihilations is shown in Fig. 4a. It was obtained using the yields of the annihilation channels given in Table 1. The peak corresponding to the $\rho\pi^0$ channel is clearly visible.

This spectrum will be drastically distorted by our apparatus. Figures 4b and 4c show the spectrum as measured under an angle θ_{12} of 40°, Fig. 4b corresponding to an angular resolution of 2 × 11°, Fig. 4c to an angular resolution of 2 × 2.3°, as achieved with the hodoscopes (see Fig. 1). The narrowness of the peak reflects directly the sharpness of the $\gamma\gamma$ correlation conditions imposed.

The sensitivities which we expect from the Monte Carlo calculations are as follows: at 200 MeV π^0 energy we need 10^{10} stopping $\bar{p}$'s in order to see a peak of 1% yield at 4σ, at an angle of $\theta_{12} \sim 110°$. Measuring at different angles θ_{12} in steps of 10°, and stopping 10^{10} $\bar{p}$'s for each setting, we would see a peak of 0.5% at 4σ.

The smallness and the rather low weight of the BGO detectors will allow for a light-weight, compact, mechanical set-up. We intend to place both detectors on one hardware construction, which will allow for precise angular adjustments and variable distances from the target. The construction will be one unit and thus easy to move.

3.6 Set-up for Jacobian peak spectroscopy

For these measurements the two BGO detectors will be placed under $\theta_{12} = 180°$ with respect to each other, each at a distance of 28 cm from the target. This corresponds to an angular resolution for the BGOs of ±1°. The angles between 30° ($E_{\pi^0} \approx 500$ MeV) and 150° ($E_{\pi^0} \simeq 140$ MeV) will be measured simultaneously by an array of 40 identical γ-ray detectors of limited energy resolution. We chose an arrangement that would keep the angular resolution constant ($\Delta\theta = 3°$). This leads to an energy-dependent energy resolution and to an energy-dependent acceptance (see Fig. 2). The solid angle of each array module is of the order of 10^{-3}, and its energy resolution is expected to be $\Delta E/E \approx (10\text{-}20)\%/\sqrt{E}$ above an energy threshold of 50 MeV.

The set-up is sketched in Fig. 5. Each counter will be vetoed for charged particles by a plastic scintillation counter.

The advantage of the method is to make full use of the Jacobian peak and, simultaneously, to be able to make a rough cut in the invariant mass, since the energies are measured. A further advantage of the method is that the γ energies in the Jacobian peak region are high. Thus the thresholds of the γ counters can be set at energies as high as about 70 MeV. Therefore the count rate and low-energy uncorrelated background problems will be largely suppressed. This is in contrast to pure Jacobian peak spectroscopy, where uncorrelated background cannot be rejected.

Monte Carlo calculations using the same Monte Carlo data as above result in the spectra shown in Fig. 6a, corresponding to $\sim 2 \times 10^8$ stopping $\bar{p}$'s. Introducing two peaks, at $\theta = 40°$ (400 MeV) and $\theta \simeq 80°$ (200 MeV), of 5% yield each, results in the spectrum of Fig. 6b. After applying the cut in the invariant mass spectrum, the background is reduced significantly at large angles (lower energies), as demonstrated in Fig. 6c.

The sensitivity reached by this method is as follows: in order to see a peak of 4σ significance in the angular spectrum of π^0's from 10^{10} stopped $\bar{p}$'s, coming from monoenergetic π^0's, the yield of these would have to be 0.5%, independent of whether the π^0 energy is 200 MeV or 400 MeV. It should be pointed out that these estimates are quite conservative, since the angular resolution may be improved significantly by a careful analysis of the shower configuration in the array modules[11)].

3.7 Set-up for the measurements of the baryonium decays

For the measurement of baryonium decaying into γ's or leptons [reactions (3a) and (3b)] it is sufficient to cover an angular interval of $130^\circ \leq \theta_{12} \leq 180^\circ$ in order to cover a mass region of $m_B \geq 1300$ MeV, supposing the baryonium is formed via reaction (1a). For more complicated formation processes the baryonium will be slower and thus the mass range will extend to lower masses. By rearranging the 40 array modules, it will be possible to cover the whole backward solid angle within the above limits.

The distinction between γ's and electrons will be done by the charged-particle-identifying plastic scintillators in front of each detector. The discrimination against heavier charged particles will be achieved by requiring electromagnetic shower characteristics in the γ detectors. The pions of reaction (3c) will be identified by additionally requiring a $\beta \geq 0.94$. This will be achieved by means of two Čerenkov detectors.

It should be pointed out that the events from reactions (3a) to (3c) show up in kinematical regions where the background from uncorrelated events is low since the energy of each decay particle is of the order of 400 MeV or higher.

3.8 Set-up for the measurements of the radiative annihilation channels

The measurements of the radiative annihilation channels require no special set-up. The channels $\bar{p}p \to \gamma\gamma$ and $\bar{p}p \to \pi^0\gamma$ will be obtained from the measurements under 180°. The channels $\bar{p}p \to \rho\gamma$ or $\omega\gamma$ will show up in the single γ spectra of each BGO detector.

4. RATES AND SENSITIVITY

Assuming a beam intensity of 10^6 $\bar{p}$/s and an initial beam momentum of 600 MeV/c, the number of stopping $\bar{p}$'s will be about 3×10^5 $\bar{p}_{stop}$/s. The average number of particles produced per annihilation being ~ 7, the total particle flux will be $\sim 2 \times 10^6$/s, half of it being γ's. For the BGO crystals 25 cm away from the target, the solid angle of one BGO module is 2.5×10^{-3} and its single rate thus 5000 s^{-1}. (This rate could be larger by as much as a factor of ~ 20 before running into count-rate problems.)

The $\gamma\gamma$ coincidence rate is then about 16 s^{-1}. This rate will again be reduced by about a factor of 10 by a fast correlation trigger (see next section), so that the final coincidence rate is of the order of $\sim 2\ s^{-1}$.

The Monte Carlo estimates discussed in Section 3.5 show that a sequence of 12 measurements at angles ranging from 150° to 40° in steps of 10°, and stopping 10^{10} $\bar{p}$'s for each setting, would reach a sensitivity of 0.5% at 4σ for energies $E_{\pi^0} < 400$ MeV. This would correspond to six days of measuring time at 600 MeV/c beam momentum, assuming ∿ 70% machine efficiency. At lower momentum (∿ 400 MeV/c) the same sensitivity would already be reached after two days of running.

The Jacobian peak method will yield somewhat higher coincidence rates since the total solid angles are larger. A coincidence rate of about 200 s^{-1} is expected if the appropriate energy cuts are applied. From the Monte Carlo estimates we conclude that with a beam momentum of 600 MeV/c we already reach the 4σ significance level for monoenergetic π^0's of 0.5% yield after half a day of running. At lower beam momenta we would stop 10^6 $\bar{p}$/s and thus reach the 4σ level for monoenergetic π^0's of 0.1% yield after about 10 days of running.

The measurements of the baryonium decays into γ's or leptons will have yields of the order of 10^{-6} per annihilation, provided the yield of baryonium is 1%. With full LEAR intensity and low beam momentum (all $\bar{p}$'s stopped), and increasing the solid angle of the two BGOs until the count-rate limit is reached, we expect a rate of 1500 events per day. The amount of correlated background as well as uncorrelated background is expected to be smaller.

5. DATA-TAKING AND OFF-LINE ANALYSIS

The data will be taken on-line with a PDP-11/44 computer. We intend to use the CERN data-acquisition system. A microprocessor system is now being developed which will reduce the amount of data already on the CAMAC level. Video-ADCs, fast dividers, and comparators will be applied to establish a fast trigger for correlated γ's.

The number of events per tape (1600 bpi) will be about 2×10^5.

Off-line data analysis will be possible partly at the PDP-11/44 and partly in our home institutes. Primary data processing will, however, have to be done at the CERN computers.

6. CERN AIDS

Although most of the detectors and electronics will be provided by the collaboration, we ask for support with regard to the following items:

- software support from CERN DD Division if changes to the CERN data-acquisition system will be necessary;

- support with standard pool electronics, essentially in case of emergency;
- workshop assistance for large hardware;
- support for the counter array;
- installation of an experimental hut and of a small on-line computer hut.

7. TIME REQUESTS, BEAM AND EXPERIMENTAL AREA

7.1 Time

We ask for a total of two periods of test time at the PS already in 1981, in order to check and tune detector components. The k_{23} beam would be particularly suitable.

At LEAR we ask for:

- four weeks of essentially parasitic beam for setting up;
- one week of main-user beam for the Jacobian peak spectroscopy;
- two weeks of main-user beam for the high-resolution π^0 spectroscopy.

Beam-time requests for the measurements of the baryonium decays will be placed when LEAR will provide low-energy beams.

7.2 Beam

The focal properties of the beam should be such as to keep the beam size below 5 mm FWHM in both directions. Moderation will be done in the focal plane. We ask for refocalization of the moderated beam, which should have a momentum of 200-300 MeV/c.

7.3 Area

We need about 2.5 m left and right from the target, about 3 m in front of the target, and 3 m behind it. The total area should thus be 5×6 m^2. We ask, in addition, that the area be well shielded from the beam dumps of areas where scattering experiments are performed.

Standard installations such as mains, pressurized air, and hydrogen exhaust will be necessary. We also would like to have the area covered with a removable plastic roof.

REFERENCES

1) R.D. Tripp, *in* Proc. 5th European Symposium on Nucleon-Antinucleon Interactions, Bressanone, 1980 (CLEUP, Padua, 1980), p. 519.

2) D. Perrin, Proc. Bressanone Symposium (1980), p. 545.

3) L. Tauscher, Proc. Bressanone Symposium (1980), p. 575.

4) P. Pavlopoulos et al., Phys. Lett. 72B, 415 (1978).

5) CERN Proposal PSC/77-41/P9 (PS 161) (1977), and following status reports.

6) P. Pavlopoulos, Proc. Bressanone Symposium (1980), p. 37.

7) R. Armenteros, *in* CERN Proposal PSCC/80-101/P28 (1980).

8) D.L. Hartill et al., Phys. Rev. 184, 1415 (1969).

9) See, for instance, G.C. Rossi and G. Veneziano, Phys. Rep. 68, 149 (1980).

10) P. Pavlopoulos et al., paper in preparation.

11) G.A. Akopdjanov et al., Nucl. Instrum. Methods 140, 441 (1977).
D.P. Barber et al., Nucl. Instrum. Methods 145, 453 (1977).

Table 1

Annihilation channels contributing to the spectrum of Fig. 4a

1)	$\omega 2\pi^+ 2\pi^-$	1.3%
2)	$\omega\pi^+\pi^-$	3.8%
3)	$\rho^+\pi^-\pi^+\pi^-$	6.4%
4)	$\rho^\pm\pi^\mp$	2.7%
5)	$\rho^0\pi^0$	1.3%
6)	$\rho^0\pi^+\pi^-\pi^0$	7.3%
7)	$\pi^+\pi^-\pi^0$	3.7%
8)	$\pi^+\pi^-2\pi^0$	9.3%
9)	$\pi^+\pi^-3\pi^0$	23.3%
10)	$\pi^+\pi^-4\pi^0$	2.8%
11)	$2\pi^+2\pi^-2\pi^0$	16.6%
12)	$2\pi^+2\pi^-3\pi^0$	4.2%

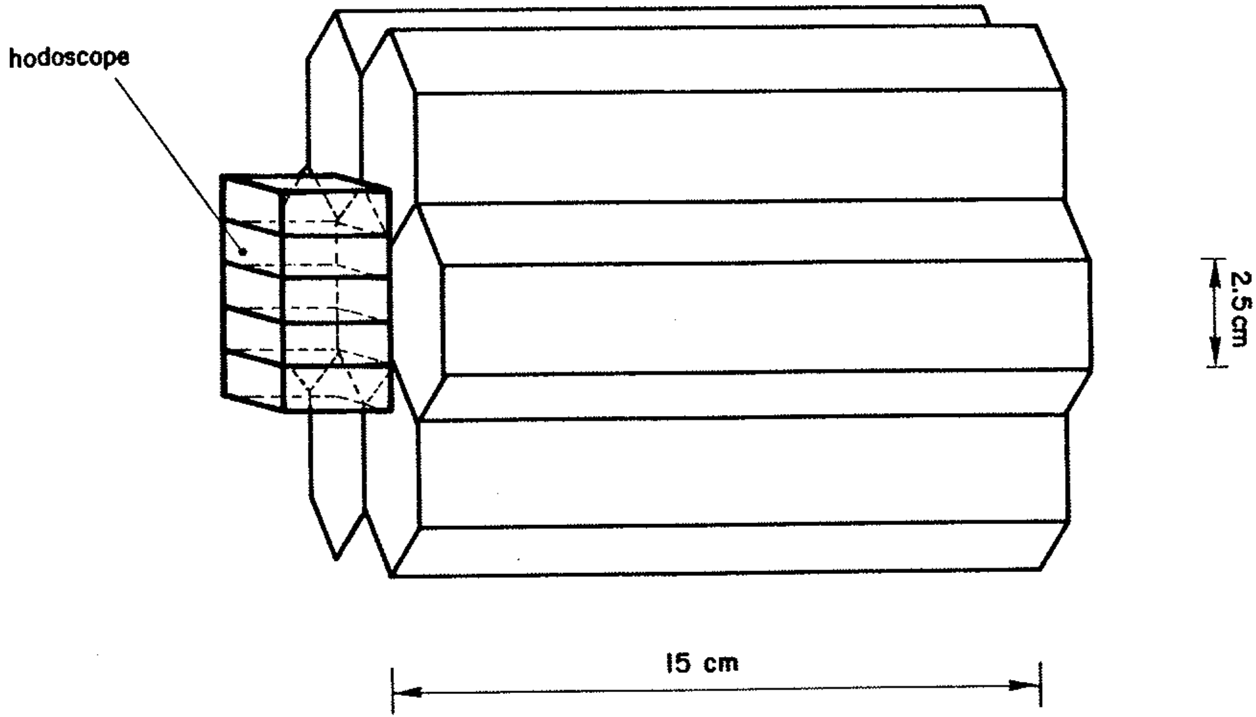

Fig. 1 BGO detector assembly

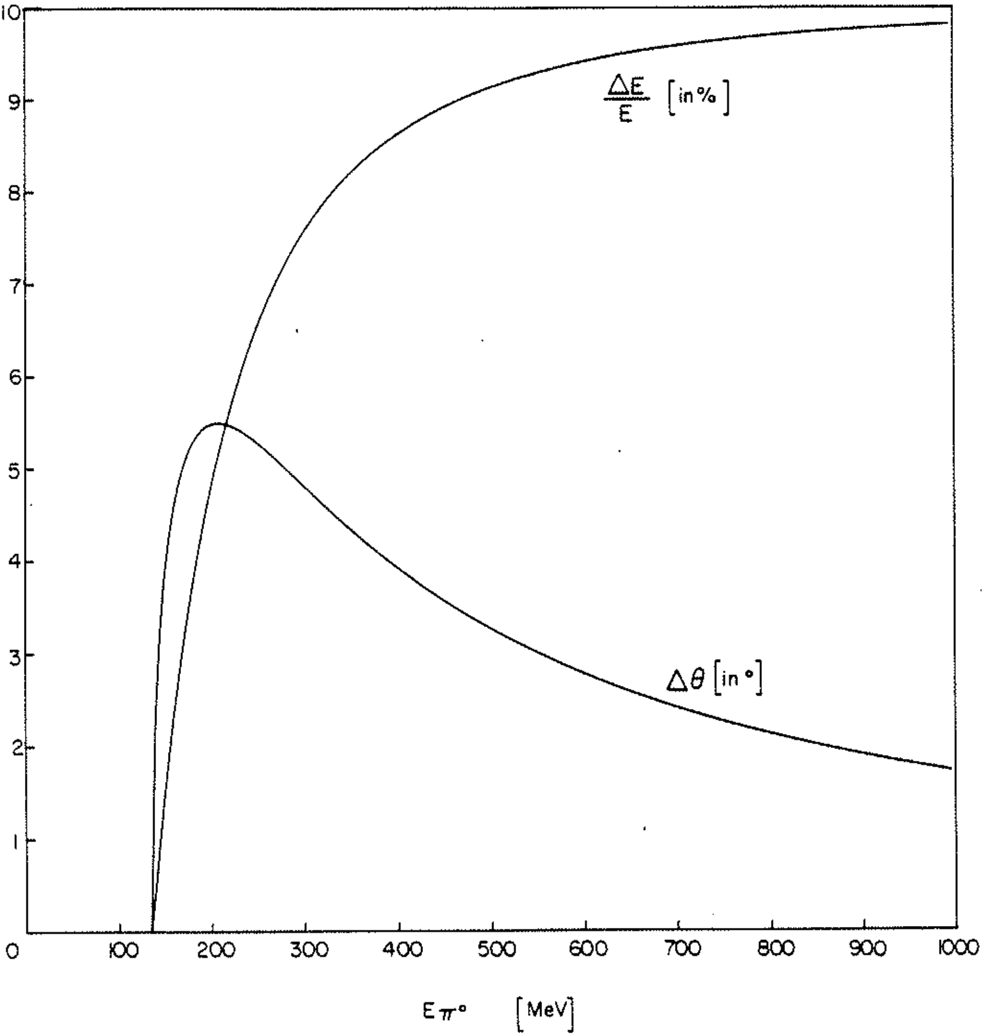

Fig. 2 Energy resolution $\Delta E/E$ (in percent) and angular interval $\Delta\theta$ (in degrees) as a function of E_{π^0}, if 40% of the Jacobian peak is accepted

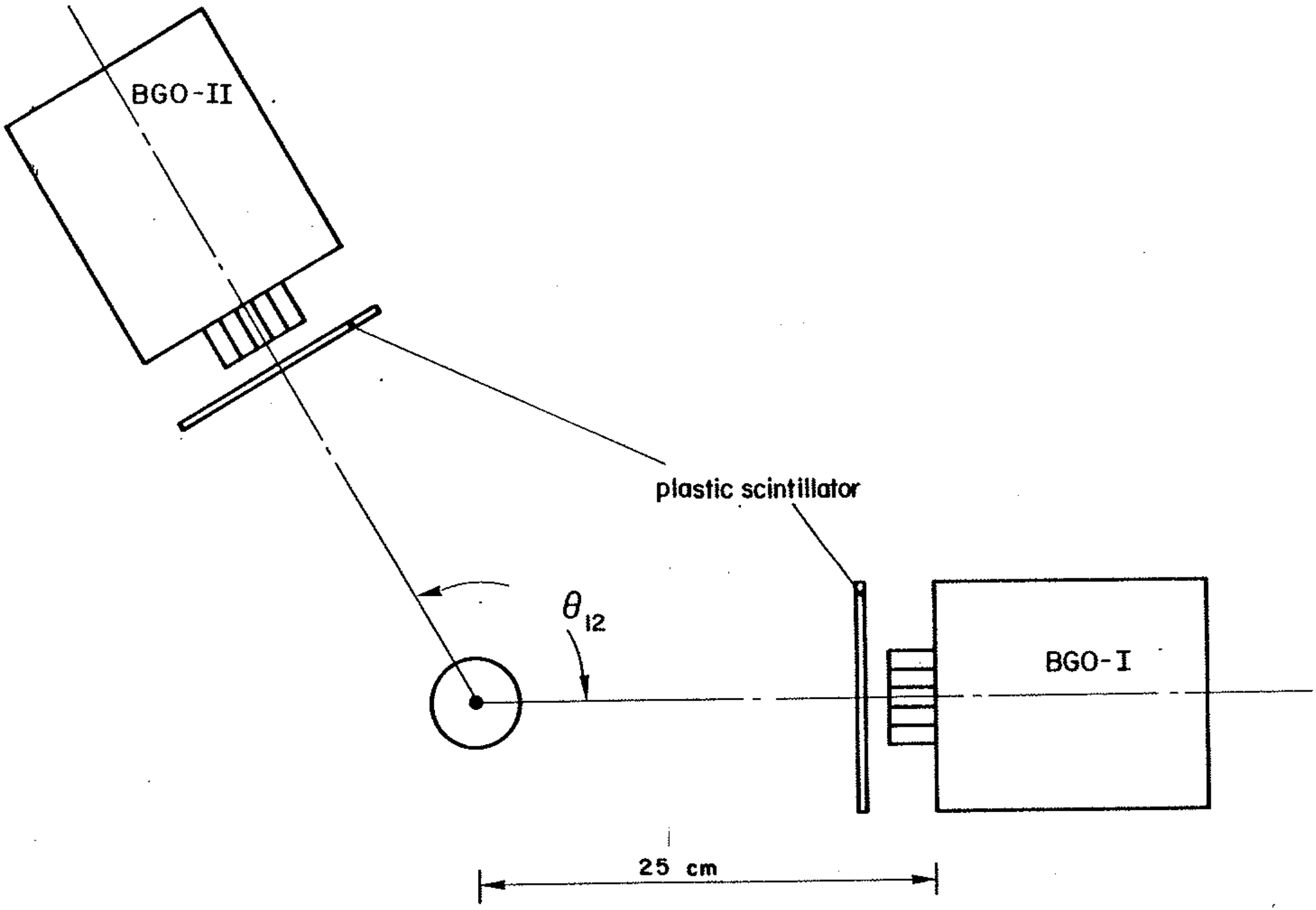

Fig. 3 Schematic view of the apparatus used for high-resolution π^0 spectroscopy

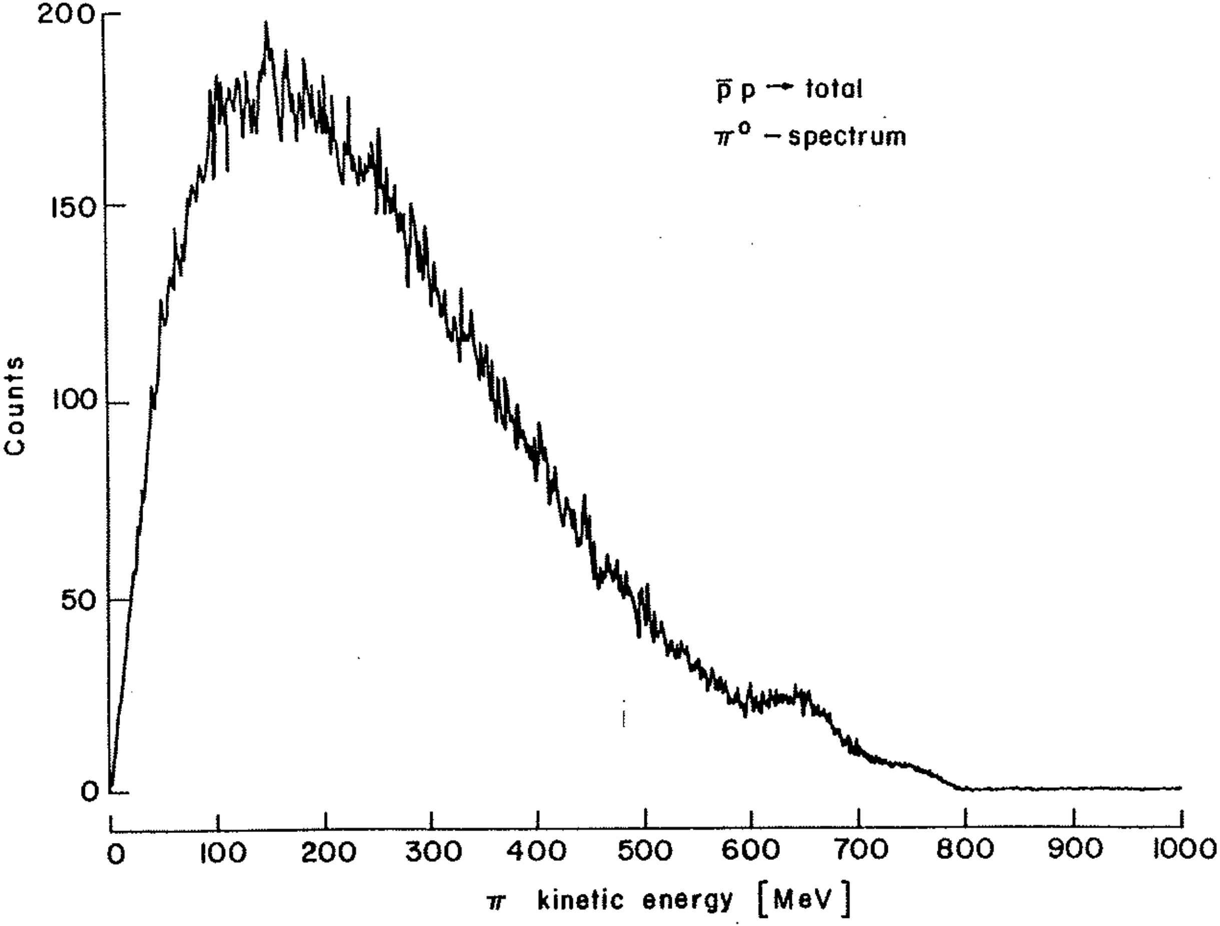

Fig. 4a The π^0 energy spectrum as obtained from Monte Carlo calculations, using the annihilation channels of Table 1 and their weights

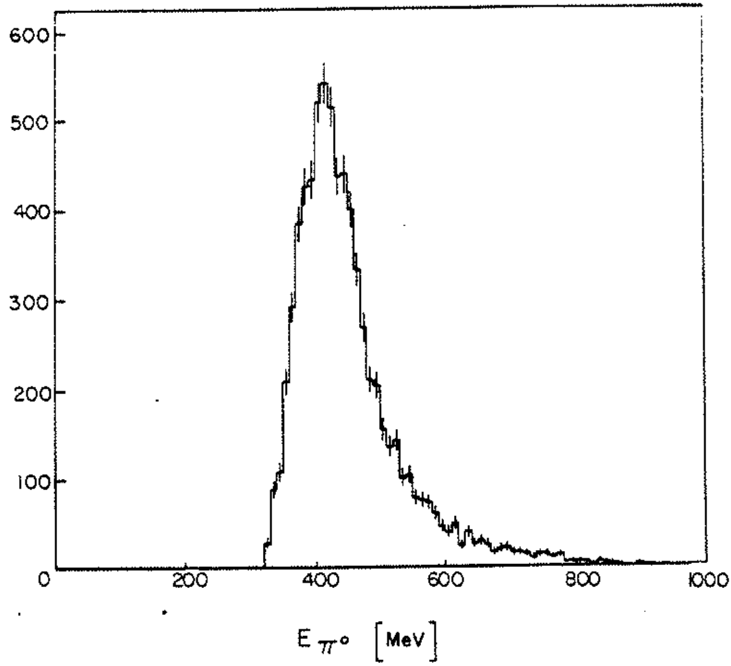

Fig. 4b The π^0 spectrum as measured by two BGO crystals under $\theta_{12} = 40°$. The angular resolution is 11° per detector.

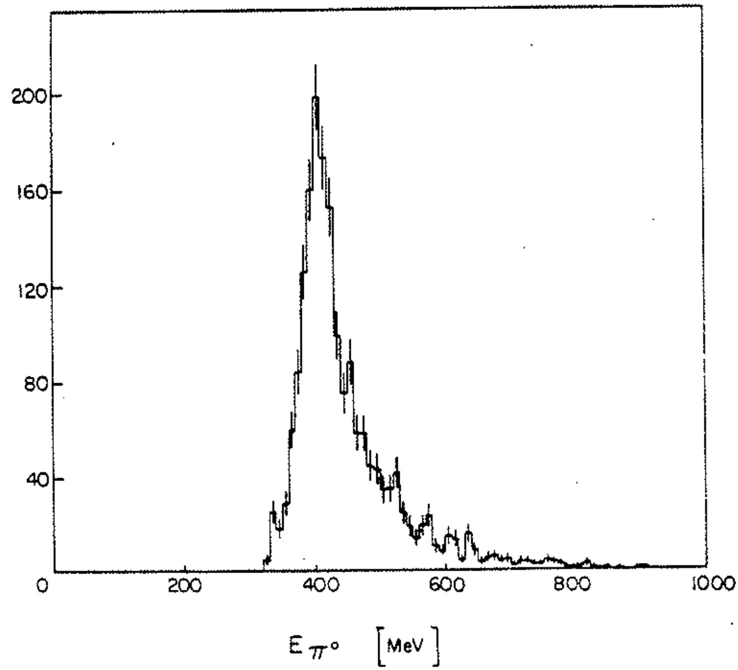

Fig. 4c Same as Fig. 4b, but now with an angular resolution of 2.3°

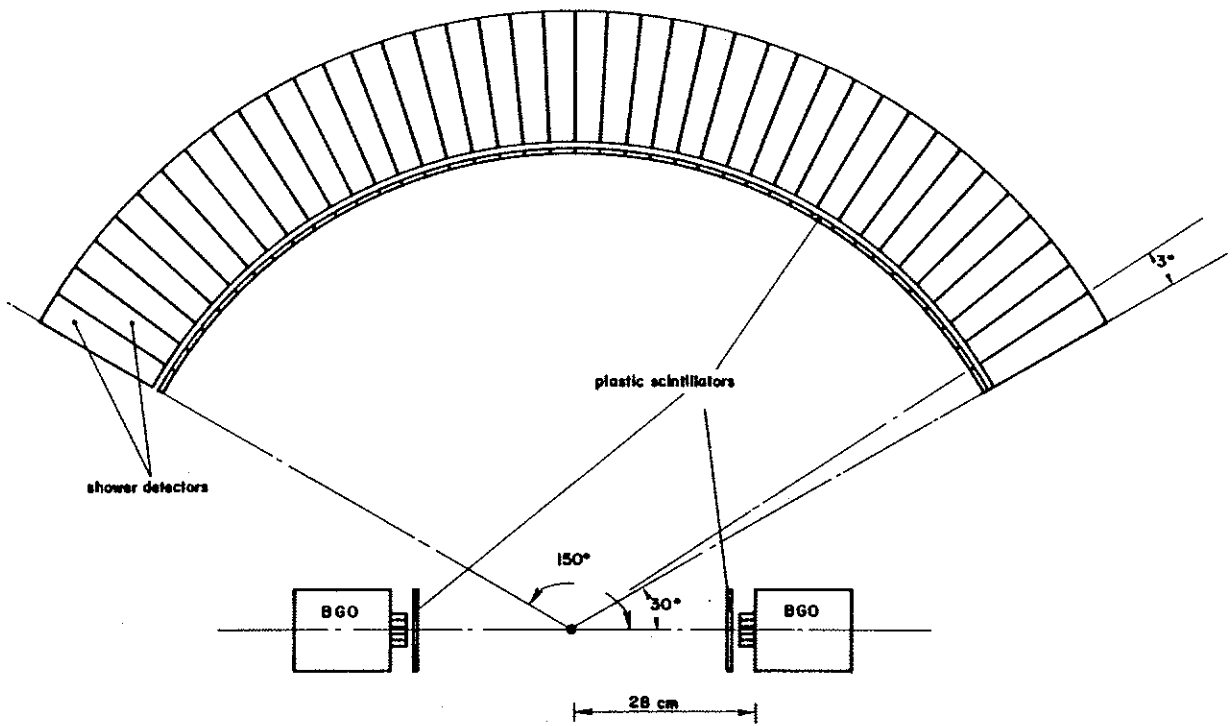

Fig. 5 Schematic view of the apparatus used for π^0 Jacobian peak spectroscopy

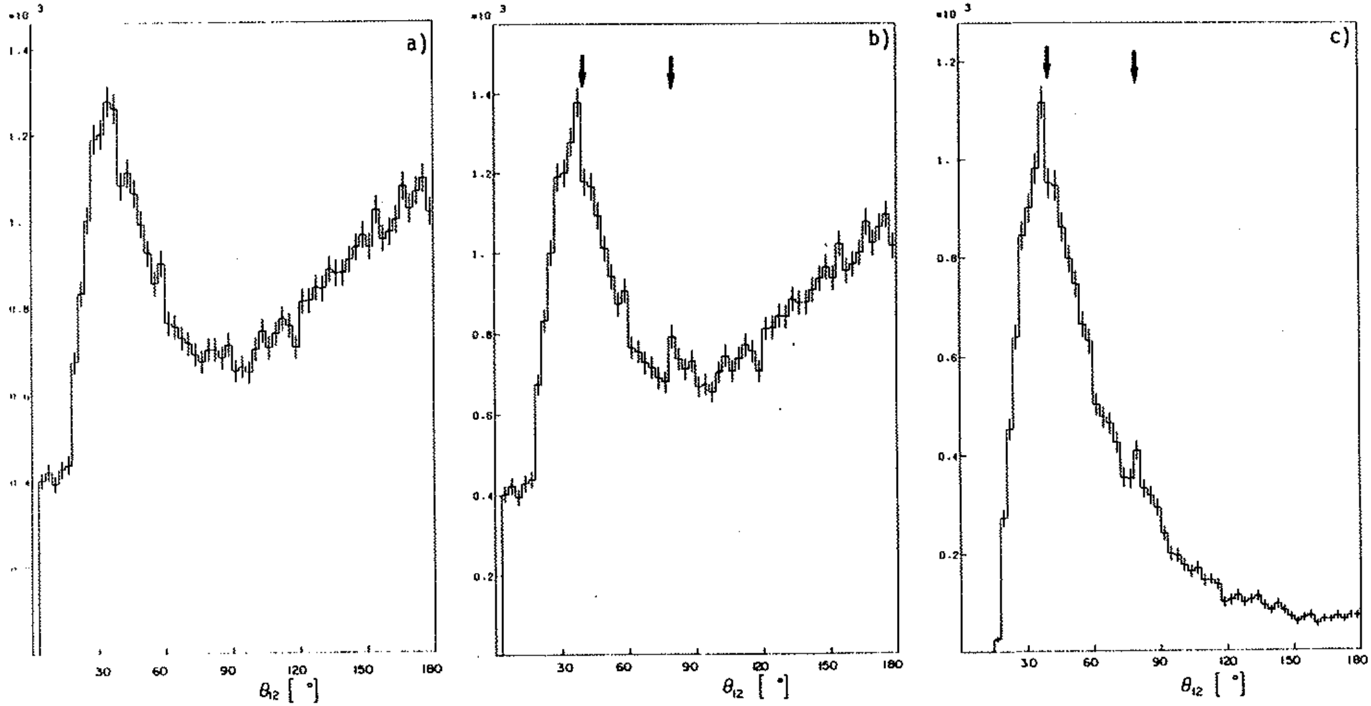

Fig. 6 Angular spectrum as obtained from π^0 decays, from $\bar{p}p$ annihilation. a) including an energy cut at 50 MeV; b) with the addition of two peaks of 5% yield each at $\theta = 80^\circ$ (200 MeV) and $\theta = 40^\circ$ (400 MeV); and c) with a further cut in the invariant mass spectrum.

REFERENCES

1. P.A.M. Dirac, Proc. Roy. Soc. **A126**(1930)360.

2. R. Armenteros and B. French, Antinucleon-nucleon interactions in high-energy physics, ed. E.H.S. Burhop (Academic Press, New York, 1969), vol. IV, p. 237.

3. C. Ghesquière, Proc. Symp. Antinucleon-nucleon interactions, ed. L. Montanet (Liblice-Prague), CERN, Geneva, CERN 74-18, 1974, p. 436.

4. R. Armenteros, CERN PS proposal CERN/PSCC/80-101 (1980).

5. G. Bassompierre et al., Proc. 4th European Antiproton Symp. Barr (Strasbourg), ed. A. Freidman (CNRS. Paris, 1979), vol. I, p. 139.

6. S. Devons et al., Phys. Rev. Lett. **27**(1971)1614.

7. M. Gell-Mann, Phys. Lett. **8**(1964)214.

8. Arnison et al. (UA1-C), Phys. Lett.**122B**(1983)103.

9. H.R. Rubinstein and H. Stern, Phys. Lett. **21B**(1966)447.

10. Particle Data Group, Review of Particle Properties, (Reviews of Modern Physics, Vol. 56, No.2, Part 2) April 1984.

11. A.M. Green and J.A. Niskanen in International Review of Nuclear Physics, Vol. 1, "Quarks and Nuclei", pp. 570, ed. W. Weise, Singapore, 1984.

12. A.M. Afrikyan, ZhETF **30**(1956)734; Sov. Phys. JEPT **3**(1956)503.

13. H. Bethe and R. Hamilton, Nuovo Cimento **4**(1956)1.

14. E. S. Birger, B. O. Kerbikov and I. S. Shapiro, Yad. Fiz. **17**(1973)1321 (Sov. J. Nucl. Phys. bf 17(1973)92).
    O. D. Dalkarov et. al., Yad. Fiz. **17**(1973)1321 (Sov. J. Nucl. Phys. **17**(1973)688).

15. D. Robson, Nucl. Phys. **B130**(1980)328-348.

16. A.S. Carroll et al., Phys. Rev. Lett. **32**(1974)247.

17. V. Chaloupka et al., Phys. Let. **61B**(1976)487.

18. P. Pavlopoulos et al., Phys. Lett. **72B**(1978)415.

19. French et al., Nouvo Cimento **52B**(1967)438.

20. Baillon et al., Nouvo Cimento **50A**(1967)393.

21. Edwards et al., Phys. Rev. Lett. **48**(1982)458.

22. G. Cosme et al., Nucl. Phys. **B152**(1979)215.

23. M. E. B. Franklin, SLAC-254

24. L. Gray et al., Phys. Rev. Lett. **26**(1971)1491.

25. G.C. Rossi and G. Veneziano, Phys. Rep. **63**(3)(1980)149.
L. Montanet et al., Phys. Rep. **63**(3)(1980)149.

26. S. Sakamoto et al., Nucl. Phys. **B158**(1979)410.

27. R.P. Hamilton et al., Phys. Rev. Lett. **44**(1980)1182.

28. R.J. Abrams et al., Phys. Rev. Lett. **18**(1967)1209 and Phys. Rev. **D1**(1970)1917.

29. M. Coupland et al., Phys. Lett. **71B**(1977)460.

30. J. Cutts et al., Phys. Rev. **D17**(1978)16.

31. I.S. Shapiro, Phys. Repts. **35C**(1978)129; Proc. V European Symposium on $\bar{N}N$ Interac-
tions, Bressanone (Italy) 1980, p. 589.

32. R.Y.M. Phillips, Rev. Mod. Phys. 39(1967)681.
R.A. Bryan and R.Y.M. Phillips, Nucl. Phys. B5(1968)201.

33. C.B. Dover and J.M. Richard, Phys. Rev. C21(1980)1466.

34. A.T.M. Aerts, thesis, The MIT Bagmodel and some spectroscopic applications, Nijmegen(1

35. H.M. Chan and H. Högaasen, Phys. Lett **72B**(1977)121,400; Nucl. Phys. **B136**(1978)401

36. G.F Chew, Nucl. Phys **B151**(1979)237; Phys. Lett. **82B**(1979)439.

37. A.A. Carter et al., Phys. Lett. **67B**(1977)117,122.
A.A. Carter, Nucl. Phys. **B127**(1977)202.
A.A. Carter, Nucl. Phys. **B132**(1978)176; **B141**(1978)467.

38. L.A.P. Balász, Phys. Lett. **71B**(1977)216.
L.A.P. Balász, Phys. Rev. **20D**(1979)233.
L.A.P. Balász and B. Nicolescu, Phys. Lett. **72B**(1977)240.
L.A.P. Balász and B. Nicolescu, Orsay preprint IPNO/TH-66 (1969).

39. R.L. Jaffe, Phys. Rev. **D15**(1976)267; Phys. Rev. **D15**(1977)281; Phys. Rev. **D17**(1978)14

40. C. Rosenzweig, Phys. Rev. Lett. **36**(1976)697;
M. Bender et al., Phys. Rev. Lett. **36**(1976)695;
F.E. Close and H.J. Lipkin, Phys. Rev. Lett. **41**(1978)1263;
S. Minami, Phys. Lett. **82B**(1979)126.

41. K. Johnson and C.B. Thorn, Phys. Rev. **D13**(1976)1934.

42. F.E. Close, An Introduction to **Quarks and Partons** Academic Press(1979)428.

43. *Ib.* 426.

45. B. Berg and A. Billore, Phys. Lett**113B**(1982)65; **114B**(182)324.

46. K. Iahikawa et al.,Phys. Lett. **116B**(1982)429; **120B**(1983)387.

47. K. Wilson, Phys. Rev. **D10**(1974)2445; Phys. Rept. **23**(1975)331.

48. R. Guigas et al. Phys. Lett. **137B**(1984)323.

R. Guigas, thesis, Untersuchung des Antiprotonischen Röntgen Spectrum der Lithiumisotope ^{6}Li und ^{7}Li, KfK 3208, Karlsruhe 1981.

49. L. Mazzone CERN target group.

50. Y. Chan et al. IEEE Trans. Nucl. Sci. **NS25**(1978)333.

51. M. Suffert et. al Nucl. Instrum. Methods **213**(1983)251.

53. Electron Gamma Shower program. There exist several versions at CERN and SLAC all based on R. L. Ford and W. R. Nelson, Report SLAC-210(1978).

54. In MINUIT a general fitting package for mini computers as well as mainframes, CERN computer library, long writeup D506.

55. G. Levman, R. Singer and T. Fields, Phys. Rev. **D21** (1980) 1.

56. I.J.R. Aitchison and A.J.G Hey,Gauge Theories in Particle Physics, Adam Hilger, Bristol(1982).
G. Källén: Elementary particle physics. Reading: Addison-Wesely 1964.
D.H. Perkins Introduction to high Energy Physics, Addison-Wesly, Massachusetts 1982.

57. Pauli first suggested the neutrino in a letter adressed to some of his friends, the letter is reprinted in R. Kronig and V.F. Weisskopf, eds, Collected Scientific Papers by Wolfgang Pauli, Vol II, Wiley-Interscience, New York (1969), p1316.

58. G. Källén: Elementary particle physics. Reading: Addison-Wesely 1964.

59. O. Andersen et al., Phys. Rev. Lett. **43**(1979)687.
O. Andersen, Thesis, Risö (Denmark), June 1980.